2003

Sediment accumulation and sedimentary diatom abundance on the continental shelf of central California

Roger C. Lewis
California State University, Monterey Bay

Sediment Accumulation and Sedimentary Diatom Abundance on the Continental Shelf of Central California

A Thesis

Presented to the Faculty of Moss Landing Marine Laboratories

In Partial Fulfillment

of the Requirements for the

Degree Masters of Science

By

Roger C. Lewis

December, 2002

APPROVED FOR MOSS LANDING MARINE LABORATORIES

Dr. Kenneth H. Coale

Dr. Kenneth S. Johnson

Dr. H. Gary Greene

APPROVED FOR THE UNIVERSITY

Abstract

This thesis consists of two papers that examine the sedimentation history of the continental shelf of the Central California coast. The first paper is the outcome of a collaborative project between the U.S. Geological Survey and Moss Landing Marine Laboratories. It examines the implications of sediment accumulation rates that are based on profiles of ^{210}Pb and other short-lived radioisotopes that were measured in sediment cores. This first paper documents the rate of sediment accumulation on a 100-year time scale on the continental shelf, between Pacifica and Monterey. The second paper examines 150cm-long sediment core for evidence of changes in primary productivity in Monterey Bay. Findings from the first paper were used to choose the site of the core that is examined in the second paper. This core comes from a flat part of the shelf in the center of Monterey Bay, at a location where sedimentation is thought to be sufficiently rapid to preserve diatoms and photosynthetic pigments before they are destroyed diagenetically. In the second paper, the abundance of certain diatoms are examined along with supporting data in order to determine if diatom productivity in Monterey Bay has changed significantly over the last 170 years. The abundance of key diatoms such as *Chaetoceros sp* and *Thalassionema nitzschioieds* varies significantly with depth. Sedimentary concentrations of Phaeophorbide-a, a decay product of chlorophyll-a, vary significantly with depth in the core. Profiles of phaeophorbide-a and total diatom abundance are similar in shape. Profiles organic carbon and sediment texture show only minor variations. The Pb-210 profile of this core indicates an anomalous sedimentation history. Subsequently, the age control for this core is uncertain.

Acknowledgements

This thesis was made possible with the help of many people. Brian Edwards and Kenneth Coale planned the sampling and analytical strategy employed in this research. Ken Johnson developed the computer program in which radioisotope data were modeled. Chuck Holmes provided detailed advice about the ^{210}Pb methodology utilized in this project. Jocelyn Douglas and Erica Burton provided ^{210}Pb data for numerous cores. Marci Marot analyzed five cores for activities of ^{210}Pb, ^{137}Cs, ^{226}Ra, and ^{234}Th. Jon Kolak prepared samples from five cores for radioisotope analysis. Jamie Arbizo analyzed sediment texture. Patrick Mitts and Charlie Paull provided results of DDT analysis. The officers and crew of the NOAA ship McARTHUR and R/V POINT SUR supported sample collection. Steve Eittreim, Gary Greene, Marlene Noble, Clark Alexander, Roberto Anima, and Jingping Xu provided insightful comments on marine geology and shelf sedimentology. Expertise on diatom identification was provided by John Barron and Elizabeth Fortunaier. This project was funded by the U.S. Geological Survey.

TABLE OF CONTENTS

LIST OF ILLUSTRATIONS

Figures in Part 1

Tables in Part 1

Figure in Part 2

Accumulation Rate and Mixing of Shelf Sediments in the Monterey Bay National Marine Sanctuary

Abstract

The distribution of excess ^{210}Pb in 30 sediment cores was used to determine modern (last 100 years) mass accumulation rates and the depth of sediment mixing on the continental shelf between Pacifica and Monterey, California. Apparent mass accumulation rates average 0.27 g cm^{-2} y^{-1} and range from 0.42 g cm^{-2} y^{-1} to 0.12 g cm^{-2} y^{-1}. Accumulation rates were highest at mid-shelf water depths (60-100m) adjacent to major rivers and near the head of the Ascension submarine canyon. Cores from water depths of less than 65 m had low, uniform ^{210}Pb activity profiles and sandy textures. The uppermost 5 to 13 cm of fifteen cores had uniform ^{210}Pb activity profiles above a region of steadily decreasing ^{210}Pb activity. This phenomenon was attributed to sediment mixing. The thickness of this upper layer of uniform ^{210}Pb activity decreased southward from 13 cm, west of Pacifica, to less than 5 cm, near Monterey Canyon. This southward decrease may be attributed to shallower bioturbation in the southern study area. ^{210}Pb inventory is a measure of how much excess ^{210}Pb is contained in the sediment column under a known area of seabed. ^{210}Pb inventories were observed to be lowest near large rivers and highest in fine sediment located away from large rivers. This observation may be explained by scavening of ^{210}Pb from the water column by fine sediment, which has undergone resuspension before final deposition.

1. Introduction

1.1 Project scope

The Monterey Bay National Marine Sanctuary was established in 1992 to preserve the marine resources and scenic beauty of Monterey Bay (figure 1). In 1995 the U.S. Geological Survey began a five-year interdisciplinary study to characterize the physical and ecological environment of the sanctuary. As part of that study, this investigation examined accumulation rates and mixing of shelf surface (<50cm) sediments in the northern sanctuary so that regional sediment transport and accumulation could be better understood. The results of this study may provide a basis for thoughtful management practices of human activities that impact the seafloor such as trawling, cable deployment, and dumping of dredge spoils. This broad survey of sediment accumulation may also provide a basis for more detailed studies of surficial sediments on smaller scales.

1.2 Physical setting

The sanctuary occupies an area of 14,000 km^2 that encompasses the continental shelf from just north of the Golden Gate south to Cambria. Our study area was the shelf of the northern sanctuary between 10 m and 130 m water depths, south of the Golden Gate and north of the Carmel River. The shelf within this area narrows to the south from 45 km width near the Farallon Islands to less than 2 km in Monterey Bay. Tertiary sedimentary rocks are exposed at the seafloor at various locations throughout the study area (Eittriem et al., 2002; Greene,1977; Greene, 1990;Wagner et al., 2000;). The Monterey Canyon is thought to be a major sediment pathway across the shelf (Greene, 1977; Hughes, 1988). Ascenscion Canyon, Pioneer Canyon Ano Nuevo Canyon, and Cabrillo Canyon, indent the shelf break of the northern study area.

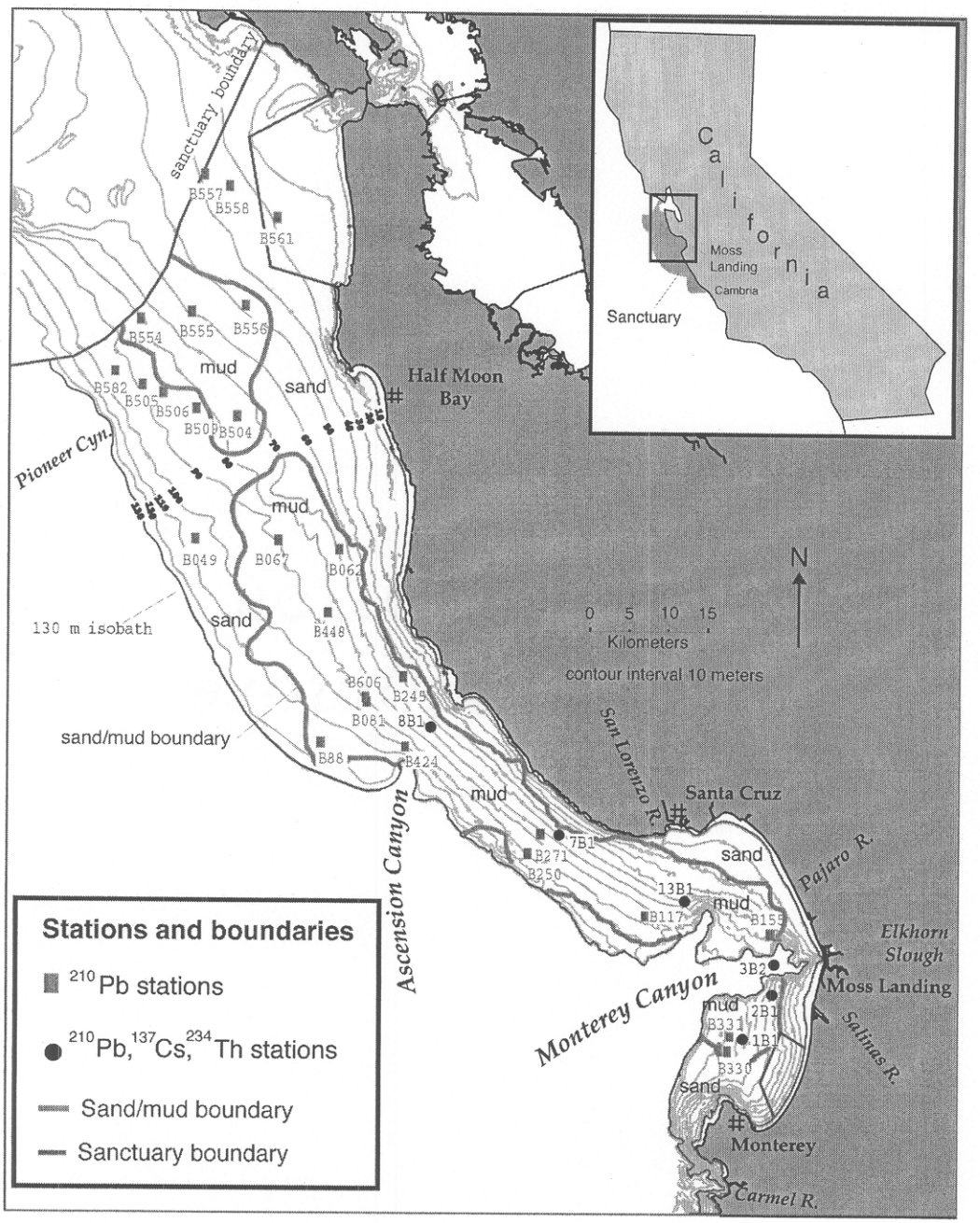

Figure 1: Area map showing study area on continental shelf of California. The bathymetric contour interval is 10m. Squares represent stations from which cores were sampled for 210Pb analysis. Circles represent stations from which cores were sampled for 210Pb, 137Cs, and 234Th analysis. The study area is between the 10 and 130 m isobaths, from Monterey to the northern boundary of the marine sanctuary.

1.3 Sediment source and transport

Sediment is supplied to the northern sanctuary primarily by stream discharge and to a minor degree by bluff erosion (Best and Griggs, 1991). Fine-grained sediment arrives as suspended solids from streams during periods of high winter discharge (Griggs and Hein, 1980). The San Joaquin and Sacramento rivers contribute 2.9 million metric tons of sediment per year to the San Fransisco Bay (Janda and Nolan, 1979; Curtis et al 1973). Sediment accumulation rates which were based on ^{210}Pb mass balance indicate 2.2 million metric tons accumulate yearly in northern San Francisco Bay (Fuller, 1982). The remaining 0.7 million metric tons of this sediment may exit the mouth of San Francisco Bay or it may remain in other reaches of the Bay. Thus, the sediment flux from San Francisco Bay is not accurately known. The Salinas, Pajaro, and San Lorenzo rivers contribute 1.8 million metric tons of sediment per year directly to the southern part of our study area (Janda and Nolan, 1979). Other streams contribute less than 0.1 million metric tons of sediment per year to the study area (Best and Griggs, 1991). Because estimates of sediment flux from the Golden Gate are not definitive, it is unknown whether the dominant sediment supply to the northern sanctuary is from the Golden Gate or from river discharge directly to Monterey Bay.

Shelf sediments are transported by a variety of currents that vary temporally and spatially. Breaker and Broenkow (1994) show that surface (0-25 m) currents within Monterey Bay are north-flowing at the surface, south-flowing at intermediate depths (25-150 m), and north-flowing at deeper level (>150 m). Current meter and sediment trap data indicate that northward bottom currents are seasonally strong enough to suspend shelf sediments (Xu et. al, 2002). As a result, northward mid-shelf sediment transport may predominate even though littoral transport is southward. Cacchione and Southard (1974) proposed that breaking internal waves at the outer shelf are sufficiently

energetic to inhibit deposition of fine-grained sediment. Wave induced resuspension of fines in the nearshore region and high energy benthic boundry transport at the outer shelf are responsible for the depositional patterns associated with fines at mid shelf.

Cross-shelf sediment pathways have been altered by sea level rise over the last 10,000 years. During the late Pleistocene, when the shoreline was to the west at the 120m isobath, Pioneer Canyon and the Ascension Canyon system (Greene, 2000; Normark, 1970) captured littoral sediment. Sea level rise has repositioned the modern shoreline eastward so that littoral transport bypasses Pioneer and the Ascension Canyon system, favoring Monterey Canyon as the cross-shelf sediment pathway for coarse sediments.

Based on shallow-seismic reflections and side-scan sonar images, Holocene sedimentation has been greatest at the mid-shelf (70-90m water depth). A Holocene sediment wedge, up to 40-m-thick, has been imaged at the mid-shelf atop what is thought to be a Pleistocene unconformity (Mullins et. al, 1985; Greene 1977). This Holocene sequence is thickest at the mid-shelf and thinnest at the near-shore (0-10m water depth) and shelf break (120m water depth). Side-scan sonar surveys of the northern sanctuary (see Eittriem et. al, 2002) indicate that rocks are exposed at the seabottom at 120-meter water depths. This indicates that modern sediment is trapped before it reaches the outer shelf or possibly that the outer shelf environment is too energetic to allow deposition of fine sediment to occur.

2. Methods

2.1 Sample collection

Sampling sites were selected randomly in the study area by the use of a site selection protocol developed by the Environmental Protection Agency. This program,

"Environmental Management Assessment Program" (EMAP), discretely designates sampling sites within the study area via a triangular point grid (Overton et. al., 1990). Discrete sampling on a triangular grid reduces sampling biases that may invalidate key assumptions of spatial statistical analysis. Over 300 box cores were collected from EMAP sites on research cruises aboard the Pt. Sur in 1995 and 1997.

Cores used for ^{210}Pb analysis were selected following several cross-shelf transects to represent depositional environments throughout the shelf region. Subcores were collected by use of a mechanical device that pressed a 9-cm-wide polycarbonate tube down into the box core. A stationary piston in the tube minimized sediment compaction upon subsampling. By use of this device, 3 or 4 subcores were collected for each box core location. Sediment samples were collected for ^{210}Pb analysis in three ways:

1) Eighteen subcores (B448, B504 - B506, B509, B554 - B558, B561, B606, 1B1, 2B1, 3B2, 7B1, 8B1, 13B1) were collected specifically for ^{210}Pb analysis and sampled aboard ship. These subcores were extruded and incrementally sampled into plastic bags or plastic jars that were immediately sealed to minimize water loss.

2) Ten subcores (B49, B62 , B67, B81, B88, B245, B250, B271, B330, B331) were split in half and sampled in the laboratory with a sectioning device. A core-sectioning device was used to cut 1/4-round slices out of the split core, leaving the other 1/4 for later analysis. Sediments adjacent to the core liners were excluded from analysis to minimize effects of sediment smearing.

3) Two cores (B117 and B115) were split in the laboratory and sampled by hand with a plastic spatula at 1 cm-thick intervals taken every 2 cm.

2.2 Radioisotope analysis

^{210}Pb activities were determined by alpha spectroscopy of the granddaughter nuclide ^{210}Po. Samples were homogenized, dried to a constant weight, and spiked with 11 dpm (2 mL) of ^{208}Pb + ^{209}Pb yield tracer. Polonium-210 was leached from the sediments in a series of three acid digestions that included 1) concentrated (12N) HCl, 2) concentrated (16N) HNO_3, and 3) aqua regia (HCl and HNO_3 in equal amounts). Each acid digestion was taken to dryness at 80-85° C. Dilute (0.5N) HCl was then added, solids were removed by centrifugation, and the supernatent was decanted and dried.

Polonium was plated onto pure silver discs for alpha counting using a method that was similar to the method described by Flynn (1968). Dried sample residues were dissolved in dilute HCl at 80° C and ascorbic acid was added to eliminate interference of iron III during auto deposition. Silver disks were cleaned and placed on custom made teflon® holders that attached to teflon® coated stirbars. Each disk was spun in the sample solution with a magnetic stirring hot plate at 80° C for 4 hours so that one side of the disk was plated. Plated disks were then set into a Tennelec TC-256 eight-channel alpha spectrometer equipped with two kinds of detectors: 1) silicon surface barrier detector, or 2) passivated ion implanted silicon detector, each with 22 KeV alpha resolution. Detectors were connected to a TC 306 digital router/multiplexer and a personal computer, running Dascon® software. Decays were counted for 12 hours to accumulate sufficient counts in the ^{208} Po, ^{209} Po, and ^{210}Po regions. Alpha spectra were integrated and transferred to a spreadsheet determine sample ^{210}Po activity. The ^{208} Po and ^{209} Po tracers were used to calculate detector efficiency and yield efficiency for the sample ^{210}Po activity. ^{210}Pb was assumed to be in secular equilibrium with ^{210}Po, so that that the sample ^{210}Pb activity could be calculated by dividing the yield-corrected ^{210}Po

activity by sample mass and count time. ^{210}Pb activity was corrected to account for decay time between sample collection and sample processing.

^{234}Th, ^{226}Ra, and ^{137}Cs activities were measured in six cores (1B1, 2B1, 3B2, 7B1, 8B1, and 13B1) by gamma spectroscopy. The <63um size fraction was ground to a fine powder and sealed in 125 milliliter counting jars. The sealed samples were stored for a minimum of 14 days to allow the in-growth of ^{214}Pb and ^{214}Bi, short-lived radiogenic progeny of ^{226}Ra. Samples were counted for a minimum of 24 hours on a Canberra high-purity germanium planar detector with an active area of 2000 mm^2 and a thin carbon composite window. Spectrum collection and analysis was performed using a PC-controlled APTEC multichannel analyzer and associated software. ^{234}Th and ^{137}Cs activities were calculated by integrating the area of the 63.3 keV and 661.6 keV photopeaks, respectively. ^{226}Ra activities were determined by averaging the activities of its daughters ^{214}Pb (295 keV, 352 keV) and ^{214}Bi (609 keV), which are assumed to be in secular equilibrium with their parent. Energy and efficiency calibrations were performed using an 11 line NIST traceable multi-gamma standard. The counting efficiency and full width-half height resolution were 9.0% and 612 eV at 60 keV and 1.3% and 1.4 keV at 661 keV. The activities are calculated for the date of sample collection to correct for decay between the time of sampling and counting. Error values were based on statistical counting errors at the 95% confidence interval.

2.3 Radioisotope data reduction

Sediment accumulation rates were determined from excess ^{210}Pb activities that decrease exponentially below the surface mixed layer (figure 2). Excess ^{210}Pb activity was determined by subtracting the average supported activity of a core from the total

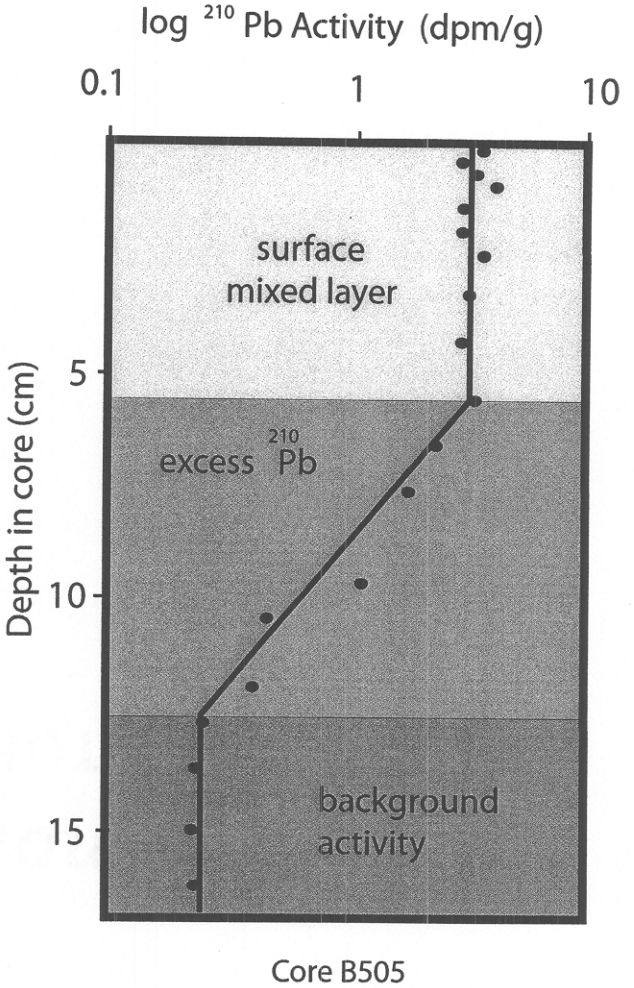

Figure 2: A 210Pb profile from core B505 showing log 210Pb activity vs. depth. A top layer of uniform 210Pb activity marks the apparent sediment mixed layer. Below is region of steady-state radioactive decay where 210Pb activity decreases with depth to background levels.

activity of each sample in that core. Supported activity was ascertained by averaging the uniform, low-level ^{210}Pb activities in the basal section of each core.

Linear sediment accumulation rate (cm y^{-1}) was calculated from the rate of decrease in excess ^{210}Pb with depth in the sediment column. A least-squares fit linear regression was applied to the natural log ^{210}Pb activity and the decay constant of ^{210}Pb (0.3108 y^{-1}) was divided by the line slope from the regression to determine linear accumulation rate (cm y^{-1}). In a similar manner, mass accumulation rates (g cm^{-2} y^{-1}) were determined by regressing natural log of excess ^{210}Pb verses cumulative mass.

The integrated excess ^{210}Pb activity in sediment cores may be used to determine mass accumulation rates by mass balance. Integrated excess ^{210}Pb activity was inventoried by summing excess ^{210}Pb activity per volume of wet sediment over the length of the core. ^{210}Pb activities in unmeasured depth intervals were extrapolated between measured sections. Uncertainties in sample volume made this approach of determining mass accumulation less favorable than by calculating mass accumulation from the line slope from the ^{210}Pb activity verses cumulative mass plot.

Calculations of sediment accumulation are based on the assumption that physical and biological mixing occurs only within the surface mixed layer. It is also assumed that the surface mixed layer coincides with the depth of uniform ^{210}Pb activity and that the thickness of surface mixed layer has remained constant with time. Activity profiles of ^{234}Th and ^{237}Cs (discussed later) indicate that these are realistic assumptions. If deep mixing were to occur below the surface mixed layer then ^{210}Pb activity would decrease more gradually with depth in the sediment column and the apparent sediment accumulation rate would be greater than the actual accumulation rate. Thus the apparent accumulation rates report in this paper should be considered as maximum estimates of the actual accumulation rates.

Apparent ^{210}Pb accumulation rates were evaluated by comparing the measured maximum depth of ^{137}Cs penetration in several cores to the depth that is predicted by the apparent accumulation rate and thickness of the surface mixed layer. If ^{137}Cs was first introduced to the seafloor in 1954 as a result of atmospheric testing of atomic weapons, then ^{137}Cs should be undetectable below a depth in the sediment column that is equal to the thickness of sediment accumulated since 1954 plus the thickness of surface mixed layer. This approach assumes that downward diffusion of ^{137}Cs is not significant, an assumption that may be invalid in some environments (Comans et. al., 1991), but is thought to be robust in this environment.

2.4 Sediment texture

^{210}Pb activity commonly varies with sediment texture (Nittrouer, 1978). This is thought to be caused by changes in the ratio of surface area to mass that results from changes in particle size. In order to avoid the confounding effects of sediment texture on ^{210}Pb activity, cores with significant textural and compositional variations were not included in this ^{210}Pb survey.

In order to screen out cores with significant textural and compositional variations, each core was scanned with a GEOTEK Multi-sensor logging system. This logging system directly measures P-wave velocity, gamma-ray attenuation, and magnetic susceptibility at 2-cm intervals along the sediment core. Changes in sediment composition and bulk density correspond to changes in the physical properties measured directly by the core logger. A more detailed discussion of this logging system is presented with examples of data in Edwards et al. (1997).

3. Results

3.1 ^{210}Pb profiles

Sedimentation rates were calculated from 22 of the 31 cores we analyzed for ^{210}Pb (figure 3). Sedimentation rates were not calculated from the remaining 9 cores because they had either unchanging or erratic ^{210}Pb profiles. Sediment accumulation rates range from 1.0 to 3.9 mm y^{-1} and mass accumulation rates range from 0.12 to .42 g cm^{-2} y^{-1} (Table I). Maximum accumulation rates are in mid-shelf regions and near major rivers. Apparent mixed-layer thickness range from 13cm in the north and decrease steadily to less than 2 cm southward along a mid-shelf transect (figure 3).

3.2 Cross-shelf trends

Apparent sedimentation rates are highest along the mid-shelf at water depths of 70-90m. These high rates fall within zones of fine surface sediments described by Edwards (2002). Cores from water depths of less than 60 m have uniform ^{210}Pb profiles that provide no evidence for modern accumulation. This is most likely due to wave action that results in resuspension of fine sediments that scavenge ^{210}Pb from the water column. Two cores from the outer shelf (B49 and B582) have ^{210}Pb profiles that provide no evidence for modern accumulation. Core B49 has constant and low ^{210}Pb activities and core B582 has erratic and low ^{210}Pb activities. These low and erratic ^{210}Pb profiles are probably due to the low concentration of fine sediment at the outer shelf.

3.3 Along-shelf trends

Apparent sedimentation rates are highest along the mid-shelf at water depths of 70-90m. These high rates fall within zones of fine surface sediments described by

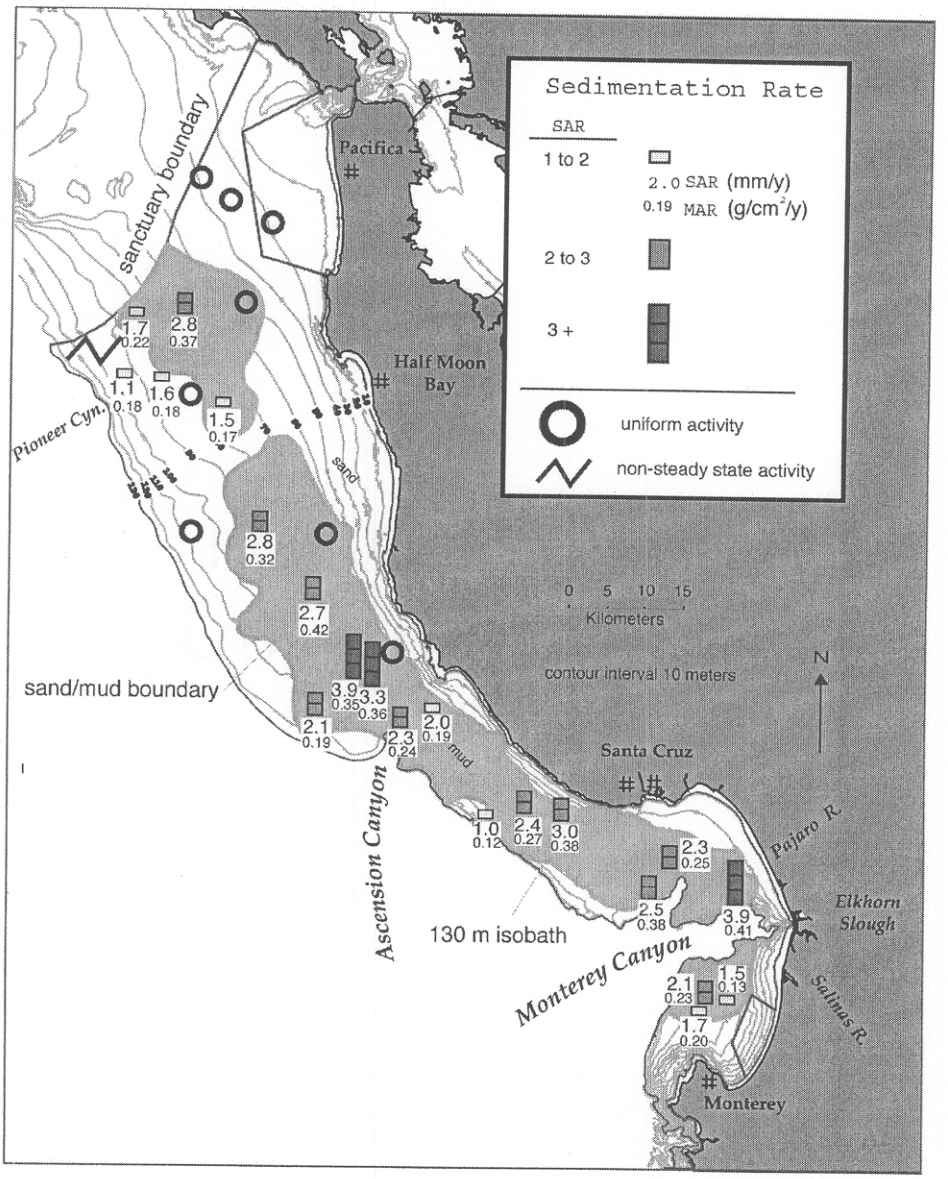

Figure 3: Area map showing distribution of sediment mass accumulation rates (upper number in large font) and mass accumulation rates (lower number in small font) within our study area on the California coast (inset). The location of each core is centered below the base of the box that represents the sedimentation rate. The shaded area in the shelf represents surface (0-2cm) sediments that have mean particle diameters of less than 63 microns.

core number	profile quality	depth (m)	sand (%)	SAR (mm/y)	MAR ($g/cm^2/y$)	Inventory (dpm/cm^2)	mean surface texture (phi)
B557	poor	39	88	-	-	-	3.5
B558	poor	35	87	-	-	-	3.6
B561	poor	31	92	-	-	-	3.5
B554	good	80	66	1.7	0.22	95	4.1
B555	good	61	56	2.8	0.37	61	4.3
B556	poor	50	65	-	-	-	4.1
B582	poor	95	94	-	-	-	3.2
B505	good	89	94	1.1	0.18	70	3.3
B506	good	85	92	1.6	0.18	79	3.4
B509	poor	82	79	-	-	-	3.9
B504	good	75	67	1.3	0.17	68	4.2
B49	poor	107	81	-	-	-	3.9
B67	good	92	54	2.8	0.32	95	4.5
B62	poor	44	92	-	-	-	3.5
B448	good	84	12	2.7	0.42	65	5.8
B88	good	123	73	2.1	0.19	68	4.1
B81	good	93	19	3.3	0.36	149	5.4
B606	good	90	15	3.9	0.35	115	6.2
B245	poor	64	60	-	-	-	4.4
8B1	good	97	-	2.0	0.19	-	-
B424	good	106	28	2.3	0.24	88	6.6
B250	good	96	36	1.0	0.12	116	5.2
7B1	good	71	-	3.0	0.38	-	-
13B1	good	80	-	2.3	0.25	-	-
B271	good	82	18	2.4	0.27	110	5.5
B117	good	85	12	2.5	0.38	83	6.2
B155	good	69	6	3.9	0.41	42	8.5
2B1	good	70	-	1.4	0.17	-	-
B331	good	95	3	2.1	0.23	114	6.7
1B1	good	93	-	1.5	0.13	-	-
B330	good	98	18	1.7	0.20	72	6.1

Table I: Summary of data from 31 cores arranged from north to south. Cores designated as "good" have ^{210}Pb activities that decrease exponentially with depth and were interpreted for sedimentation rate. Cores designated as "poor" have ^{210}Pb activities that are uniform with depth and were not interpreted for sedimentation rate. Apparent sediment accumulation rate (SAR) is a linear sedimentation rate in units of millimeters per year. Apparent mass accumulation rate (MAR) is as grams of dry sediment per square centimeter of sea floor, per year. Inventory is the integrated excess ^{210}Pb in units of decays per minute, per square centimeter of seafloor.

Edwards (2002). Cores from water depths of less than 60 m have uniform ^{210}Pb profiles that do not evidence modern accumulation, as do two cores from the outer shelf (B49 and B582). Core B49 has uniform and low ^{210}Pb activities and core B582 has erratic and low ^{210}Pb activities. The low and uniform ^{210}Pb activity in core B49 suggest that sediment mixing is high relative to the sedimentation rate. Sediment textural changes in core B582 indicate that its erratic ^{210}Pb profile may be attributed to a slump or change in composition.

4. Discussion

4.1 Sediment accumulation rates

The modern accumulation rates ascertained from ^{210}Pb profiles are slightly lower than average Holocene rates that were determined by previous workers who interpreted seismic reflection profiles (Chin et. al, 1987; Greene, 1977; Mullins et. al, 1985). Average Holocene sedimentation rates were calculated by measuring the thickness of sediments above a Pleistocene erosional unconformity and dividing that thickness by 10,000 y, the approximate time scale of the Holocene. Mullins and others (1985) mapped a Holocene sequence between Point Ano Nuevo and Santa Cruz that was up to 22 m thick, indicating an average sedimentation rate of 2.2 mm y^{-1} (22m/10000y). The modern rates we determined from ^{210}Pb profiles were 1.0-2.5 mm y^{-1}. Greene (1977) mapped a Holocene sequence southwest of Santa Cruz that averaged 25m in thickness with a maximum thickness of 40m near the Soquel canyon head. Modern accumulation rates in that area have an average of about 2.5 mm y^{-1}. Chin and others (1987) mapped a lobe of Holocene sediment that is up to 35m thick and thins outward from the Salinas River mouth. This study has determined modern rates of 2.1 and 1.7 mm y^{-1} on the outer fringe of the sediment lobe mapped by Chin and others (1987). Recent

sedimentation rates are typically greater than long-term rates because hiatuses in sedimentation reduce average long-term rates.

4.2 Mass accumulation rates

Apparent mass accumulation rates are highest at core B155, near the Pajaro River, and at cores B606 and B81, near the head of Ascenscion Canyon (figure 3). The high accumulation rate in core B155 is due to its close proximity to the Salinas and Pajaro Rivers, the two largest sediment sources to Monterey Bay. Terrestrial sediment input from streams and cliff erosion in the vicinity of cores B606 and B81 is comparatively small (Best and Griggs, 1991). Seismic reflection profiles show that cores B606 and B81 were sampled from an area of thin (<5m) sediment cover just north of bedrock outcrops (Eittreim et al., 2002). The high sedimentation rates at cores B606 and B81 are not explained by nearby terrestrial sediment input or average Holocene sedimentation rate.

The outer shelf and inner shelf experience low net deposition of fine sediment. Sites shallower than 65 m have low and uniform ^{210}Pb activities, an indication that sediment is being deeply mixed or that no net deposition occurs shallower than 65 m. Site B49 and site B582 have low and constant or erratic ^{210}Pb activity profiles. This is interpreted as evidence of non-deposition or deep mixing on the outer shelf. Both cores are located in greater than 90 meters water depth and are outboard of areas of sediment accumulation. Griggs and Hein (1988) described flood water plumes that extended past the outer shelf, an indication that a mechanism exists for fine sediment delivery to the outer shelf. Non-deposition on the outer shelf may therefore be due to resuspension by surface or internal waves rather than a lack of new sediment.

The Salinas River is one of the largest sources of fine sediment to the Southern Monterey Bay. A large sediment lobe extends several kilometers west of the Salinas River mouth (Chin et al., 1987; Greene, 1977). Cores B330 and B331 are within three kilometers of this sediment lobe and have low (< 0.3 g cm^{-2} y^{-1}) mass accumulation rates. This can be explained if bottom-currents at these two sites are sufficiently strong to inhibit the deposition of fine sediment.

4.3 Sediments from rivers

Rivers are the dominant source of sediment to this study area. Though most of this fluvial sediment is fine grained, a small fraction (about 16%) is trapped as near shore sand, which is entrained in the predominantly southward littoral drift (Best and Griggs, 1991). Best and Griggs (1991) also note that this fluvial sediment accounts for about 75 percent of input to the littoral cell. Resuspension by wave action inhibits the deposition of fine sediment in near shore environments. Fine sediment is more easily deposited at the mid-shelf due to the more quiescent conditions that exist there.

The average sedimentation rate calculated from ^{210}Pb profiles is in accord with estimates of sediment loads from major rivers. The San Lorenzo, Pajaro, and Salinas Rivers contribute an estimated 1.8 million metric tons of suspended sediment directly to the Monterey Bay (Griggs and Hein, 1988). The suspended sediment load to the San Francisco Bay estuary is estimated to be over 2.9 million metric tons yearly. It's also estimated that 2.2 million metric tons accumulate yearly in northern San Francisco Bay (Fuller, 1982). If the remaining 0.7 million metric tons are deposited along with sediment from major rivers entering the Monterey Bay, then the total fluvial sediment load would amount to 2.9 million metric tons. The mean mass accumulation rate for the 23 cores mid-shelf cores is 0.26 g cm^{-2} y^{-1}. Deposition at this rate over the1100 km^2

zone of fine (>4 phi) mid-shelf sediment mapped by Edwards et al (2002) accounts for approximately 2.9 million metric tons of deposition per year. Thus, it is possible that most of the fine sediment load from Monterey Bay and San Francisco Bay is deposited at the mid-shelf. These estimates do not take into account the episodic contributions of fine sediment from small streams which annually contribute approximately 0.1 million metric tons directly to the central study area (Best and Griggs, 1991). Coastal erosion of bluff and dunes contributes less than 0.1 million metric tons of sediment annually to the mid-shelf(Best and Griggs, 1991; Griggs and Hein, 1988). Large uncertainties exist in estimates of sediment contribution from San Francisco Bay so significant errors may exist in this sediment budget.

4.4 Apparent mixed-layer thickness

The apparent mixed layer is the uppermost portion of a ^{210}Pb profile that contains high, uniform ^{210}Pb activities. Along the shelf, the apparent mixed layer increases in thickness toward the northwest from less than 2 cm, near Monterey, to more than 11 cm, west of Pacifica (figure 4). Figure 4 shows profiles of ^{210}Pb activity that indicate a northward thickening of the apparent sediment mixed-layer. Most likely this is due to a northward increase in mixing by bioturbation, though a tenfold increase in sedimentation may also be a cause. This trend in apparent mixed layer thickness follows a transect of cores that contain the same mean particle size in the uppermost few centimeters (Edwards, 2002). High rates of sedimentation commonly result in low ^{210}Pb activities because particle flux may outpace the input of ^{210}Pb. This would explain why cores B555 and B504, in the northern study area, have ^{210}Pb activities that are half those of cores further south that have similar sediment texture. However, physical property logs of these cores do not show any sudden change in bulk density that would

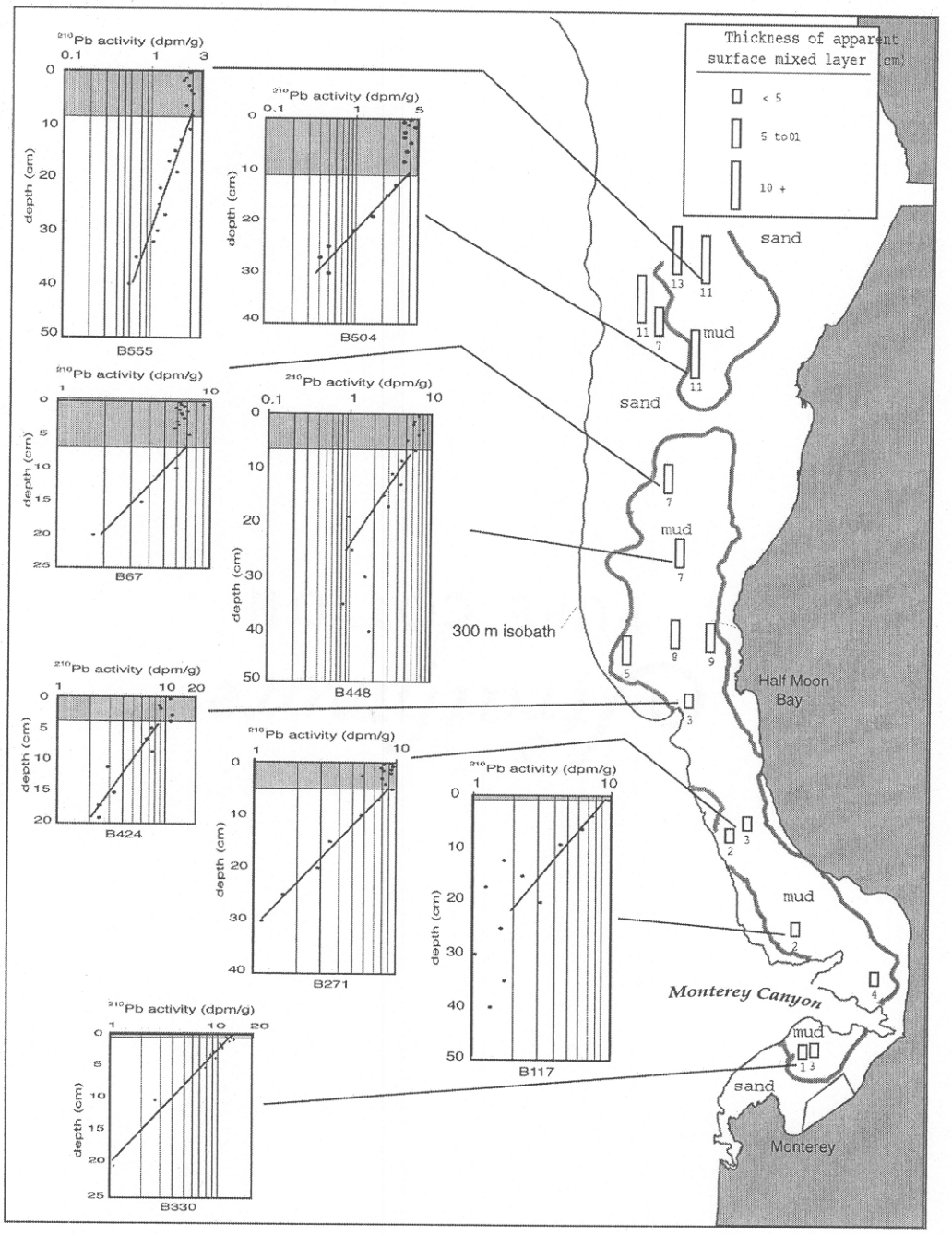

Figure 4: Area map showing the thickness of apparent surface mixing as ascertained from 210Pb activity profiles. Activity profiles show total 210Pb activities in decays per minute per gram of dry sediment and depth in cm. The shaded area in the upper part of each activity profile approximates the thickness of the apparent mixed layer. The small rectangular symbols depict the depth to which surface sediment exhibit uniform 210Pb activity. The number at the base of the rectangular symbol approximates the depth of uniform 210Pb activity. The apparent depth of surface mixing is greatest to the north.

most likely be associated with a sudden increase in sedimentation. A numerical model was used to test if either bioturbation or increased sedimentation could be ruled out as causes of the apparent change in sediment mixing.

4.5 Numerical Modeling

Sediment mixing by physical and biological processes affects the distribution of ^{210}Pb in the sediment column. This effect becomes increasingly significant if the depth of vigorous mixing increases and sedimentation rate decreases. The combination of deep mixing and slow sedimentation can have a profound effect on the apparent accumulation rate ascertained from ^{210}Pb profiles. Deep mixing reduces the slope of the part of the ^{210}Pb profile that is used to calculate a sedimentation rate. The apparent sedimentation rate of a deeply-mixed ^{210}Pb profile may dramatically overestimate the true sedimentation rate.

The effect of sediment mixing on ^{210}Pb activity profiles was evaluated with the numerical model of Peng and Broecker (1979). The rate of mixing in this model decreases exponentially with depth in the sediment. The effect of this downward decrease in mixing rate becomes more pronounced as the mixed depth increases or sedimentation rate decreases. This model assumes that the ^{210}Pb activity per gram of new sediment remains constant with time and that the depth and rate of sediment mixing also remain constant with time.

Modeled ^{210}Pb activity profiles most closely matched measured profiles when apparent accumulation rates and apparent mixed depth were used. Cores in the southern study area, near Monterey Canyon, had modeled mixing coefficients of 2-3 $cm^2\ y^{-1}$. These mixing coefficients compared favorably with other modeling studies of shelf environments that have mixed depths and sedimentation rates similar to Monterey Bay

(Boudreau, 1994). Cores in the northern study area, near Half Moon Bay, required dramatically higher mixing coefficients (30-40 $cm^2\ y^{-1}$) to reproduce observed ^{210}Pb activity profiles. When the mixing model was altered so that mixing rate was constant to the base of the mixed layer, then the lower mixing rate of 2-3 $cm^2\ y^{-1}$ reproduced the ^{210}Pb activity profiles observed in northern cores. On this basis, the discrepancy in mixing coefficients is due to the downward-decreasing mixing rate of the Peng and Broeker (1979) model.

Numerical modeling was used to test if a pulse of rapid sedimentation could cause the uniform ^{210}Pb activities observed in the upper 8-11cm of cores from the northern study area. If pulse sedimentation could be ruled out then bioturbation would be the most likely mechanism for these uniform ^{210}Pb activities. Model results matched the observed profiles when sedimentation rate in the top 8-11cm was increased ten times as the ^{210}Pb activity of new sediment was reduced by half. If sediment deposition increases by a factor of ten as the ^{210}Pb activity of new sediment decreases by half, then the rate of ^{210}Pb deposition increases by five-fold. This increase in ^{210}Pb deposition would cause the total excess ^{210}Pb in sediments to be higher in cores from the northern study. Such an increase in total excess ^{210}Pb is not observed in the northern study area (figure 5). Thus, the uniform ^{210}Pb activities in the upper 8-11cm of cores from the northern study area are most likely due to sediment mixing, not rapid sedimentation.

4.6 Integrated excess ^{210}Pb

Integrated excess ^{210}Pb is commonly influenced by factors such as sediment texture, water depth, sedimentation rate, and atmospheric deposition rate of ^{210}Pb. However, if ^{210}Pb accumulation is limited primarily by sediment flux then the highest integrated ^{210}Pb values should be near river mouths. The distribution of integrated

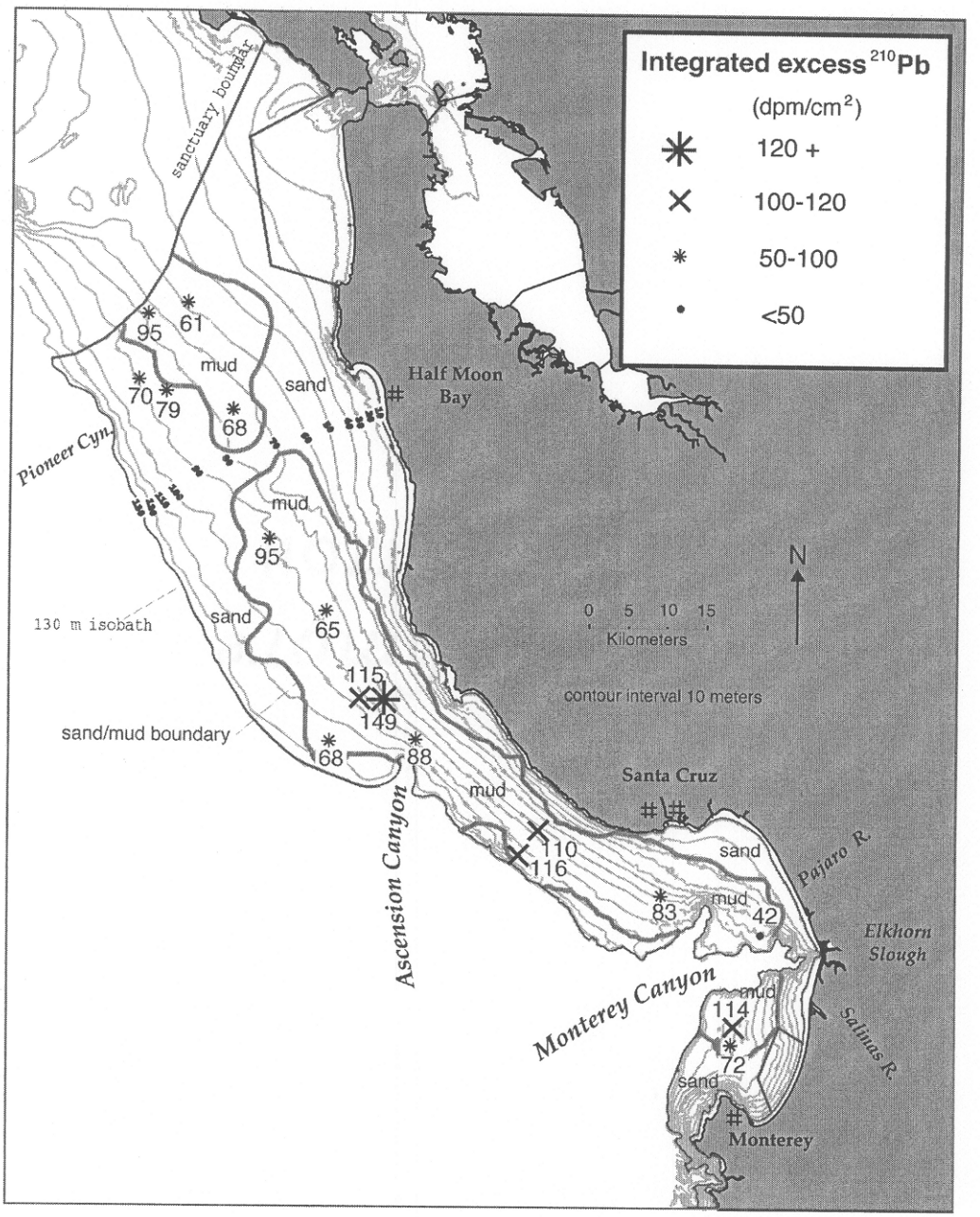

Figure 5: Area map showing integrated excess 210Pb activities as decays per minute, per square centimeter of seafloor. Integrated activity is highest in the mid-shelf near the head of Ascension Canyon and lowest near the mouth of the Pajaro River. Integrated 210Pb activities are greatest where sediment sources are small.

excess ^{210}Pb shows the opposite to be true (figure. 5). Values are lowest near the Pajaro River, a major sediment source, and highest near Point Año Nuevo, where sediment flux is low. The cores near the Pajaro River indicate that high sediment flux does not result in high integrated ^{210}Pb activity. Cores B155 and B117, near the Pajaro River, have mean particle diameters that are similar to cores B81 and B606, near point Año Nuevo, yet cores B81 and B606 have almost twice as much ^{210}Pb stored in them (Table 1). Consequently, ^{210}Pb deposition depends on more than just sediment flux or sediment texture.

Sediment transport can theoretically increase the rate of ^{210}Pb deposition by sediment focusing. If fine-grained sediments are suspended from a large area and subsequently deposited in a small area, then particle-bound ^{210}Pb deposition may be focused to an area of seafloor. If ^{210}Pb flux to the sea floor is constant over the study area, then the large amounts of excess ^{210}Pb in the seafloor near Point Año Nuevo may be explained by sediment focusing. Alternately, it is possible that sediments near Año Nuevo have more surface area per mass than the sediments near the Pajaro River. Increased surface area may result in enhanced ^{210}Pb scavenging by suspended sediment particles. At this time, neither sediment focusing nor enhanced ^{210}Pb scavenging can be ruled as mechanisms responsible for the large excess ^{210}Pb near Point Año Nuevo.

4.7 ^{137}Cs and ^{234}Th

Activity profiles of ^{234}Th and ^{137}Cs were used to evaluate the mixed depths and apparent accumulation rates that were ascertained from ^{210}Pb profiles. The depth to which excess ^{234}Th exists in the sediment column is assumed to coincide with the depth of particle mixing on time scales of less than five months. Significant deposition of ^{137}Cs is assumed to have begun in 1954 as a result of extensive atmospheric testing of

atomic weapons. The depth of penetration of ^{137}Cs is therefore expected to coincide with 45 years of sedimentation, plus the apparent mixed depth. In order for measured ^{137}Cs penetration to match measured penetration, the apparent rates of sediment accumulation and depth of mixing depth must both match the actual values. It is also assumed that mixing and sedimentation remained constant through time and that ^{137}Cs did not diffuse past the base of the mixed layer in 1954.

The five cores analyzed for ^{234}Th and ^{137}Cs (1B1, 2B1, 3B2, 7B1, 8B1, and 13B1) are located along the mid-shelf, south of Ascension Canyon (figure 1). The depth of excess ^{234}Th penetration in these cores is 1-2cm shallower than the depth that is predicted from ^{210}Pb profiles. This indicates that, south of Ascension Canyon, mixing on time scales of several years is only slightly deeper than mixing on time scales of several months. The depth of ^{137}Cs penetration in all five cores is within 2 cm of the depth predicted by ^{210}Pb profiles. Thus the depth of surface mixing and sedimentation rates ascertained from ^{210}Pb profiles are consistent with ^{234}Th and ^{137}Cs penetration depths.

5. Conclusions

Radioisotope profiles of ^{210}Pb, ^{234}Th and ^{137}Cs indicate that modern (last 100 years) apparent mass accumulation rates on the shelf of the northern Monterey Bay National Marine Sanctuary range from 0.42 g cm^{-2} y^{-1} to 0.12 g cm^{-2} y^{-1}. The apparent depth of surface mixing decreases from 13 cm, in the northern study area, to less than 5, in the southern study area. It is possible, however unlikely, that this trend in apparent mixing may also be due to a sudden increase in sedimentation to the north. It is observed that cores from less than 65m have uniform ^{210}Pb activity profiles and cores from the outer shelf have low and erratic ^{210}Pb profiles. It is also observed that the

highest sedimentation rates are at mid-shelf (65-100m) These observations may be explained by active processes such as resuspension by surface waves and internal waves that result in deposition of fine sediment at the mid shelf. Sedimentation rates are also high near rivers in the southern study area and in an area just north of the Ascension Canyon head. High integrated excess ^{210}Pb activities near Ascension Canyon indicate that high sedimentation rates in that area result from deposition of fine sediment that has been transported from a broad area. Low integrated excess ^{210}Pb activities near rivers indicate that the water column residence time is low for sediment particles deposited near rivers.

References

Best, T.C., and Griggs, G.B., 1991. A sediment budget for the Santa Cruz littoral call, California, From shoreline to Abyss. SEPM Special Pub. No. 46, 35-50.

Breaker, L.C., and Broenkow, W.W., 1994. The circulation of Monterey Bay and Related Processes. Oceanography and Marine Biology: an Annual Review, 32, 1-64.

Boudreau, B.P., 1994. Is burial velocity a master parameter for bioturbation? Geochimica et Cosmochimica Acta. Vol 58, No. 4 143-1249.

Cacchione, D.A., and Southard, J. B, 1974. Incipient sediment movement by shoaling internal gravity waves. Journal of Geophysical Research. 79 (15), 2237-2242

Chin, J.L., Clifton, E. H., Mullins, H.T., 1987. Seismic stratigraphy and late Quaternary shelf history, south-central Monterey Bay, California. Marine Geology. 81, 137-157.

Comans, R. N. J., Haller, M., De Preter, P., 1991. Sorption of cesium on illite: Non-equilibrium behavior and reversibility. Geochimica et Acta. Vol. 55, pp. 433-440.

Curtis, W.F., Culbertson, J, K., and Case, E.B., 1973. Fuluvial sediment discharge to the oceans form the contemporaneous U.S. Geol. Surv. Cir. 670, 17.

Edwards, B.D. 2000. Variation in sediment texture on the northern Monterey Bay National Marine Sanctuary continental shelf. Marine Geology. 181, 83-100.

Edwards, B. D., Gardner, J.V., and Medrano, M.D., 1997. Grain size, organic carbon, and CaCO3 of surface sediments from the southern Monterey Bay continental shelf seafloor. In: S. I. Eittriem, Ed. Southern Monterey Bay continental shelf investigations: former Fort Ord restricted zone. U.S. Geological Survey Open File Report 97-450, 22-75.

Eittriem, S., Anima, R.J., and Stevenson, A.J. 2002. Seafloor geology of the Monterey Bay area continental shelf. Marine Geology. 181, 3-34.

Flynn, W.W., 1968. The Determination of low levels of Polonium-210 in environmental Materials. Analytica Chemica Acta, v. 43, 221-227.

Fuller, C.C, 1982. The use of Pb-210, Th-234, and Cs-137 as tracers of sedimentary in San Pablo Bay, California. University of Southern California thesis USCSG TD-01-82. 251p.

Greene, H. G., 1977. Geology of the Monterey Bay region". Open-file report U.S. Geological Survey, OF-77-718. 347.

Greene, H. G., Hicks, K.R.,1990. Ascencion-Monterey canyon system: history and development. In: Garrison, R.E., Greene, H.G., Hicks, K.R., Weber, G.E., Wright, T.L.(Eds.), Geology and tectonics of the central California coastal region, San Francisco to Monterey. American Association of Petrolium Geologists, Pacific Section, Volume and Guidebook, GB 67, 229-250.

Griggs, G.B., and Hein, J.R., 1980. "Sources, dispersal, and clay mineral composition of fine-grained sediment off Central and Northern California". Journal of Geology, 88, 541-566.

Hughes, W.L., 1988. Recent Sediment Accumulation Rates on the Monterey Fan. M.S Thesis. Moss Landing Marine Labs.

Janda, R. S., Nolan, K.M., 1979. Stream and sediment discharge in Northwestern California. In: Guidebook for a fieldtrip to observe on natural and management-related erosion in San Franciscan terrane of Northern California, Cordilleran Section. San Jose, Geol. Soc. Amer. P. IV-1-IV-27

Mullins, H.T., Nagel, D.K., Dominguez, L.L., 1985. Tectonic and eustatic controlls of late Quaternary shelf sedimentation alonf the central California (Santa Cruz) continental marin: high-resolution seismic stratigraphic evidence. Sedimentary Geology. 44, 327-347.

Nittrouer, C.A., 1978, The Process of Detrital Sediment Accumulation in a Continental Shelf Environment: an Examination of the Washington Shelf. University of Washington thesis.

Normark, W.R, 1970. Channel piracy on the Monterey deep-sea fan. Deep Sea Research, 17 837-846.

Overton, S.W., White, D., and Stevens, D.L., 1990. Design Report for EMAP Environmental Monitoring and Assessment Program. U. S. Environmental Protection Agency report 600/3-91/053.

Peng, T.H., Broeker, W.S., and Berger, W.H., 1979. Rates of benthic miging in deep sea sediments as determined by radioactive tracers. Quaternary Research, v.11, p.141-149.

Wagner, D.L., Greene, H.G., Saucedo, G.J., Pridmore, C.L., 2000. Geologic map of the Monterey Bay Region, California: A plot from a digital database. California Depart. Of Mines and Geology, 3 sheets, scale 1:200,000

Xu, J. P., Noble, M., Eittreim, S.L. 2002. Suspended sediment transport on the continental shelf near Davenort, California. Marine Geology. 181, 171-194

Diatom Abundance in a 150-cm-long Sediment Core

from Monterey Bay, California

Abstract

A 150-cm-long sediment core from the continental shelf of central Monterey Bay was studied for evidence of changes in primary productivity and sedimentation rate. Excess ^{210}Pb activity in the 40-80cm depth interval of the core indicates that sedimentation has occurred at a rate of 0.76cm/y. Low excess ^{210}Pb in the upper 25cm may be attributed to a recent pulse of high sedimentation. Pheophytin-a, a degradation product of chlorophyll-a, was measured as a proxy of primary production. The diatom assemblage was dominated by the genus *Chaetoceros*, which is linked to late summer upwelling. *Thalassionema nitzschiodes*, which is linked to early spring upwelling, was also common in this core. The genus *Pseudonitzschia*, which is linked to toxic bloom events, was present in small amounts throughout the core. Diatom abundance in this core varies by an order of magnitude.

1 Introduction

1.1 Scope

The purpose of this study is to document changes in the abundance and taxonomic composition of diatoms in a 150cm-long sediment core from Monterey Bay. Diatoms and chlorophyll-related pigments in this core record approximately 200 years of primary productivity with an age resolution of about 2 decades. Abundant diatoms such as *Chaetoceros* and *Thalassionema nitzschiodes* record fluctuations in upwelling-related oceanic conditions such as water temperature and nutrient concentration. The genus, *Pseudo-nitzschia*, though rare in this core, is of special interest because it is linked to the production of domoic acid, a neurotoxin that is responsible for amnesic shellfish poisoning in higher vertebrates. Decade-scale variations in primary productivity have been observed (Pennington and Chavez, 2000), but century-scale variations in Monterey Bay are not well constrained. This study attempts to estimate changes in diatom productivity on a two-century time scale so that the relative importance of modern variations may be better understood.

In order to interpret diatom abundance in this historical context it is necessary to have a depositional chronology for this core. A profile of the naturally-occurring radioisotope ^{210}Pb provides a 100-year average of the rate of sedimentation in this core. Human-introduced tracers such as residues of the pesticide DDT and the radioisotope ^{137}Cs may be used to independently verify the ^{210}Pb-based sedimentation rate. Sediment was examined for changes in texture and color that may be linked to pulses of rapid sedimentation or increased physical reworking. Organic carbon was measured

quantitatively in order to detect changes in the rate of burial of organic matter. Pulses of rapid sedimentation and changes in the deposition of organic material affect diatom abundance. Phaeophytin-a, a diagenetic product of chlorophyll-a, was measured as a proxy of export production that would likely vary with diatom abundance.

1.2 Setting

Monterey Bay is a semi-enclosed embayment located approximately 200 km south of San Francisco Bay (Figure 1). Hydrographic conditions in Monterey Bay commonly consist of an upwelling period from approximately February to September, an oceanic period from September to October, and surfacing of the Davidson Current from November to February (Smethie, 1973). Coastal upwelling develops in response to persistent northwest winds that predominate in the spring and early summer months. High standing stocks of chlorophyll-a, primarily marine plankton diatoms, commonly correspond to upwelling periods (Malone 1971; Garrison, 1979; Bolin and Abbott 1963). The length of the upwelling season varies and may be affected by large-scale hydrographic events along the California coast such as El Nino Southern Oscillation (ENSO). The 1983 ENSO event was associated with decreased upwelling and oceanic conditions (Simpson, 1984) that resulted in relatively low chlorophyll-a standing stocks.

The Monterey Submarine Canyon intercepts southerly littoral sediment transport (Best and Griggs, 1991). Mean surface flow in Monterey Bay is generally cyclonic at about 10 cm/sec, resulting in northward dispersal of fine sediments (Breaker and Broenkow, 1994). The three major sources of terrigenous sediment are the San Lorenzo,

Pajaro and the Salinas rivers, which have annual sediment loads of 0.14, 0.22 and 1.4 million metric tons, respectively (Janda and Nolan, 1979).

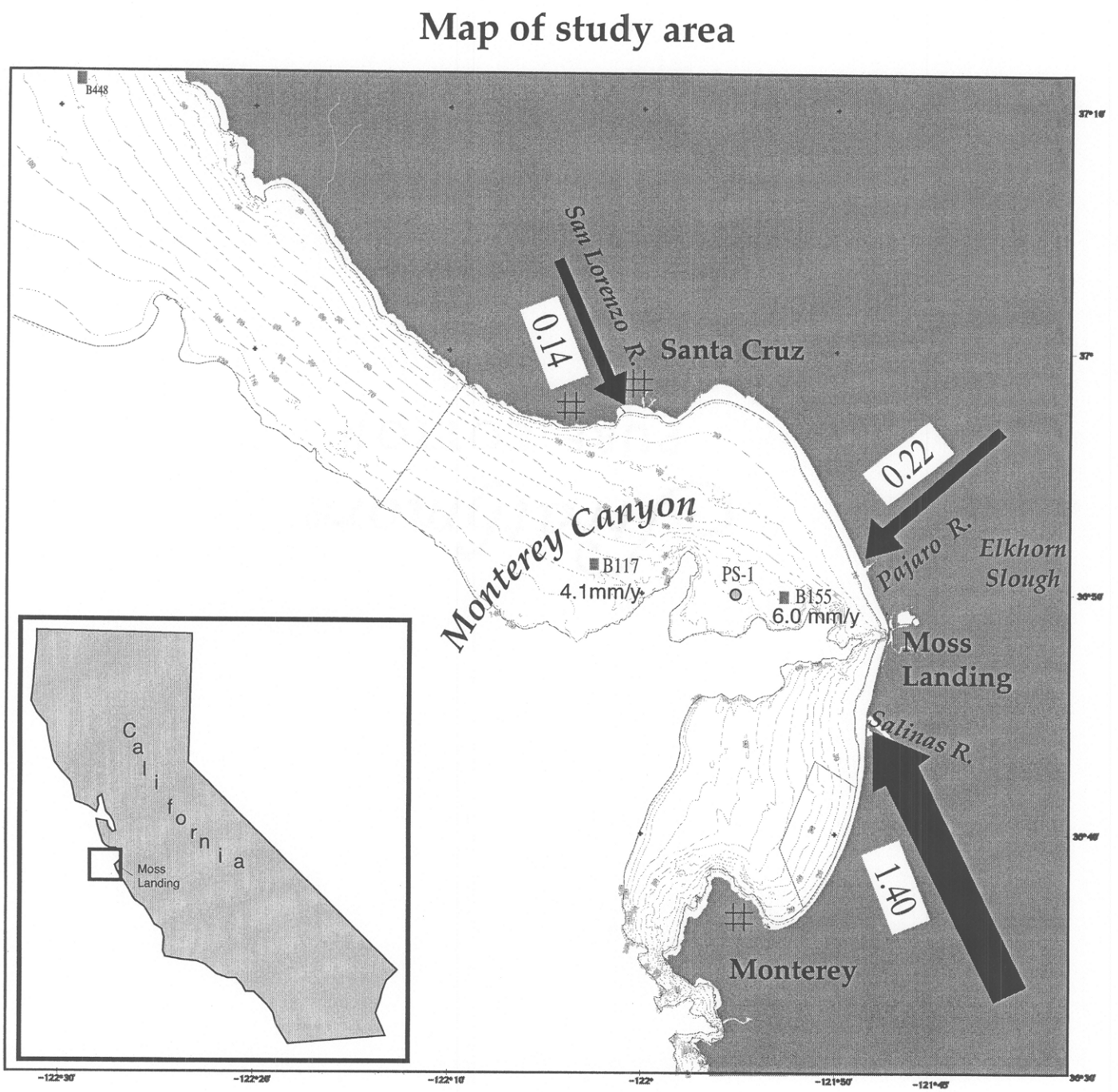

Figure 1. Map of Monterey Bay, located on the California coast. Core PS-1 is located in a broad area of the shelf, near the center of the bay. Sedimentation rates of 4.1 mm/y and 6.0 mm/y were determined for cores B117 and B155 by Pb-210 dating techniques. Major sediment sources are the San Lorenzo, the Pajaro, and the Salinas Rivers which contribute 0.14, 0.22, and 1.40 million metric tons of sediment annually.

Though the Salinas River is by far the largest source of sediment to Monterey Bay, the relative sediment input to the shelf from this river is poorly constrained for several reasons. Prior to armoring of the Moss Landing Harbor in the 1940s, the location of the Salinas river mouth migrated north and south of Moss Landing. Because the head of Monterey Canyon divides the shelf directly at Moss Landing, the shifting location of the Salinas River mouth influenced which part of the shelf received sediment from the Salinas River. When the Salinas River emptied north of Moss Landing, sediment would have been deposited on the northern shelf of Monterey Bay. Alternately, when the Salinas river emptied south of Moss Landing, sediment was deposited on the southern shelf of Monterey Bay. During normal flows, the Salinas River discharges several kilometers south of Moss Landing Harbor. However, at peak discharge, the Salinas River discharges at Moss Landing Harbor in addition to its usual river mouth. Instrumental records indicate that discharge from the Salinas River during extreme floods may occur as high-density flows (Johnson et. Al, 2001) that enter Monterey Canyon. These high-density flows may result in little or no net deposition on the shelf. Thus, sediment input from the Salinas River to the shelf of Monterey Bay is dependent not only on the location of the river mouth but also on the magnitude of discharge. Moreover, the extreme floods that carry the largest pulses of sediment down the Salinas River may result in only minor deposition on the shelf.

The diatoms discussed in this study are from PS-1, a 150cm-long core that was collected on the northern shelf on Monterey Bay. This site was chosen on the basis of previous work (Lewis et. al, 2002), which showed that sedimentation rates to the north

and west of this area are relatively high (0.25-0.39 mm/y) and that the depth of surface mixing was shallow (2-4 cm). The combination of rapid accumulation and shallow mixing that was thought to occur here would result in rapid burial of diatoms. Rapid burial increases the temporal resolution of the sedimentary record and reduces the corrosive effect of seawater on diatoms.

Sediment mixing diffuses pulses of diatom deposition. Consequently, sediment cores commonly record diatom deposition and preservation averaged over several years. A combination of shallow mixing and rapid sedimentation results in a high-resolution sedimentary record. A combination of deep mixing and slow accumulation, on the other hand, results in a low resolution sedimentary record. If the rate of sedimentation and depth of surface mixing at PS-1 were comparable to sites that were cored to the north and west, then core PS-1 should contain a 500 to 750-year-long record with a temporal resolution of 7 to 20 years. ^{210}Pb was measured in PS-1 after most other work was completed. The shape of this ^{210}Pb profile indicates that the sedimentation rate in this core is twice a high as expected and that surface mixing most likely occurs to 15 cm. Thus, this core contains a sedimentary record that spans approximately 170 years with an age resolution of 20 years.

The diatoms preserved in the sediment column are not necessarily representative of the diatoms found in the overlying water column because some diatoms are especially prone to breakage and dissolution. Preservation tends to favor diatom taxa that have strong valves and are especially numerous. Two such taxa, *Chaetoceros spp.* and *Thalassionema nitzschiodies*, are common in Monterey Bay and have previously

been used to document changes in Holocene productivity of the Northern California Current System (Sanchetta et. al, 1992). Sanchetta et al (1992) reported that *Chaetoceros* spores were found in nearshore sediment traps with greatest relative abundance during spring and fall (July and November). This is a flora that is a characteristic component of late-stage upwelling in coastal regions. *Thalassionema nitzschiodies* is most abundant in early spring (March-April) and is a reliable indicator of early spring production. Though not all diatom taxa are preserved in the sediment column, *T. nitzschiodies* and *Chaetoceros,* are shown to be reliable indicators of coastal upwelling. Furthermore, these are robust taxa that are readily preserved in shelf sediments of Monterey Bay.

The occurrence of the toxic diatom genus *Psuedo-nitzschia* is of special interest because it is linked to the production of domoic acid (Fryxell et. al, 1990; Miller and Scholin, 1996). Though not all the diatoms in this genus produce domoic acid, toxic blooms of *Psuedo-nitzschia* have been associated with the death of seabirds and other fauna in Monterey Bay. *Psuedo-nitzschia* has been present in Monterey Bay at least as far back as 1930 (Bigelow & Leslie, 1930). Prior to that, little is known about the significance of *Psuedo-nitzschia* in Monterey Bay. This 170-year sedimentary chronology indicates that of *Psuedo-nitzschia* has existed in Monterey Bay long before 1930. *Psuedonitzschia,* however, is a relatively delicate diatom that is prone to breakage and dissolution. Moreover, it is difficult to distinguish between certain species of *Psuedonitzschia,* with a light microscope. Thus, taxonomic identification by light microscope was verified with the aid of an electron microscope.

2. **Methods**

2.1 Sampling

Sediment core PS-1 was collected aboard the RV Point Sur in September of 1999 with a 2-m-long gravity core that was lined with a 10-cm-wide polycarbonate tube. The sampling site is located in 83 m water depth, 10 km west of Moss Landing, on the north side of the Monterey Canyon (36 49.27N, 121 56.47W). The core was refrigerated within 3 hours of collection and stored upright until it was split and sampled. A plastic spatula was used to sample the core and careful attention was paid to prevent cross-contamination. Sediment samples were sealed in plastic bags that were immediately placed in an opaque box and kept away from sunlight until the time of processing. Four samples were sealed in acid-cleaned screw-capped plastic centrifuge tubes that were frozen and kept away from sunlight until later analyzed for pesticide residues. These four samples were analyzed among a much broader survey of DDT in Monterey Bay that is described by Paull et al, 2002.

2.2 Radioisotope analysis

Activities of ^{210}Pb and ^{137}Cs were measured by gamma spectrometry in 12 samples from core PS-1. Thirty-gram samples of dried sediment were ground to a fine powder and sealed in plastic counting jars. Each jar was counted for a minimum of 24 hours on a Canberra high-purity planar germanium detector with an active area of 2000 mm^2 and a thin composite window. Spectrum collection and analysis was performed by using a

PC-controlled Canberra multichannel analyzer and Genii® 2000 software. ^{210}Pb, ^{214}Pb, and ^{137}Cs activities were calculated by integrating the area of the 46.5, 352, and 661.6 keV photopeaks, respectively. Energy and efficiency calibrations were performed using an 11-line NIST traceable multigamma standard. Self-adsorption of gamma rays by the sample matrix was corrected for by a height-based calibration that was based on sediments from the Northern California margin. Supported ^{210}Pb activity was calculated by subtracting the mean ^{214}Pb activity in the core from total ^{210}Pb activity. Radioisotope activities were calculated for the date of sample collection to correct for decay between the time of sampling and counting. Error values were based on statistical counting errors at one standard deviation.

2.3 Textural analysis

Sediment texture was analyzed at 10-cm intervals in core PS-1 to test for particle size variations that might be linked to a change in sedimentation rate. Quantitative analysis of sediment grain size followed a standardized procedure in which known weights of sediment were oxidized in 30% hydrogen peroxide. Samples were treated with hydrogen peroxide until all organic material was oxidized and then washed with de-ionized water through a 63-micron sieve to separate sand from silt and clay. Sand fractions were dried and weighed. Silt and clay fractions were washed into1000mL-graduated cylinders that were then filled with water to 1000mL. After each cylinder was mixed, a 20mL aliquot was withdrawn and dried. The mass of fine

sediment in each sample was determined by multiplying the mass of the dried aliquot by 50. The mass percent of fine material was calculated by the following:

[F/(F+C)]x100
where F is the mass of silt and clay (<63um)
and C is the mass of sand (>63um)

2.4 Organic carbon

Organic carbon was measured in a two-step process that uses two dried and powered aliquots of each sample. The first step measures total carbon by combusting 0.03-0.07 mg of dried sediment in pure oxygen at 1000C°. Carbon dioxide from this combustion is sent to a Coultronics® coulometer that determines the total amount of carbon from the sample. The second step of the analysis measures inorganic carbon by treating a 0.5-1.0 mg sample with perchloric acid. Carbon dioxide from this reaction is sent to the coulometer that measures the inorganic carbon in the sample. Total carbon and inorganic carbon values are normalized by the weights of their respective aliquots and inorganic carbon is subtracted from total carbon to determine the organic carbon content of the sediment.

2.5 Photospectrometric chlorophyll assay

Phaeophorbide-a, a diagenetic product of chlorophyll-a, was measured as a proxy for export production. Pheophorbide-a was extracted from a known volume of wet sediment with 5mL of 90% acetone. The adsorption of solution was measured on a

spectrophotometer at 666nm and background adsorbance was measured a 750nm. The concentration of the solution was determined by the following:

$C = (Ap-Ab)/K$
Where C is the concentration of pheophorbide-a, Ap is the adsorbance at 666nm, Ab is the adsorbance at 750nm, and K is the coefficient of adsorbance

The solution concentration was divided by 200,000 and again by the sediment volume to determine the ug of pheophorbide-a per cc of wet sediment.

2.6 Diatom Abundance

Diatom abundance was measured quantitatively with a method that allows for direct comparison of changes in species composition from sample to sample (Battarbee, 1973). An Olympus HB microscope with phase-contrasts optics was used to scan one 30mm-long transect along a microscope slide at 630x. The microscope slides were made by settling a known mass of sediment through a water column onto a cover glass. Diatoms on these slides are distributed randomly over the cover glass, so that the orientation of transects does not skew the diatom count. The common practice of preparing strewn slides by transferring an aliquot of sediment directly onto a glass cover slip is known to distribute diatoms non-randomly (Battarbee, 1973). As a result, absolute numbers of diatoms cannot be determined unless the entire sample is scanned. In the case of this study, it was not necessary to scan the entire slide because diatoms were randomly distributed. Full-length transects were scanned for diatoms and diatom fragments until a count of 300 was achieved.

The microscope slides used in this study were prepared by a method that first involves chemical pretreatment of the sediment, followed by a sediment dispersal procedure, and finally mounting of the cover glass. Approximately 2 cc of sediment was treated with 10 mL 30% Hydrogen Peroxide at 70C° for 45 minutes and then allowed to cool. The sample was then treated with 5 mL of 30% hydrochloric acid at 70C° for 45 minutes. The acid was removed from the sediment by repeatedly centrifuging at 800 RPM for 10 minutes and rinsing with deionized water until the sample pH was neutral. The sample was then mixed with ten parts water to one part centrifuged sediment. While the sample was stirred, two 40uL aliquots were drawn. One aliquot was dried and weighed to determine the amount of material that was used to make the microscope slide, while the replicate aliquot was used to make the slide.

The replicate aliquot was dispersed into a 250mL beaker that was half filled with deionized water and additional deionized water was then sprayed into the beaker to mix the sample evenly. The dispersed sediment settled onto two 20x30mm cover glasses that were mounted with rubber cement to a 5-cm-wide glass disk that was placed at the bottom of the beaker before the sediment was added. A thin layer of unflavored gelatin on one of the two cover glasses prevented the clumping of sediment that occurs as a result of static attraction between clay particles. The other cover glass was kept free of gelatin to assure that one slide does not discolor with age. After the beaker stood covered for 24 hours, most of the water was slowly drawn out with a capillary tube that was attached by a hose that is connected to a vacuum bottle. The water was drawn to within 5mm of the surface of the cover glass and the beaker was not

moved so that the sediment remained evenly dispersed on the cover glass. The remaining water evaporated . The glass disk that holds the cover glasses was then removed from the beaker with tongs. The cover glasses were then mounted to glass microscope slides with a mounting medium with a high refractive index (1.74), such as Naphrax or Hyrax.

The mass of the material mounted to the cover glass is equal to the mass of the dried replicate aliquot multiplied by the fraction of the beaker cross-sectional area that is taken up by the cover glass. In this case, each cover glass comprised a 0.218 fraction of the bottom of the beaker. A typical aliquot dispersed 13.8 mg of sediment into the beaker. Thus, a typical cover glass is holds 3.01mg of dry sediment. Each 30mm-long scan examined a 0.114 fraction of the cover glass. The total number of diatoms on the slide was calculated by normalizing the counted number of diatoms to the area of the slide that was scanned. Diatom abundance was calculated by normalizing the the total number of diatoms on the slide to the mass of sediment on the slide. Diatom abundance was expressed as valves per mg of dry sediment.

Diatoms were identified to species level, when possible. Broken diatoms that were missing more than half the valve were counted as fragments. All species, except *Thalassionema Nitzschiodies,* (figure 2) were later grouped to genus level. Resting spores of *Chaetoceros sp.* were grouped together with vegetative cells because vegetative cells were rare. The genus *Psuedo-nitzschia* was treated as a group because light microscopy did not resolve subtle differences between certain species of this genus. Samples at 18 cm and 123cm were examined with an electron microscope to

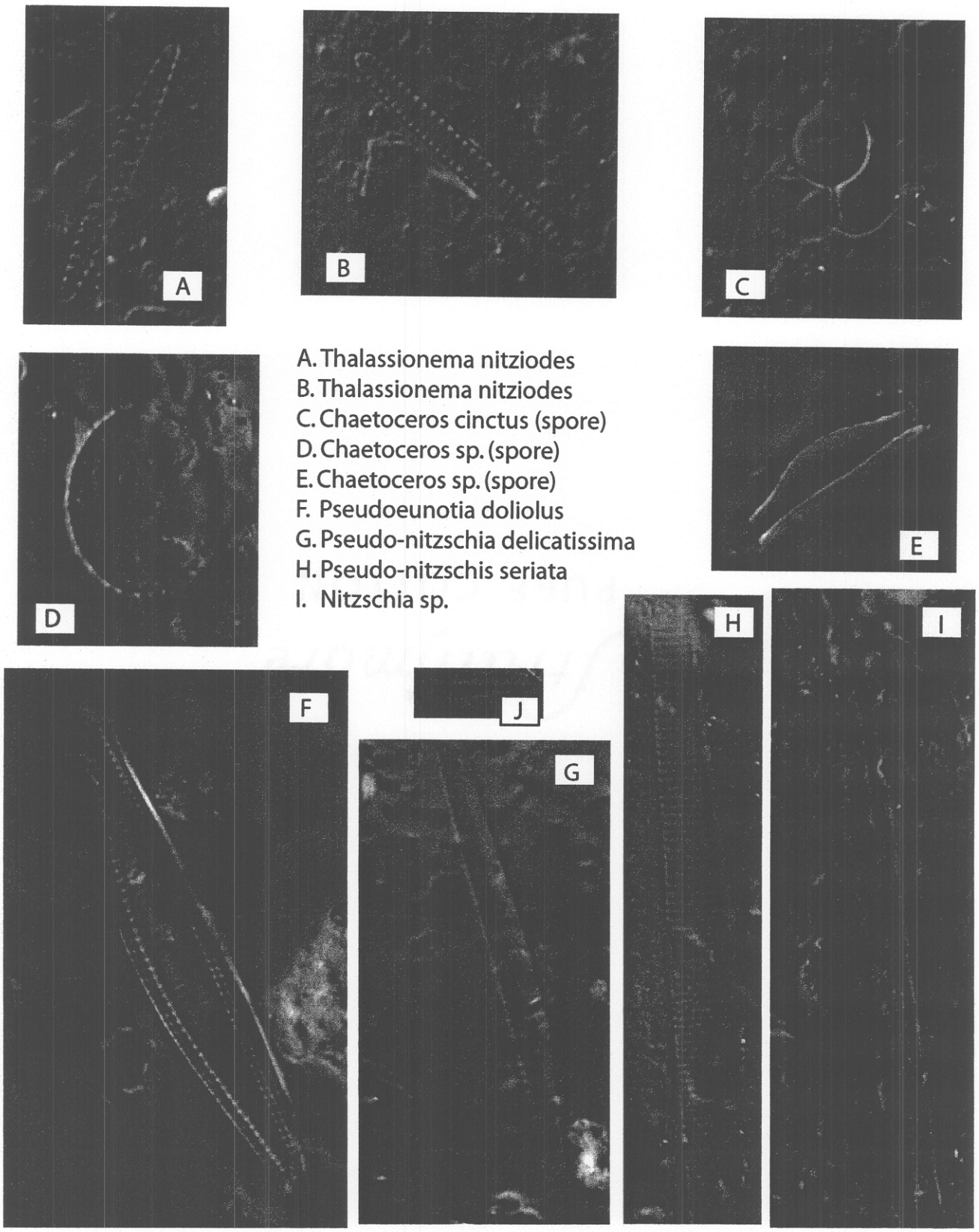

Figure 2. Photomicrographs of significant diatoms in core PS-1. Thalassionema nitzschiodes (A,B) and the genus Chaetoceros (C,D,E) comprised the bulk of the diatom assembalge. Pseudoeunotia doliolus (F) and the genus Pseudonitzschia (G,H,I) were rare, but present throughout the core. The black line in the gray box at the center of the figure (J) is 10 micrometers long. All the photos are to the same scale.

verify the presence of *P.pungens* (figure 3) in both samples. It is possible, however unlikely, that the non-toxic diatom *Psuedoeunotia doliolus* was occasionally mistaken for *P.pungens* in other samples that were studied only by light microscope. *Psuedoeunotia doliolus* is similar in valve view, but it is rounder ends and greater relief than the toxic diatom *P. pungens.*

3 Results

3.1 Sediment texture

The texture and color of sediment in core PS-1 show subtle variations with depth. Overall, the sediment in this core was olive green fine sandy clay with light olive green medium sandy clay horizons (figure 4.a). The strongest color change is at a diffuse 5cm-thick silty-clay layer at 111 cm. Changes in apparent sediment texture did not coincide with changes in quantitatively measured sediment texture (figure 4.b). Sediment texture ranges 78-98% mud with minor amounts of sand and no detectable shell fragments. Bands of fine sediment may correspond to flood-borne pluses of deposition. If this is true, then the horizons of very fine in this core may be interpreted as flood layers. However, the lack of correspondence between color and sediment texture complicates the interpretation of fine horizons as flood layers.

3.2 ^{210}Pb, ^{137}Cs, and DDT

The radioisotope ^{210}Pb is useful for dating sediments that were deposited within the last 100 years. Excess ^{210}Pb is atmospherically deposited in surface waters where it

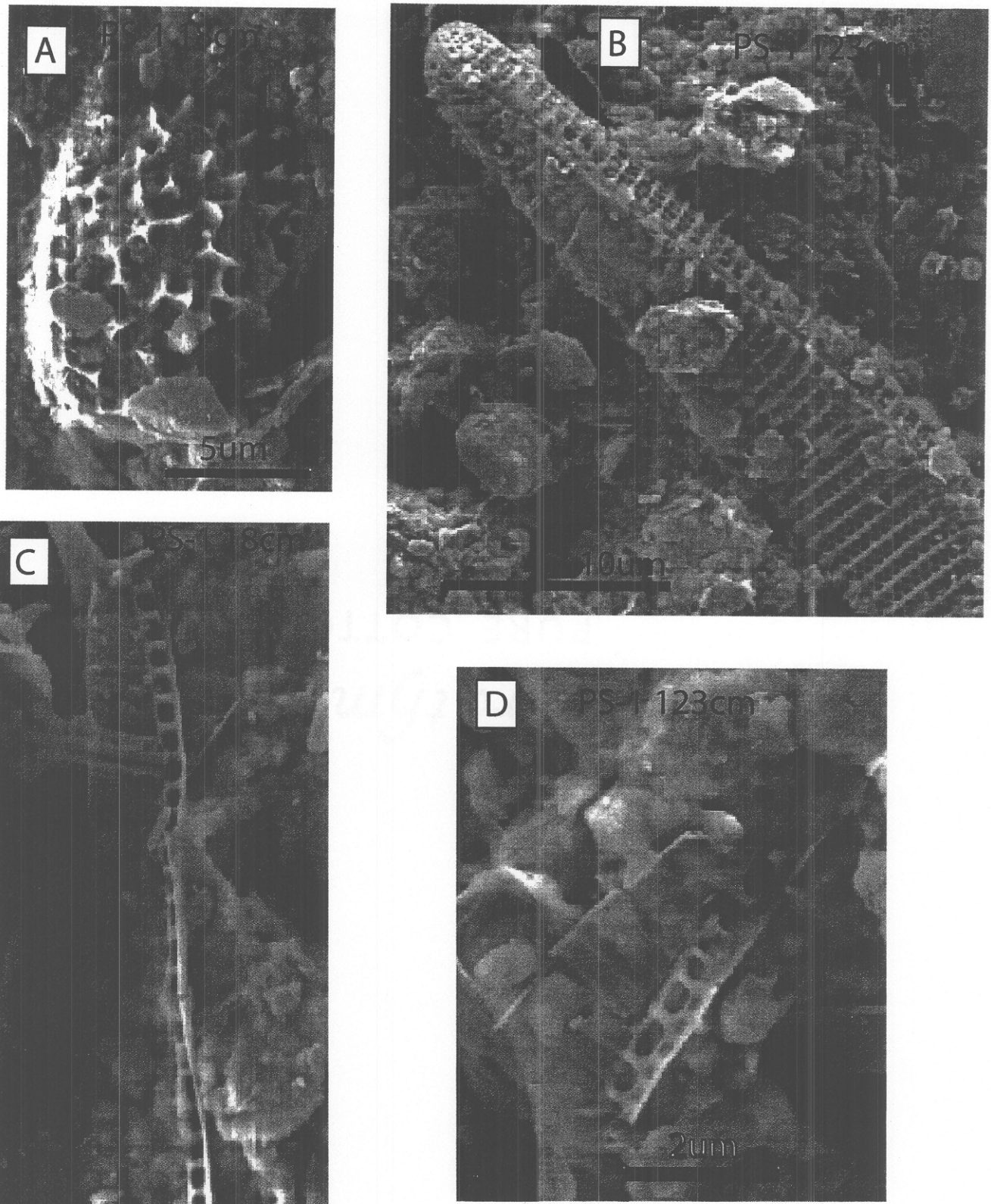

Figure 3. Scanning elecron micrographs of diatoms from core PS-1. Chaetoceros sp. spores (A) were common in the core. Differences between Pseudoeunotia doliolus (B) and Pseudonitzschia pungens (C,D) were recognizable when studied by electron microscope.

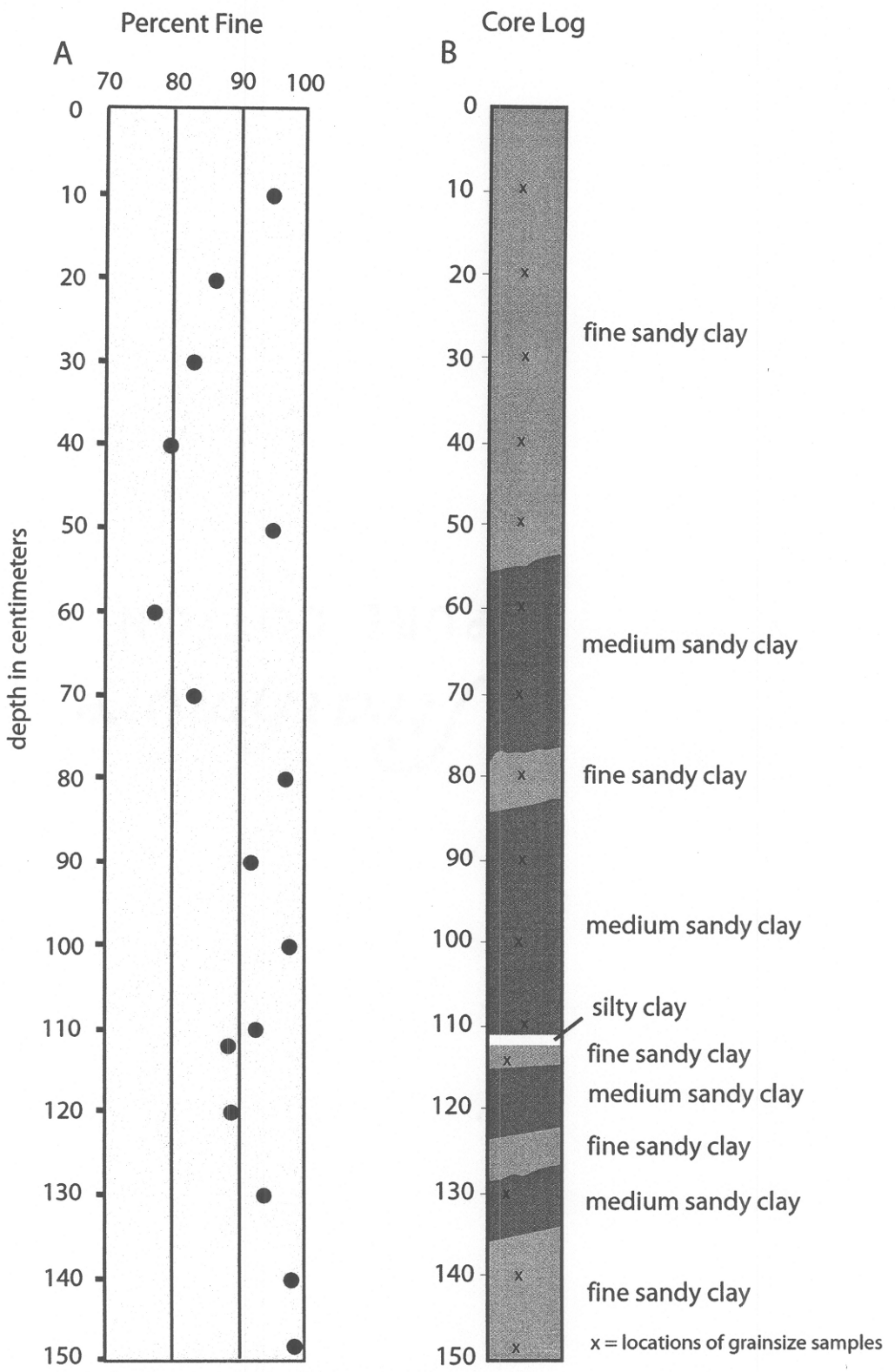

Figure 4. Descriptive log of core PS-1. A vertical profile of sediment texture (A) shows the weight percent of particles less then 63 microns in diameter. A qualitiative log of sediment color and apparent texture (B) shows that only minor variations in sediment texture and color were discernable by hand. The sediment in the core is nearly homogenous.

is scavenged into sediment particles. Profiles ^{210}Pb measured in sediment cores from the mid continental shelf commonly exhibit a layer of constant and high activity in the upper few centimeters that is generally construed to result from surface mixing of newly deposited sediment. Below this layer of surface mixing, ^{210}Pb activity decreases exponentially downward to background activities that are supported by the decay of uranium-238 series radioisotopes that are present in the mineral grains of the sediment. A sedimentation rate may be ascertained from the part of a ^{210}Pb profile that decreases exponentially below the zone of surface mixing (Lewis et al 2002).

Unlike ^{210}Pb, the radionuclide ^{137}Cs and the pesticide DDT are not naturally occurring. ^{137}Cs and DDT were both introduced to the marine environment in the middle 20^{th} century as a result of human activities. The timing of their first introduction is well constrained and their persistence in the environment is long lived. Consequently, ^{137}Cs and DDT may be used to bracket sedimentation rates on time scales of less than 60 years. The first significant deposition of ^{137}Cs occurred in 1954 as a result of atmospheric testing of atomic weapons. Thus, sediments with measurable amounts of ^{137}Cs were either deposited after 1954 or have been mixed with sediments that were deposited after 1954. DDT was first used agriculturally in the Salinas and Pajaro Valleys in 1945 (Paull et al 2002). DDT and the chemical breakdown products of DDT are collectively referred to as DDTr. These compounds are persistent in the environment and the timing of their introduction to the Monterey Bay region is well constrained. Consequently, DDTr is an excellent tracer of post-1945 input from the Salinas and Pajaro Rivers. The depth of penetration of ^{137}Cs and DDT independently

test the sedimentation rate that was estimated from the profile of ^{210}Pb that was measured in core PS-1.

^{210}Pb activities in core PS-1 are unusual and possibly problematic. ^{210}Pb activity in this core increases downward in the upper 25cm (figure 5). Below 25cm, ^{210}Pb activity is constant to 40cm. The zone of exponentially decreasing ^{210}Pb activity occurs between 40 and 70cm. ^{210}Pb profiles from most of the sites from an earlier survey of the Monterey Bay shelf showed that surface mixing occurs to less than 5cm (Lewis et al, 2002). If the upper 25cm of core PS-1 were missing, then the profile of ^{210}Pb activity in this core would be like many ^{210}Pb profiles measured from shelf sediments elsewhere in Monterey Bay. It is likely that the low ^{210}Pb activities in the upper 25cm of core PS-1 reflect a recent and unique surge of rapid deposition.

If it may be assumed that the upper 25cm of this core was deposited recently in a short period of time, then a sedimentation rate can be calculated from the 25 to 70cm section the ^{210}Pb profile. Based on this assumption, the horizon of surface mixing occurs between 25 and 40cm and the horizon of exponential decay occurs between 40 and 70cm. Consequently, the surface mixed layer is 15cm thick and the horizon between 40 and 70cm may be used for age dating. When the natural log of excess ^{210}Pb of the 40 to 70cm horizon is plotted against depth, the slope of the resulting line indicates that the sedimentation rate is 0.76 cm/y.

Taken independently, this ^{210}Pb-based sedimentation rate is somewhat speculative. However, penetration depths of ^{137}Cs and DDT in core PS-1 are consistent with this sedimentation rate. ^{137}Cs was measured from 4 to 131cm, but only detected in

depth interval (cm)	mean depth (cm)	depth error (cm)	excess Pb 210 (dpm/g)	excess Pb-210 error (dpm/g)	Cs-137 (dpm/g)	Cs error (dpm/g)	ln (xsPb-210)
4-6	5	1	5.17	0.49	0.48	0.11	
13.5-14.5	14	1	6.91	0.48	0.46	0.09	
24-26	25	1	9.42	0.80	0.48	0.17	
34-36	35	1	9.55	0.38	0.46	0.07	
39-41	40	1	**9.81**	0.57	0.18	0.11	**2.28**
43-45	44	1	**7.90**	0.38	0.48	0.07	**2.07**
64-66	65	1	**3.26**	0.36	0.59	0.09	**1.18**
69-71	70	1	**2.93**	0.60	0.10	0.14	**1.07**
74-76	75	1	0.00	0.62	ND	ND	
87-88	87.5	1	0.00	0.20	ND	ND	
89-91	90	1	0.00	0.44	ND	ND	
129-131	130	1	0.00	0.36	ND	ND	

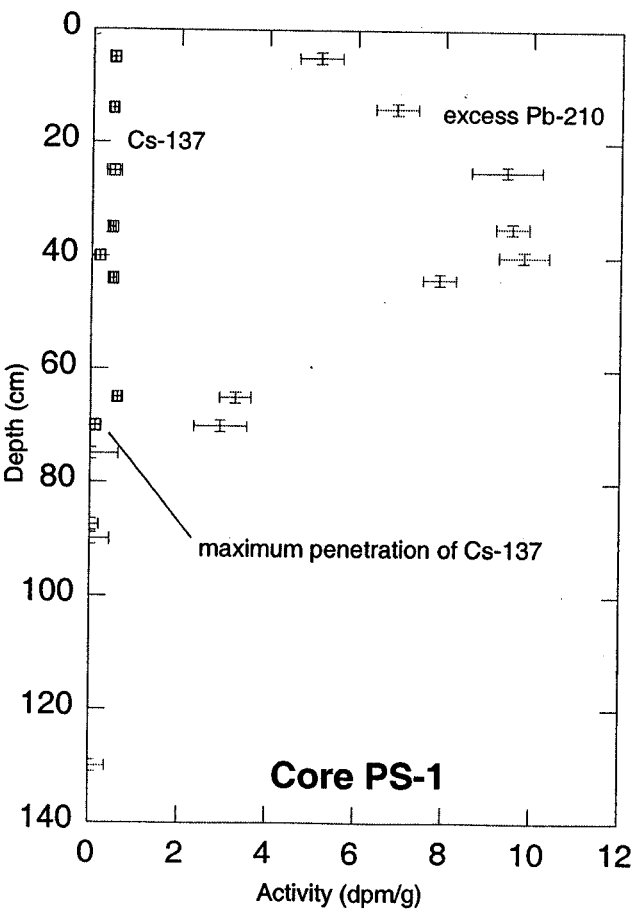

	R^2	0.995
	m	-0.041
	n	4
Pb	SAR	0.76
first Cs	predicted	72
first Cs	measured	71

Figure 5. Activities of excess Pb-210 and Cs-137 are shown from core PS-1. Excess Pb-210 activitiy increases with depth in the upper 25 cm and then decreases to supported levels below 40 cm. A sedimentation rate of 0.76 cm/y is ascertained from Pb-210 activities from the 40-70 cm interval. Cs-137 was detected in the upper 71 cm. The shape of the Pb-210 profile suggests that Cs-137 should be measurable to 72 cm.

the upper 71cm of the core. All four samples measured between 7 and 43cm tested positive for DDT and related degradation products. The maximum penetration of ^{137}Cs and DDT in core PS-1 should be equivalent to the thickness of the surface mixed layer, plus the total amount of deposition that has occurred since the initial introduction of the tracer. In the case of ^{137}Cs, the maximum penetration should be equivalent to 45 years of deposition at 0.76cm/y (34cm), plus the combination of the 15-cm-thick mixed layer and 25-cm-thick top layer of rapidly-deposited sediment (40cm). Thus, the anticipated maximum depth of ^{137}Cs penetration should be 74cm. The anticipated depth of ^{137}Cs penetration matches the measured depth to within the next deepest sample in the core. Following the same rationale as before, the maximum penetration depth of DDT should be 81cm, which equivalent to 54 years of accumulation (41cm) plus 40cm. No samples deeper than 43cm were analyzed for DDT, so the anticipated maximum penetration of DDT can not be tested with the available data. However, DDT penetration independently shows that at least the upper 43 cm of the core has most likely been mixed with sediment that is younger than 1945. Taken together, the depth of penetration of ^{137}Cs and DDT provide maximum and minimum sedimentation rates that are consistent with the ^{210}Pb-based rate.

3.3 Organic compounds

Sedimentary concentrations of organic carbon and phaeophytin-a both decrease with depth in the sediment column (figure 6). Organic carbon decreases steadily with depth from 1.1% to 0.9% and shows only one minor variation between 45 and 70cm.

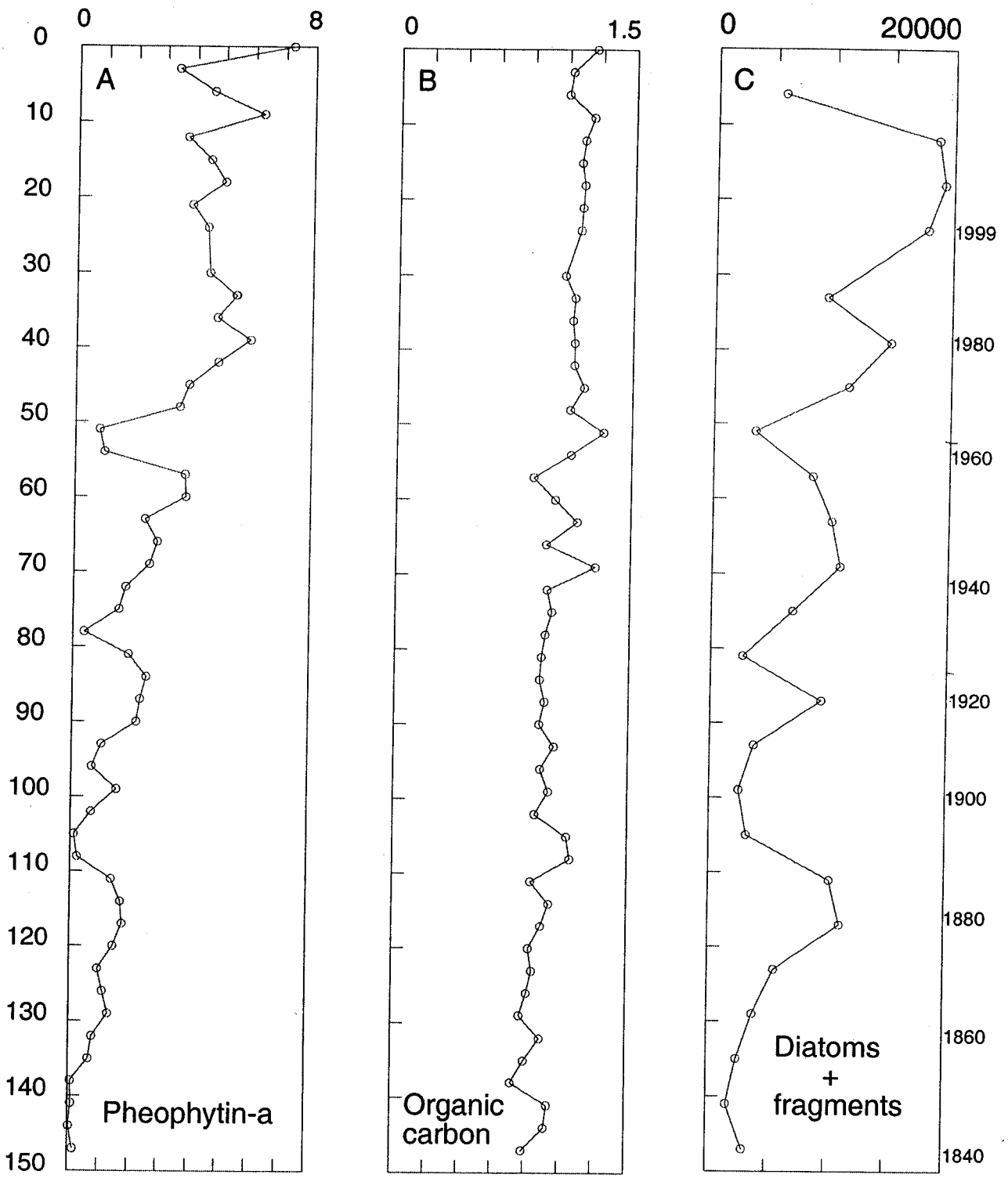

Figure 6. From core PS-1, Pheophytin-a in ug per my dry sediment (A), percent weight organic carbon (B), and abundance of ditoms and fragments per mg of dry sediment. Sedimentary pheophytin-a concentration and diatom abundance vary with depth. Organic carbon does not vary significantly with depth.

The low variation in carbon content suggests that carbon preservation was constant with time. The gradual decrease in carbon with depth may be attributed to diagenetic loss. Pheophytin-a decreases erratically with depth from 7 to 0.2 micrograms pheophytin-a per milligram of dry sediment (ug/mg). Pheophytin-a degrades more rapidly than bulk organic carbon, so the ten-fold decrease in pheophytin-a may possibly be explained by degradation in the sediment column. The erratic variation in this compound, however, is most likely due to variations in export production.

3.4 Diatom abundance

Diatom abundance was measured as valves per mg of dry sediment (v/mg) at 6cm intervals in core PS-1. The abundance of all diatom components (ie. valves and fragments) decreases erratically with depth in the sediment column (figure 6c). The highest abundance of all diatom components occurs between 12 and 24cm. Depth horizons with low (<4000 v/mg) diatom abundance occur at irregular intervals within the core. Diatom fragments and *Chaetoceros sp.* consistently comprise over 75% of the diatom assemblage of this core. *Thalassionema nitzschiodes*, which comprises 0-8% of the assemblage, is the next abundant diatom. *Pseudo-nitzchia sp.* are relatively rare, comprising less than 4% of the assemblage. The rest of the taxa in this core comprise 4-20% of the diatom assemblage, with no group exceeding 4% of the total. Variations in

diatom fragments resemble variations in abundance of *Thalassionema nitzschiodes* and *Chaetoceros sp.*, indicating that loss of these species due to crushing is insignificant (figure 7).

4 Discussion

4.1 Sedimentary chronology

In order to tie changes in diatom abundance to a meaningful time line, a sedimentary chronology for core PS-1 is necessary. The low ^{210}Pb activities in the upper 25cm of this core complicate such a chronology and undermine confidence the accuracy of this time line. If the upper 25cm are indeed the result of a recent pulse of rapid sedimentation, then the modern surface is represented by the upper 25cm of the core. Below 25cm, the ^{210}Pb-based sedimentation rate of 0.76cm/y results in a sedimentary chronology that extends 170 years into the past. If this chronology is accepted, then the upper 25cm represents sediment deposited in the 1990s and the bottom of the core represents sediment deposited in the1830s. If the thickness of the 15-cm-thick surface mixed layer has remained constant with time, then any horizon below 25cm represents envoronmental signals that are averaged over 20 years. Despite uncertainties in the accuracy of the sedimentary chronology for this core, the absence of ^{137}Cs below 71cm is a clear indication that lower sections of the core are composed entirely of sediment older than 45 years. Moreover, the absence of excess ^{210}Pb below 74cm indicates that the lower half of the core represents sediment that older than 100 years.

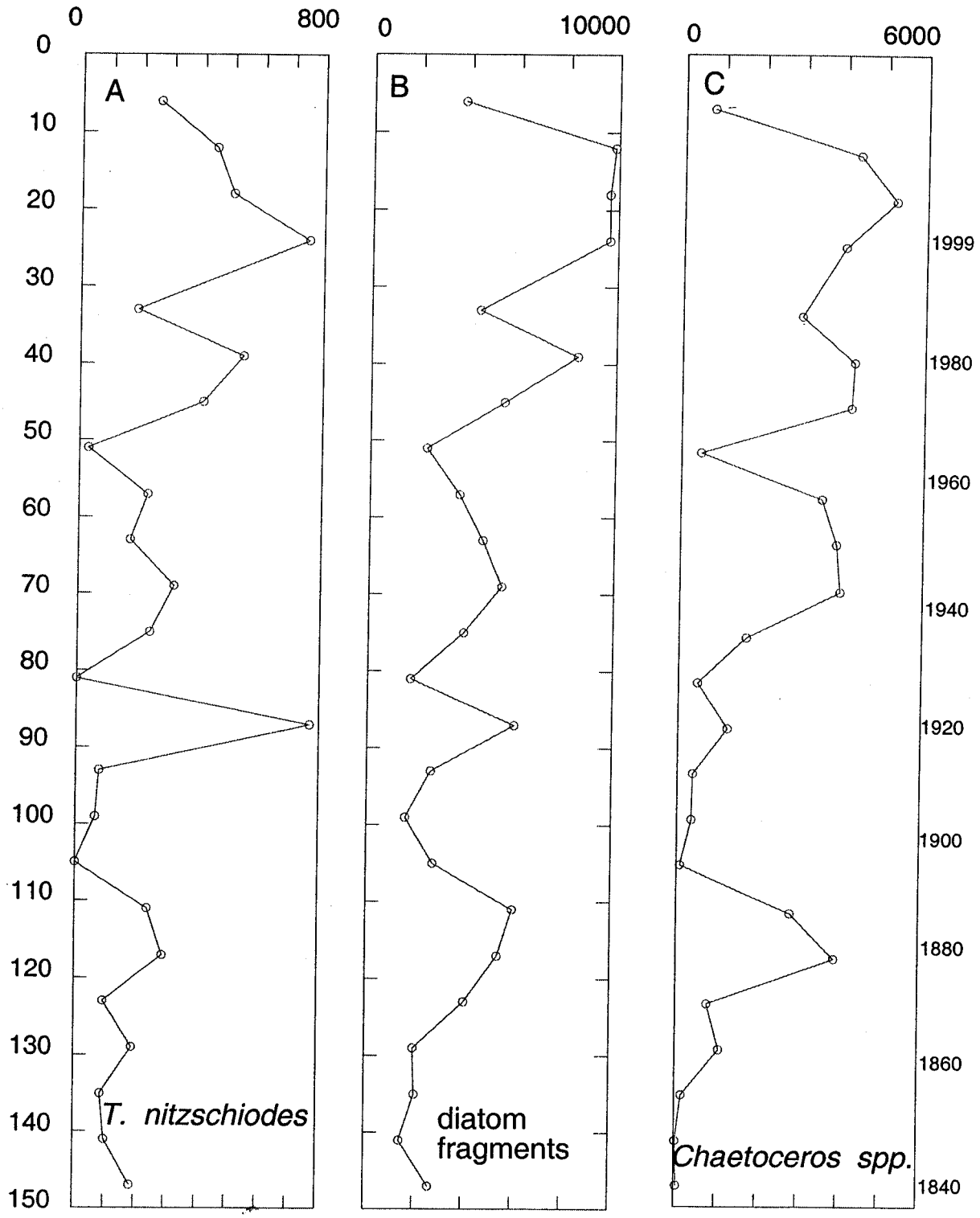

Figure 7. The abundance of *T. nitzschiodes* (A), diatom fragments (B), and the genus *Chaetoceros* (C), all measured as number of valves per gram of dry sediment.

The cause of the low ^{210}Pb activities in the upper 25cm of this core remains an open question. Low ^{210}Pb activities have been associated with flood deposits elsewhere on the California Margin (Mullenbach et al, 2000). The Monterey Bay region experienced significant flooding in 1996 and 1997 as a result of powerful storms that were associated with strong El Niño events. Thus, the low ^{210}Pb activities in the upper 25cm of the core may represent a flood layer. It is not possible to disprove that flood layers exist lower in the core. However, the shape of the ^{210}Pb profile in the 24 to 71 cm depth interval of the core does not exhibit the upward-decreasing activities evident in the top 25cm. It is therfore unlikely that flood layers exist in the 24 to 71cm depth horizon.

4.2 Diatom abundance

Sedimentary concentrations of phaeophytin-a and diatom abundance are excellent proxies for diatom productivity, provided that sedimentation has been more or less uniform. If the age model for this core is correct, then these proxies may be linked to environmental factors such as sea surface temperature and precipitation. Profiles of phaeophytin-a and total diatom abundance (figure 6) resemble each other shape. Sharp decreases in Phaeophytin-a concentration and diatom abundance occur in the core at 6cm, 51cm, 78cm. The abrupt decrease diatoms and pheophytin-a suggest that diatom productivity was low during the late 1990s, the early 1960, and the late 1920s. Such a decrease would also be explained by an increase in sediment input that would dilute the signal of these two proxies. Slight increases in the percentage of fine sediment near these depth horizons suggest increased sediment input may be the cause for the apparent

decrease in productivity. However, the percent fine sediment is also high near 80cm and 110cm where both proxies indicate that productivity was high. Thus, the subtle variations in sediment texture do not support or rule out the possibility that these proxies have been skewed by pulses of sediment input.

El Niño events are commonly associated with reduced coastal upwelling and increased stream flow in Coastal California (Simpson, 1994). Both these El Niño-related effects would result in lower sedimentary concentrations of pheophytin-a and reduced diatom abundance. *Chaetoceros* is associated with late-stage upwelling. Thus, the reduction in upwelling that occurs during a strong El Niño event would result in decreased *Chaetoceros* productivity. Overall diatom abundance would also be decreased in response to higher input of fluvial sediment that may occur during strong El Niño events. As a result of sediment mixing, the sediment column is more likely to record a sequence of closely spaced El Nino events, rather than one isolated El Niño event. A strong El Nino event occurred in 1983 and a series of El Nino events occurred during the late 1990s. Abundance of *Chaetocero* is generally high in the upper 45 cm of the core, but at sharp decreases are evident at 6 cm and 33 cm (figure 7). These decreases in diatom abundance are consistent with decreased production that would be associated with the El Niño events that occurred in 1983 and the late 1990s.

Abundance profiles of *Thalassionea nitzschioes* and *Chaetoceros* generally appear similar, except that *Chaetoceros* are more numerous by an order of magnitude. An increase in *T. nitzschioes* at 87cm, however, is not mirrored by any increase in *Chaetoceros*. The meaning of this increase is not clear, but it may indicate that early

spring upwelling was stronger during years when late summer upwelling was weak. *Thalassionea nitzschioes* is associated with oceanic water, whereas *Chaetoceros* is associated with near-shore water. Thus, an alternate explanation of the increase in *T. nitzschioes* is that production in Monterey Bay was strongly influenced by oceanic water during about 1920, when the 87cm-depth-interval was deposited.

If the proposed age mode for core PS-1 is correct, then it is possible to compare diatom abundance with historical environmental factors such as rainfall and sea surface temperature. El Niño events commonly result in higher than normal rainfall and warmer sea surface temperature in Monterey Bay. Primary productivity decreases as a result of reduced upwelling during El Niño events. Thus, diatom abundance should be lower at age horizons that correspond to times of warmer sea surface temperature and higher than normal rainfall. However, when a time line of diatom abundance is compared to historical sea surface temperature and rainfall, this relationship is not evident (figure 8). For example, diatom abundance is relatively constant during the early 1940s and late 1960s when rainfall was high and the sea surface was warm. This suggests that dilution of diatom abundance by fluvial sediment during wet years may not be significant.

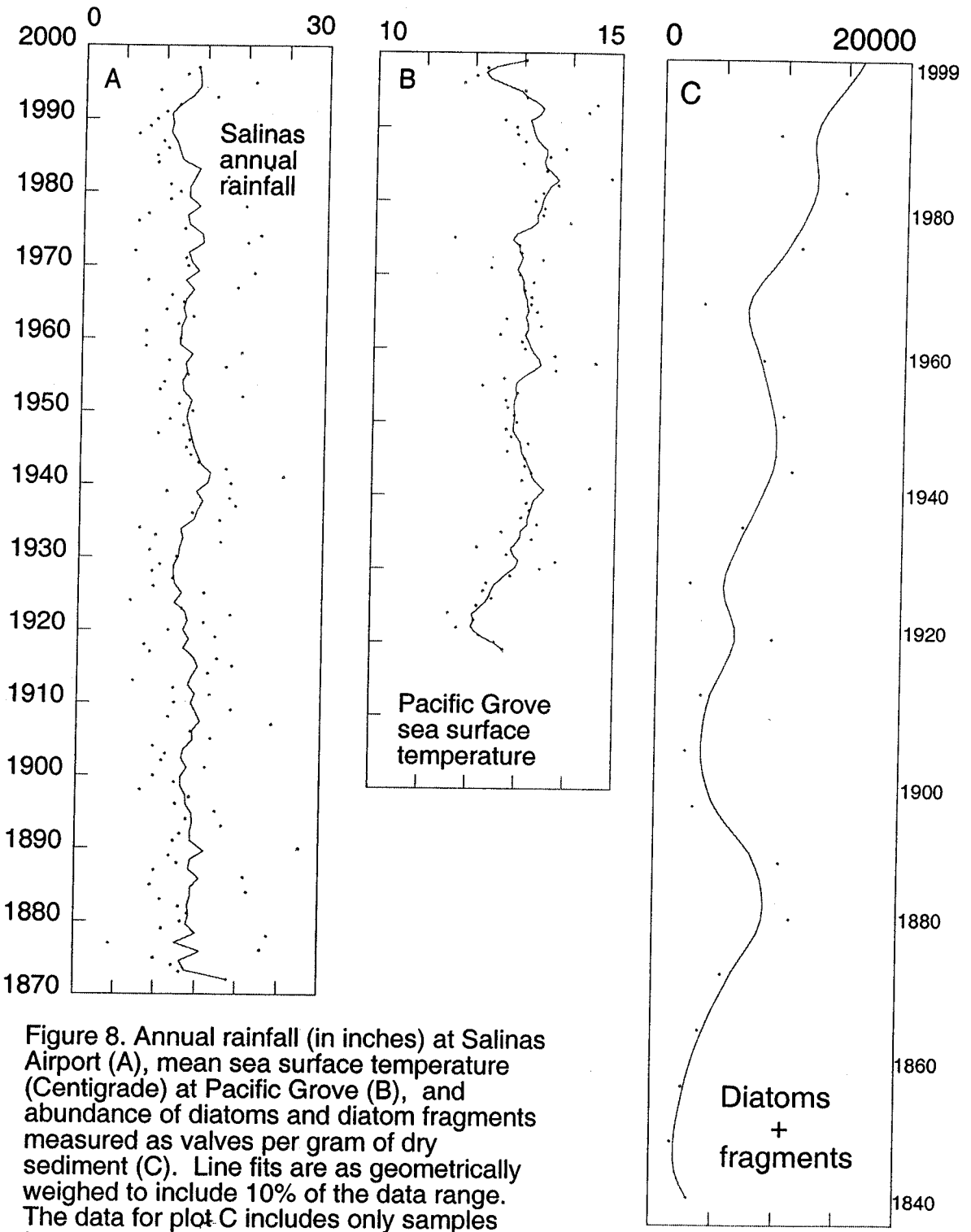

Figure 8. Annual rainfall (in inches) at Salinas Airport (A), mean sea surface temperature (Centigrade) at Pacific Grove (B), and abundance of diatoms and diatom fragments measured as valves per gram of dry sediment (C). Line fits are as geometrically weighed to include 10% of the data range. The data for plot C includes only samples from below 25cm because the upper 25cm is most likely a flood deposit.

The genus *Pseudo-nitzschia*, which is linked to toxic bloom events, was present in small amounts throughout the core. The highest number was counted at 18 and 39cm, which had abundances of 615 and 214 valves per gram, respectively. The deepest interval that contained unbroken valves that were identifiable as *Pseudo-nitzschia* occurred at 123 cm. Deeper sections of the core contained fragments of *Pseudo-nitzschia*, but they were counted only as fragments. If the bottom of core PS-1 represents sediments that are 170 years old, then the distribution of *Pseudo-nitzschia* indicated that this genus has existed in Monterey Bay until at least the early 1800s.

The effectiveness of fossil diatoms as proxies of paleoproductivity is limited by a number of factors. Silica preservation in marine sediments is poorly understood. Thus, it may be argued that depth-horizons that contain few diatoms may record periods of diatom dissolution as opposed to periods of low productivity. This argument is countered by the observation the horizons in core PS-1 that contain low diatom abundance also contain well preserved diatoms. Episodic inputs of fluvial sediment may also confound the productivity recorded by total diatom abundance. If pulses of fluvial sediment are not homogenized evenly by sediment mixing, then depth horizons with few diatoms may actually represent pulses of fluvial sediment.

5. Conclusion

Sediments on the continental shelf of Monterey Bay preserve a record of environmental conditions that extends backward in time to before written history. The sedimentary record that was sampled by core PS-1 represents less than the most recent 200 years of that environmental record. This study attempted link historical environmental conditions to diatom abundance, so that ancient environmental conditions could be documented by studying deeper sediments. An accurate sedimentary chronology is key to linking historical climate records and diatom productivity. ^{210}Pb and other chemical tracers were used to establish a sedimentary chronology for core PS-1.

The accuracy of the sedimentary chronology for core PS-1 is questionable. The shape of the ^{210}Pb profile suggests that the sedimentation history of the top 25cm of the core is unlike deeper levels. Possibly, the upper 25cm of the core was deposited as a result recent flooding. If this true, then core PS-1 was affected by pulses of rapid sedimentation that would distort the record of diatom productivity that is recorded by the core. ^{137}Cs and DDT help to constrain the sedimentation rate of 0.76cm/y that was estimated from the profile of ^{210}Pb. Additionally, the absence of excess ^{210}Pb below 74cm indicates that the lower half of the core is older than 100 years. If the sediments below 25cm accumulated at a rate of 0.76cm/y, then sediments at the base of the core are about 170 years old.

The result of this work shows that diatom abundance and phaeophytin-a varies significantly in the sediments of the northern Monterey Bay shelf. These sediments potentially contain a meaningful record of primary productivity. The techniques used in this study would likely unlock this record if they were applied to deeper cores with better age control. The key lesson to future workers, is that firm age control should be established on sediment cores before additional analysis are performed.

References

Battarbee, R.W. 1973. A new method for the estimation of absolute microfossil numbers,with reference especially to diatoms. Limnology and Oceanography, vol.18, no.4, pp. 647-653.

Best, T.C., and Griggs, G.B., 1991. A sediment budget for the Santa Cruz littoral call, California, From shoreline to Abyss. SEPM Special Pub. No. 46, 35-50.

Bigelow, H.B. and Leslie, M. 1930. Reconnaissance of the waters and plankton of Monterey Bay, july, 1928. Bulletin of the Museum of Comparative Zoology, Harvard. 70, pp.429-581.

Bolin, R.L., and Abott, D.P. 1963. Studies on the marine climate and phytoplankton of thecentral coastal areas of California, 1954-1960. Calif. Coop. Oceanic Fish. Invest. Rep 9:23-45.

Breaker, L.C., and Broenkow, W.W., 1994, The circulation of Monterey Bay and Related Processes. Oceanography and Marine Biology: an Annual Review, 32: 1-64.

Fryxell, G.A., Reap, M.E., and Valencic D.L. 1990. *Nitzschia Pungens* Gunow f. *multiseries* Hasle: observations of a known neurotoxic diatom. Nova Hedwigia, Beiheft. 100, pp. 171-188.

Garrison, D.L. 1979. Monterey Bay phytoplankton. I. Seasonal cycles of phytoplankton assemblages. Journal of Plankton Research, v1, no.3 pp. 241-265.

Janda, R. S., Nolan, K.M., 1979. Stream and sediment discharge in Northwestern California. In: Guidebook for a fieldtrip to observe on natural and management-related erosion in San Franciscan terrane of Northern California, Cordilleran Section. San Jose, Geol. Soc. Amer. P. IV-1-IV-27

Johnson, K.S., C.K. Paull, J.P. Barry and F.P Chavez. 2001. A decadal record of underflows from a coastal river into the deep sea. Geology, 29: 1019-1022.

Lewis, R.C., Coale, K.H., Edwards, B.D, Douglas, J, Burton, E. 2002. Sedimentation rate and Mixing of shelf sediments in northern Monterey Bay Marine Sanctuary. Marine Geology. 181, 157-169.

Malone, T.C. 1971. The relative importance of nannoplankton and netplankton as primary producers in the California Current system. Fishery Bulletin. 69, 799-820.

Miller, P. E. and Sholin, C.A., 1996. Identification of cultivated *Pseudonitzschia* (Bacillariophycae) using species-specific LSU rRNA-targeted flourescent probes. Journal of Phycology. 32, 646-655.

Mullenbach, B.L. and Nittrouer, C.A., 2000. Rapid deposition of fluvial sediment in the EelCanyon, northern California. Continental Shelf Research. 20, 2191-2212

Ortlieb, L. and Machara, J. 1993. Former El Nino events: records from western South America. Global and Planetary Change, vol.7, no. 1-3, 181-202.

Paull, C. K., Greene, H.G., Ussler, W., Mitts, P.J. 2002. Pesticides as tracers of sediment transport through Monterey Canyon. Geo-Marine Letters (in press)

Pennington, J.T. and F.P. Chavez (2000) Seasonal fluctuations of temerature, salinity, nitrate, chlorophyll and primary production at station H3/M1 over 1989-1996 in Monterey Bay, California. Deep Sea Research II, 47, 947-973.

Sanchetta, C., Mitchell L., Heusser L., 1992. Late-Glacial to Holocene Changes in Winds, Upwelling, and Seasonal Production of the Northern California Current System. Quaternary Research. 38, 359-370.

Simpson, J.J. 1984. El Nino-induced onshore transport in the California Current during 1982-1983. Geophysical Research Letters, v11, no.3 pp. 241-242.

Smethie, Jr. W.M. 1973. Some aspects of the temperature, oxygen, and nurtient distributions in Monterey Bay, California. Moss Landing Marine Laboratories, Technical Report, no73-1. 97p.

Appendix A: Plots of radioisotope activity measured by gamma spectrometry

1. Excess ^{210}Pb, total ^{137}Cs, in PS-1
2. Total ^{210}Pb, ^{234}Th, ^{137}Cs, ^{214}Pb, ^{137}Cs, ^{226}Ra, ^{214}Bi in 1B1 & 2B1
3. Total ^{210}Pb, ^{234}Th, ^{137}Cs, ^{214}Pb, ^{137}Cs, ^{226}Ra, ^{214}Bi in 3B2 & 7B1
4. Total ^{210}Pb, ^{234}Th, ^{137}Cs, ^{214}Pb, ^{137}Cs, ^{226}Ra, ^{214}Bi in 8B1 & 13B1

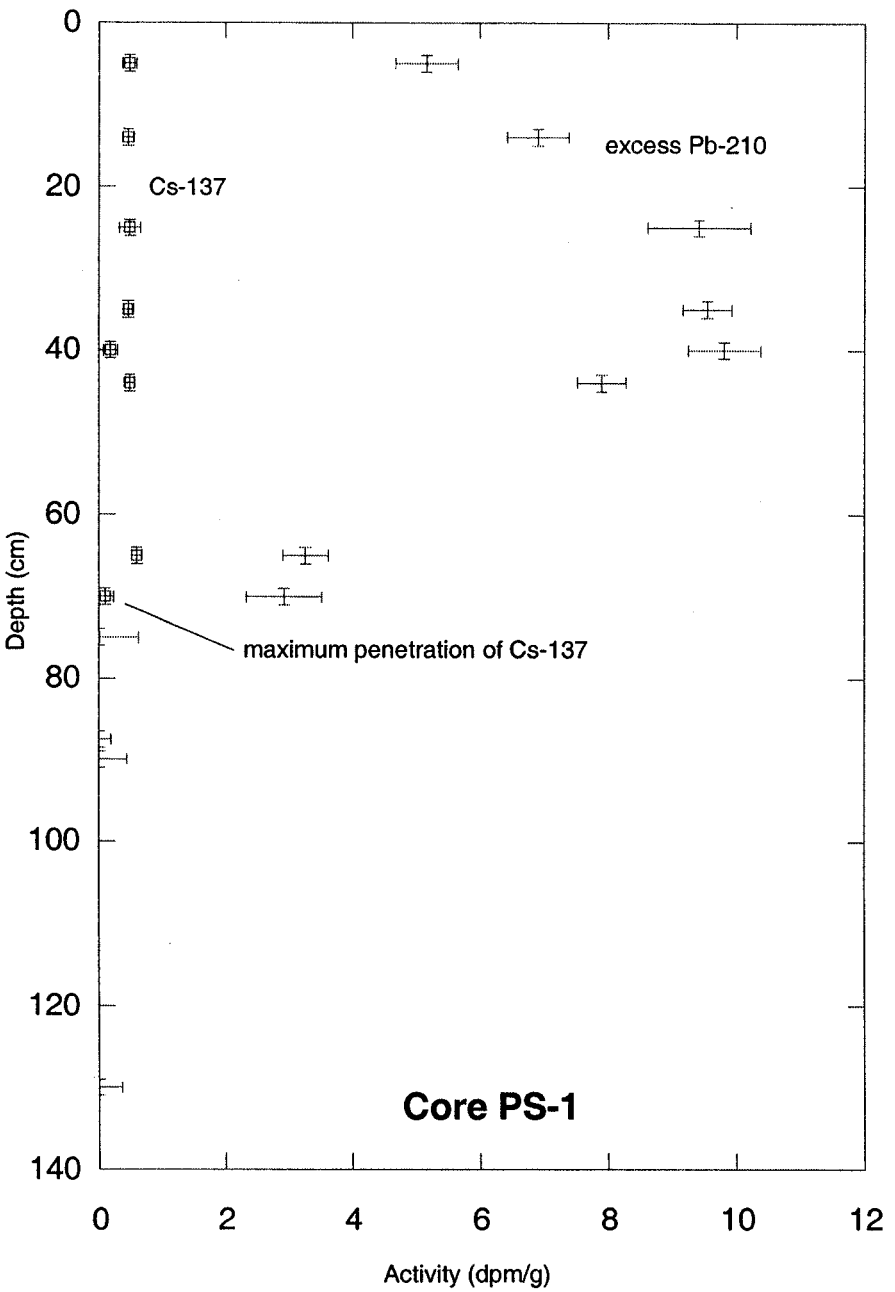
0
20
40
60
80
100
120
140
Depth (cm)
excess Pb-210
Cs-137
maximum penetration of Cs-137
Core PS-1
0
2
4
6
8
10
12
Activity (dpm/g)

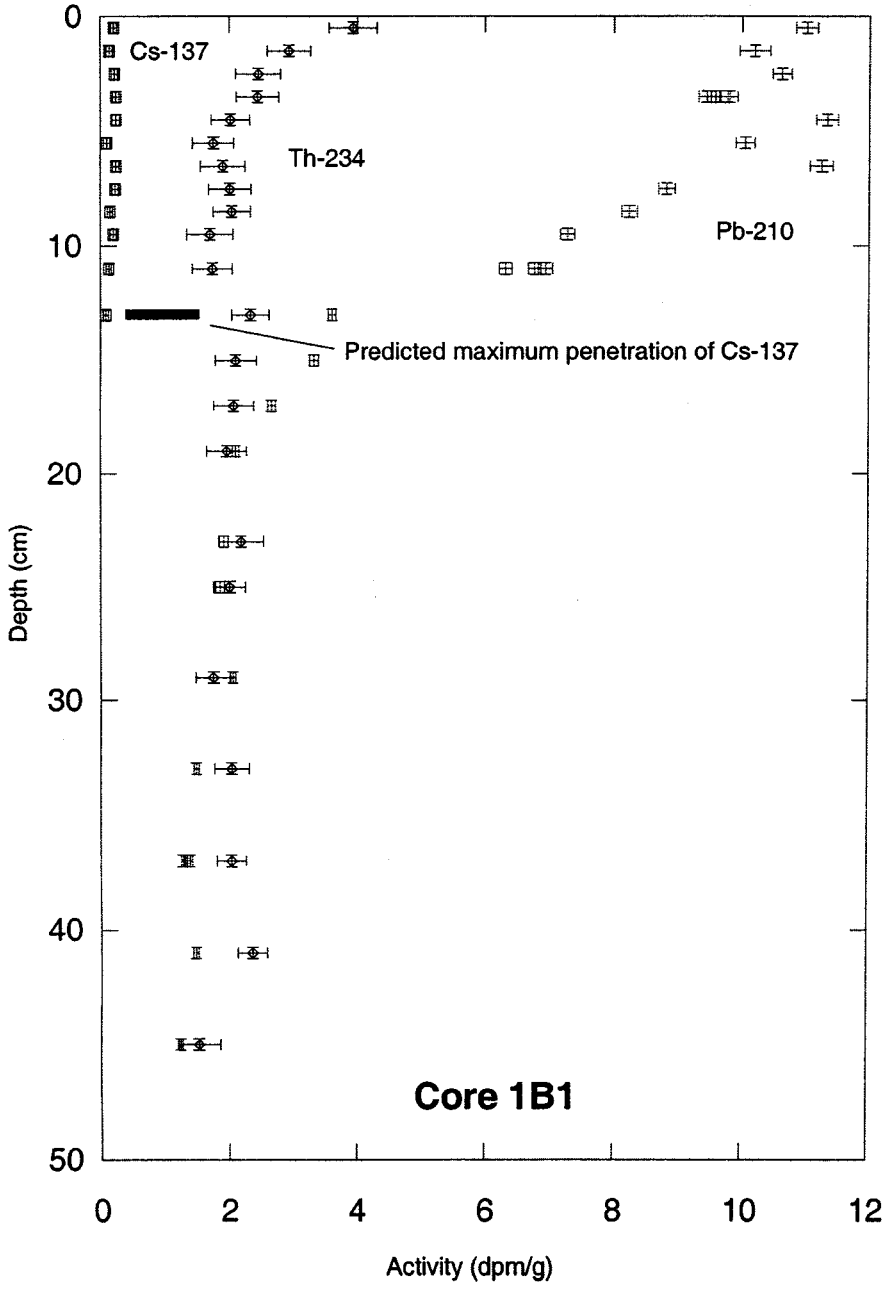
Cs-137
Th-234
Pb-210
Predicted maximum penetration of Cs-137
Core 1B1
Depth (cm)
Activity (dpm/g)
0
10
20
30
40
50
0
2
4
6
8
10
12

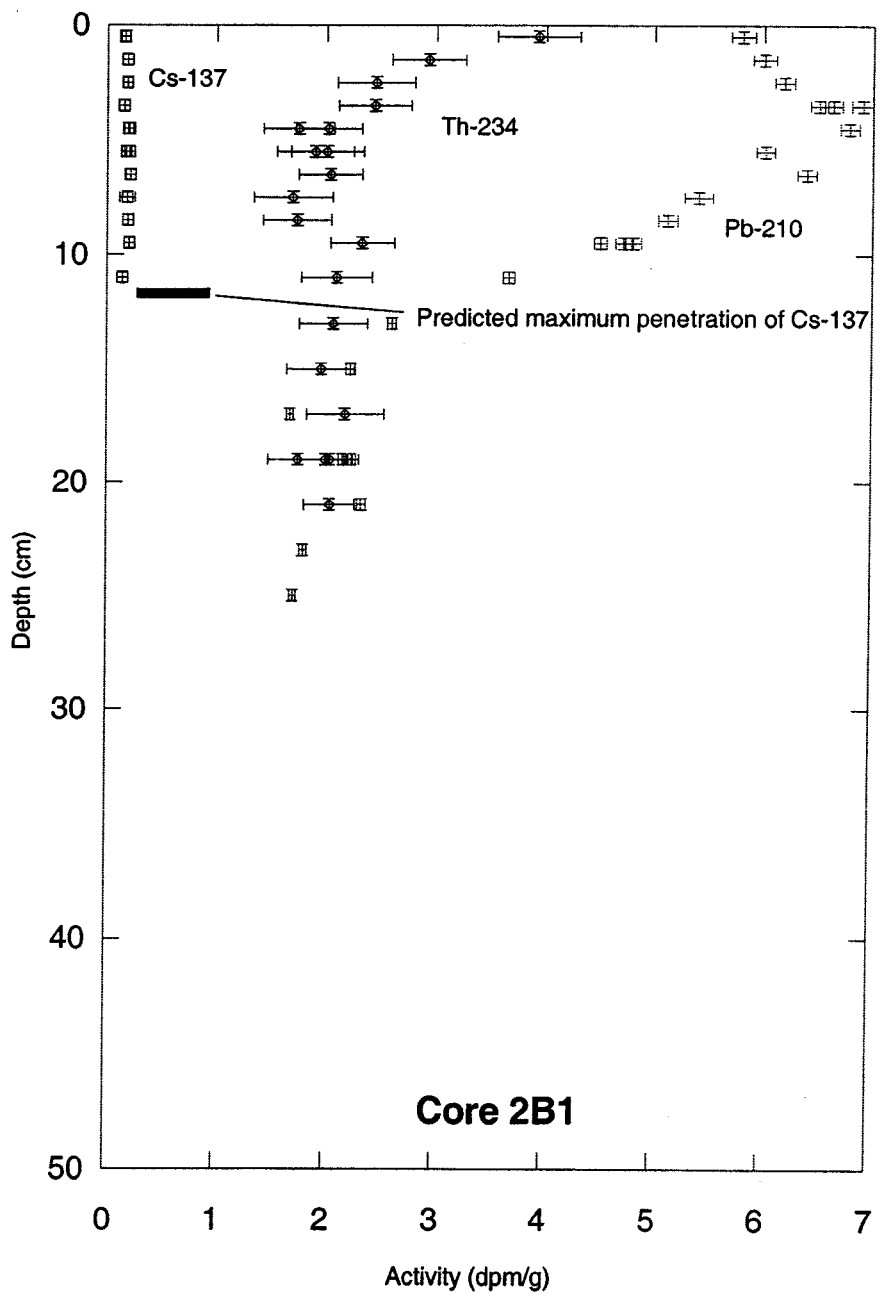
Cs-137
Th-234
Pb-210
Predicted maximum penetration of Cs-137
Core 2B1
Depth (cm)
Activity (dpm/g)
0
10
20
30
40
50
0
1
2
3
4
5
6
7

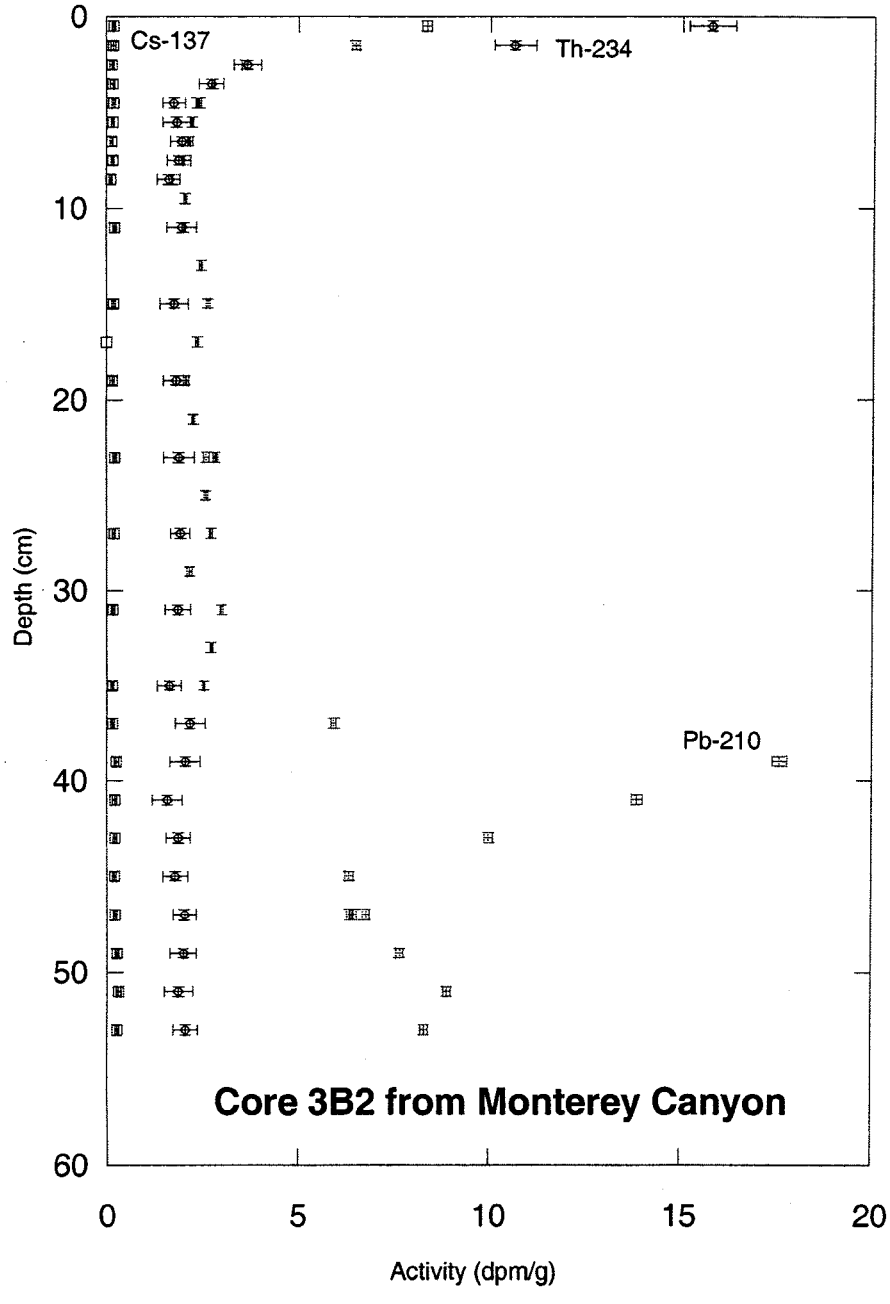
Cs-137
Th-234
Pb-210
Depth (cm)
0
10
20
30
40
50
60
0
5
10
15
20
Activity (dpm/g)
Core 3B2 from Monterey Canyon

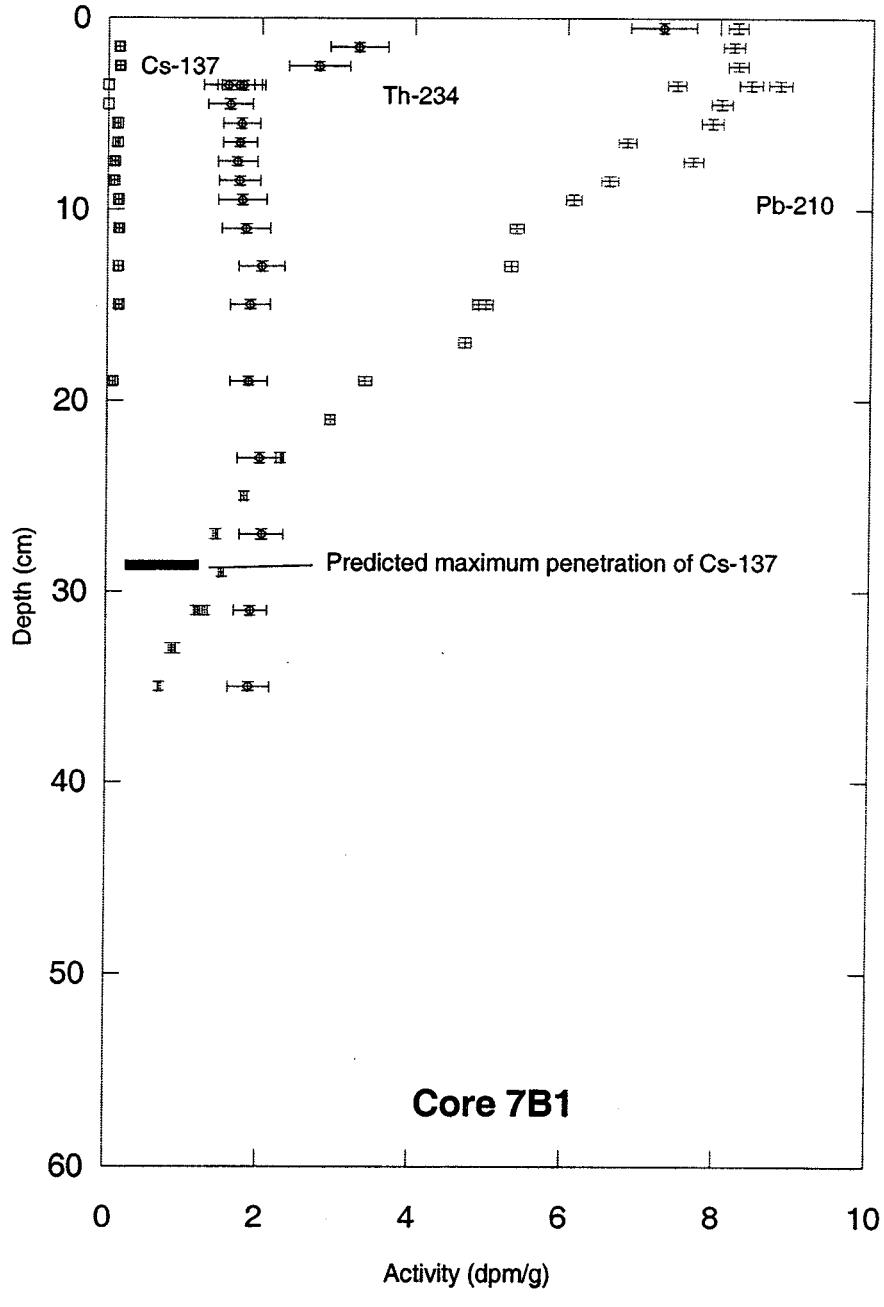
Cs-137
Th-234
Pb-210
Predicted maximum penetration of Cs-137
Depth (cm)
0
10
20
30
40
50
60
0
2
4
6
8
10
Activity (dpm/g)
Core 7B1

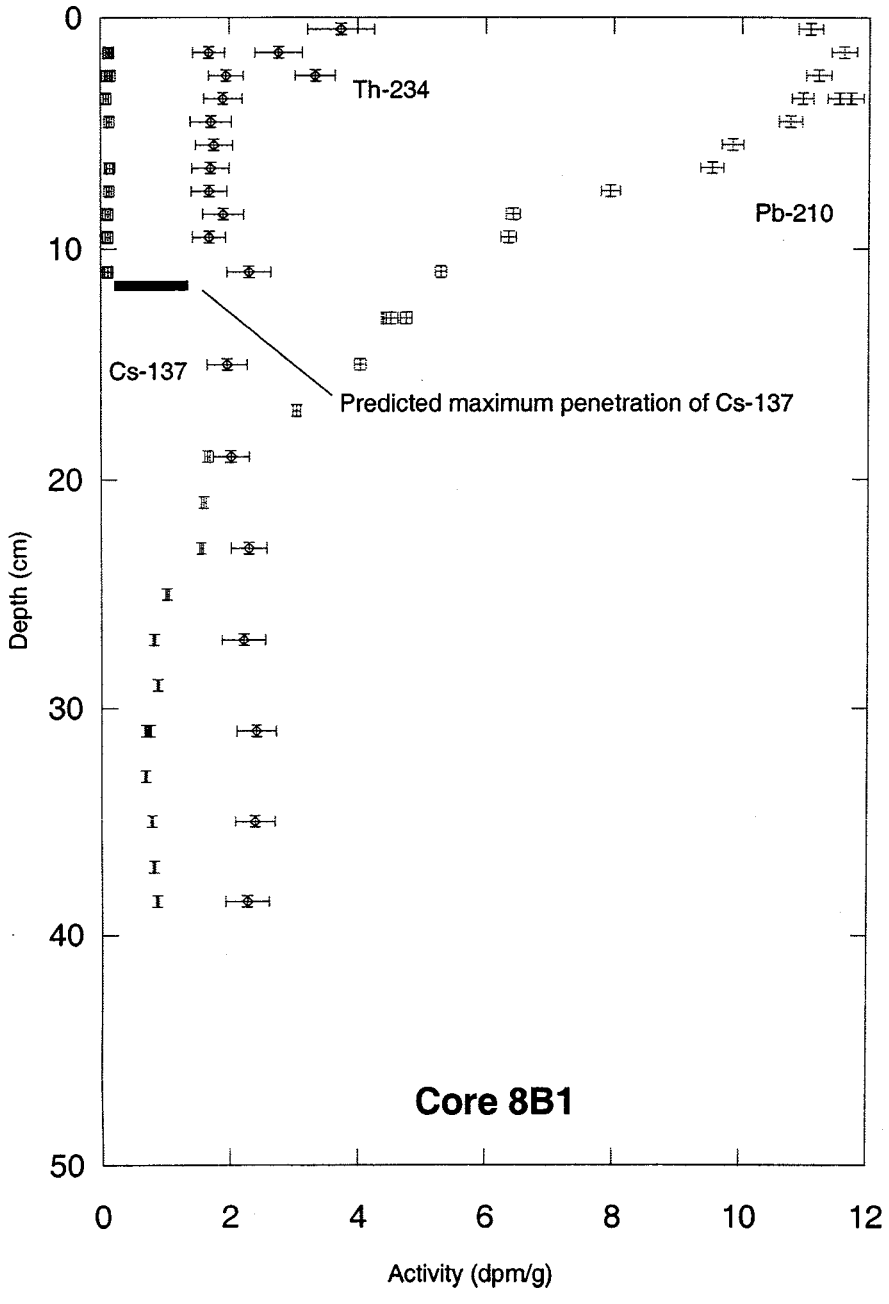
Th-234
Pb-210
Cs-137
Predicted maximum penetration of Cs-137
Core 8B1
Depth (cm)
Activity (dpm/g)
0
10
20
30
40
50
0
2
4
6
8
10
12

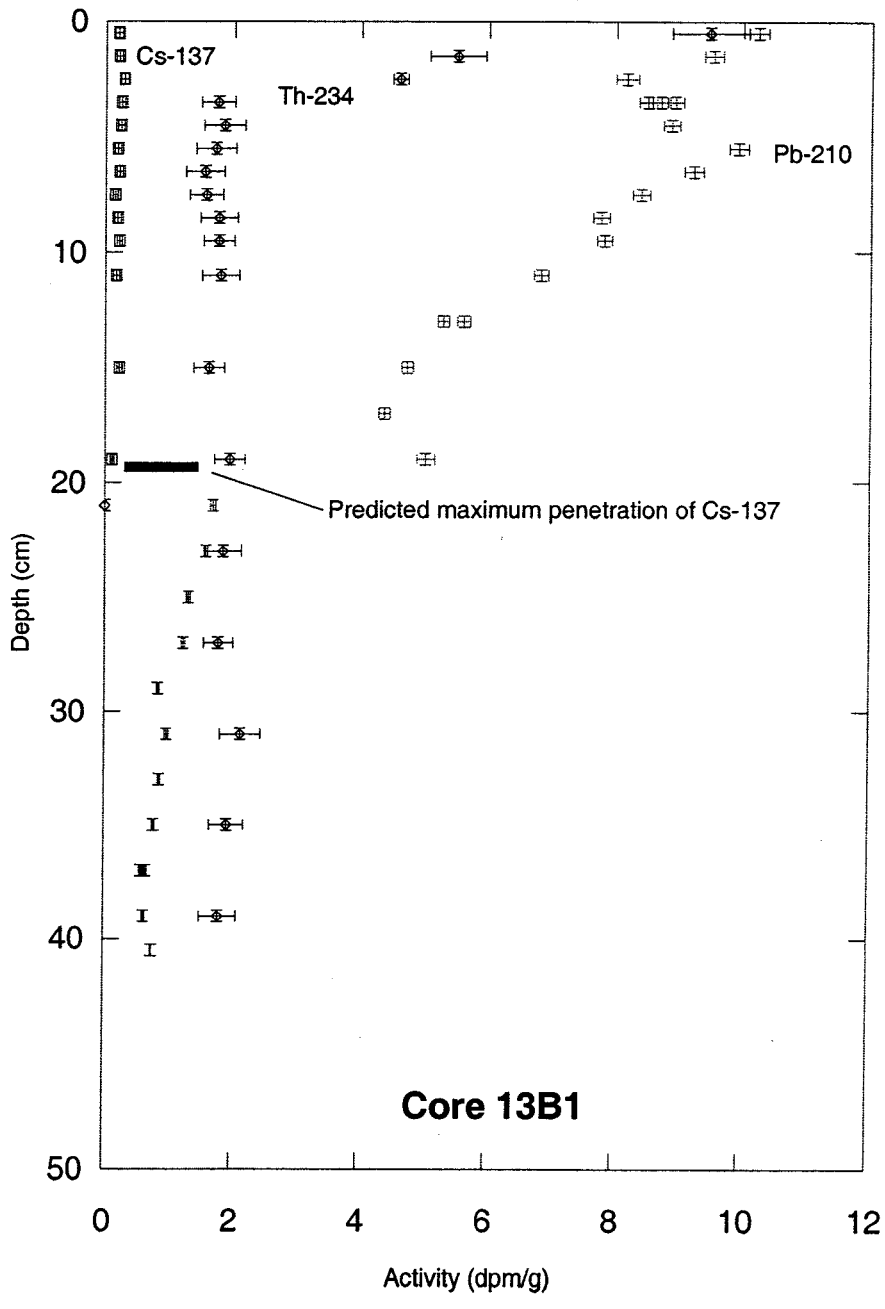
Cs-137
Th-234
Pb-210
Predicted maximum penetration of Cs-137
Core 13B1
Depth (cm)
Activity (dpm/g)
0
10
20
30
40
50
0
2
4
6
8
10
12

Appendix B: Plots of radioisotope activity measured by alpha spectrometry

1. Excess ^{210}Pb in core B557, B558, B554, B555,
2. Excess ^{210}Pb in core B556, B561, B582, B505
3. Excess ^{210}Pb in core B506, B509, B504, B49
4. Excess ^{210}Pb in core B67, B62, B448, B245,
5. Excess ^{210}Pb in core B606, B81, B117, B88
6. Excess ^{210}Pb in core B424, B271, B250, B155
7. Excess ^{210}Pb in core B330 and B331

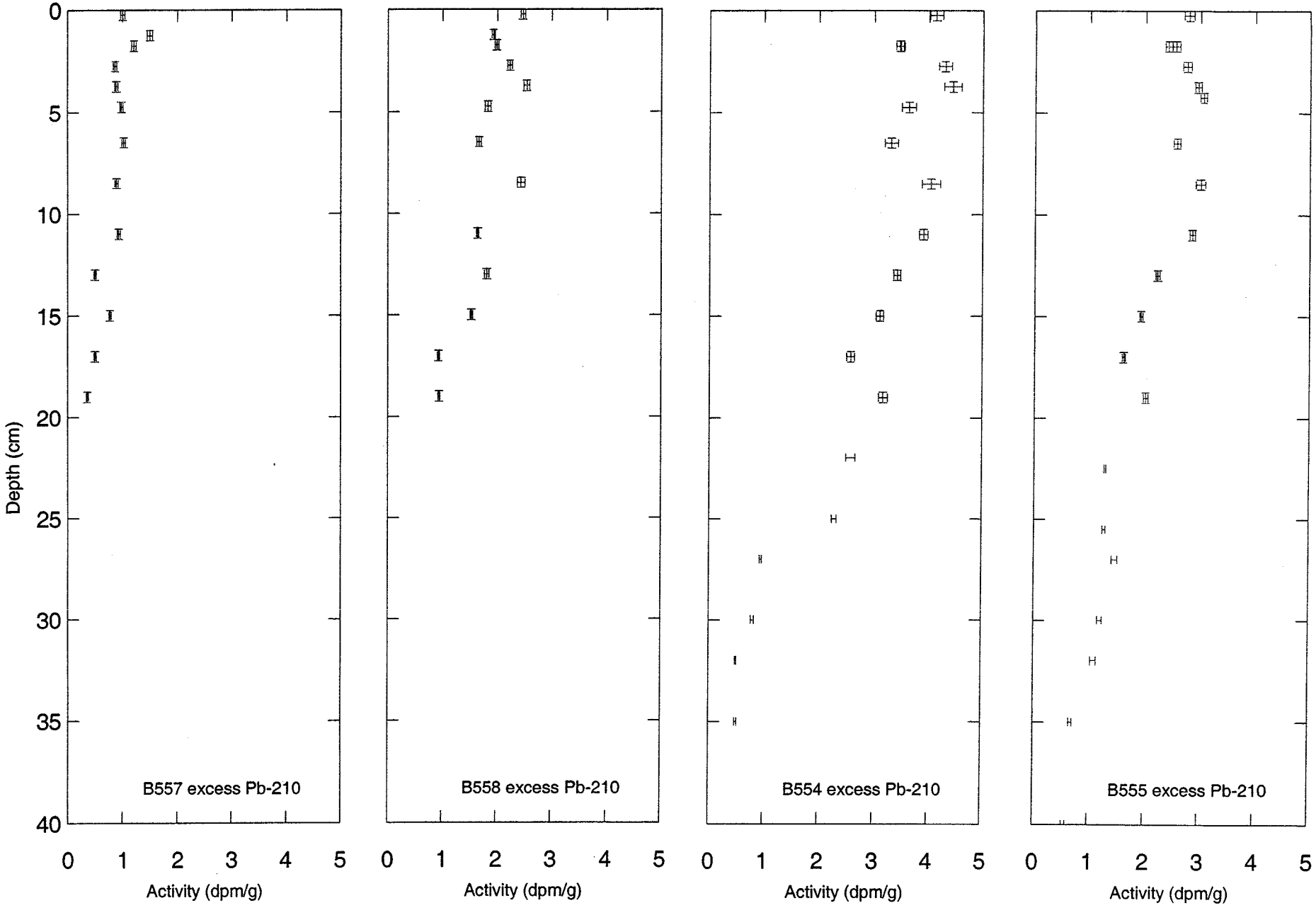
Depth (cm)
0
5
10
15
20
25
30
35
40
B557 excess Pb-210
B558 excess Pb-210
B554 excess Pb-210
B555 excess Pb-210
0 1 2 3 4 5
Activity (dpm/g)

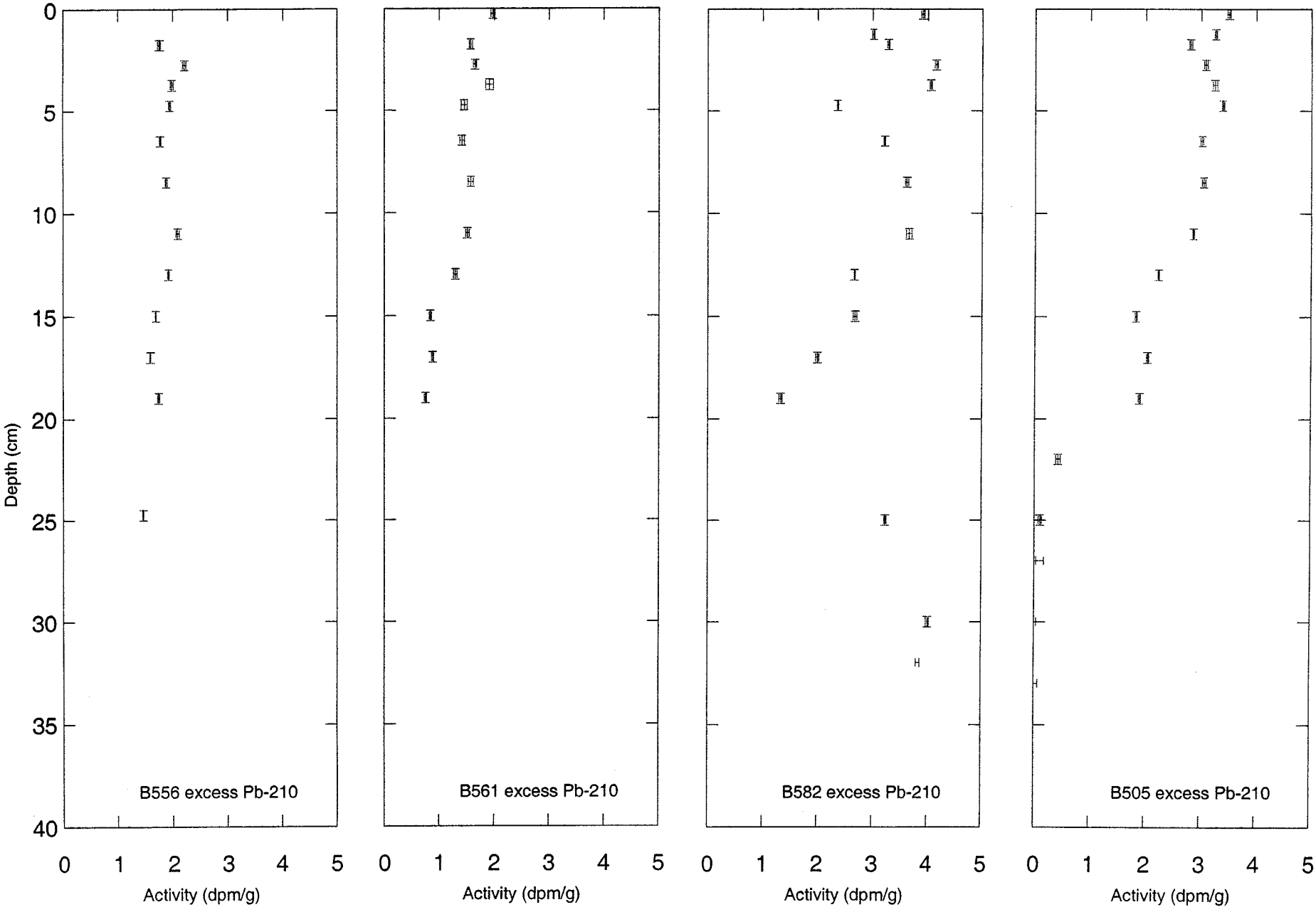
Depth (cm)
0
5
10
15
20
25
30
35
40
B556 excess Pb-210
B561 excess Pb-210
B582 excess Pb-210
B505 excess Pb-210
0 1 2 3 4 5
Activity (dpm/g)

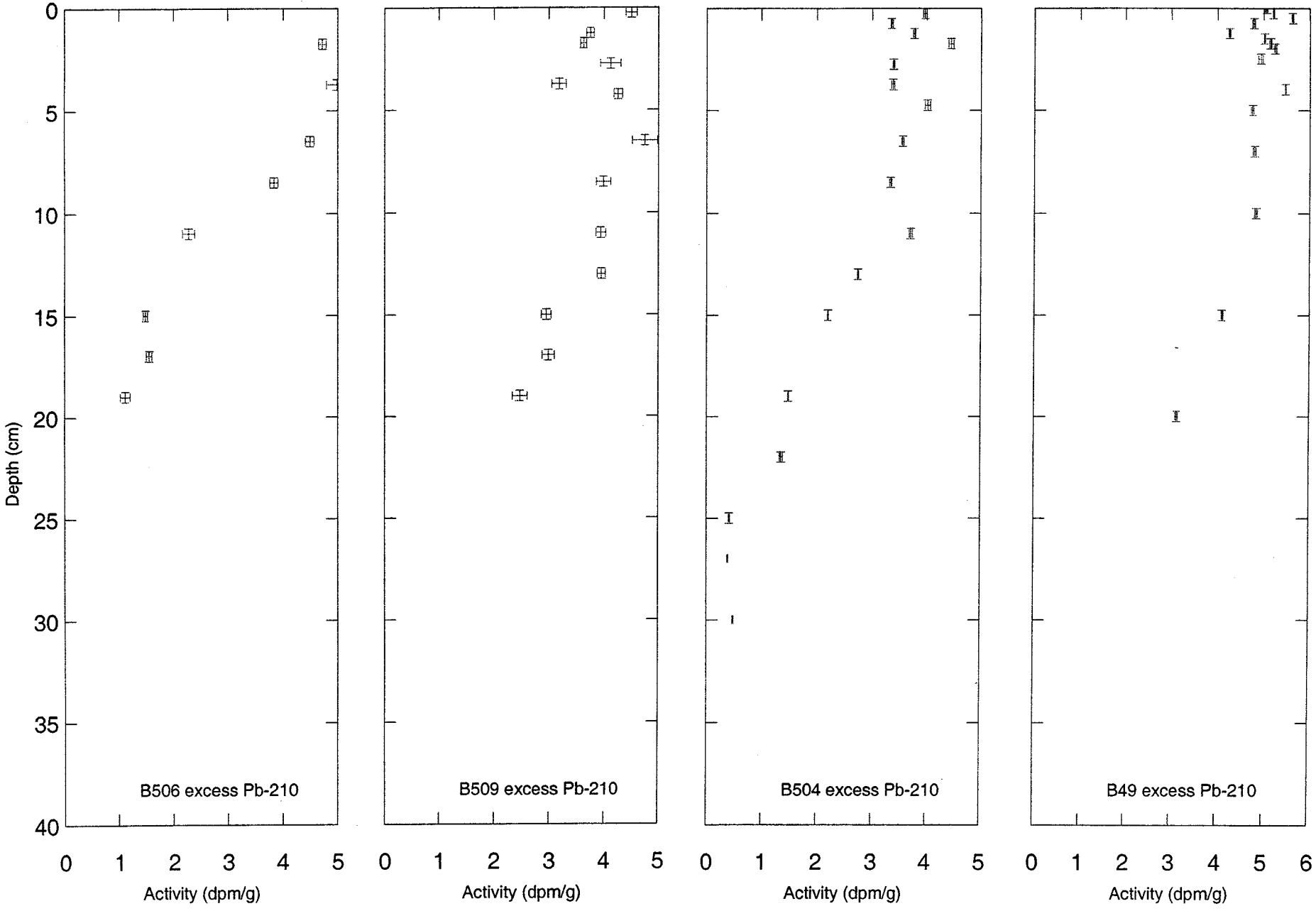
Depth (cm)
0
5
10
15
20
25
30
35
40
B506 excess Pb-210
B509 excess Pb-210
B504 excess Pb-210
B49 excess Pb-210
0 1 2 3 4 5
0 1 2 3 4 5
0 1 2 3 4 5
0 1 2 3 4 5 6
Activity (dpm/g)
Activity (dpm/g)
Activity (dpm/g)
Activity (dpm/g)

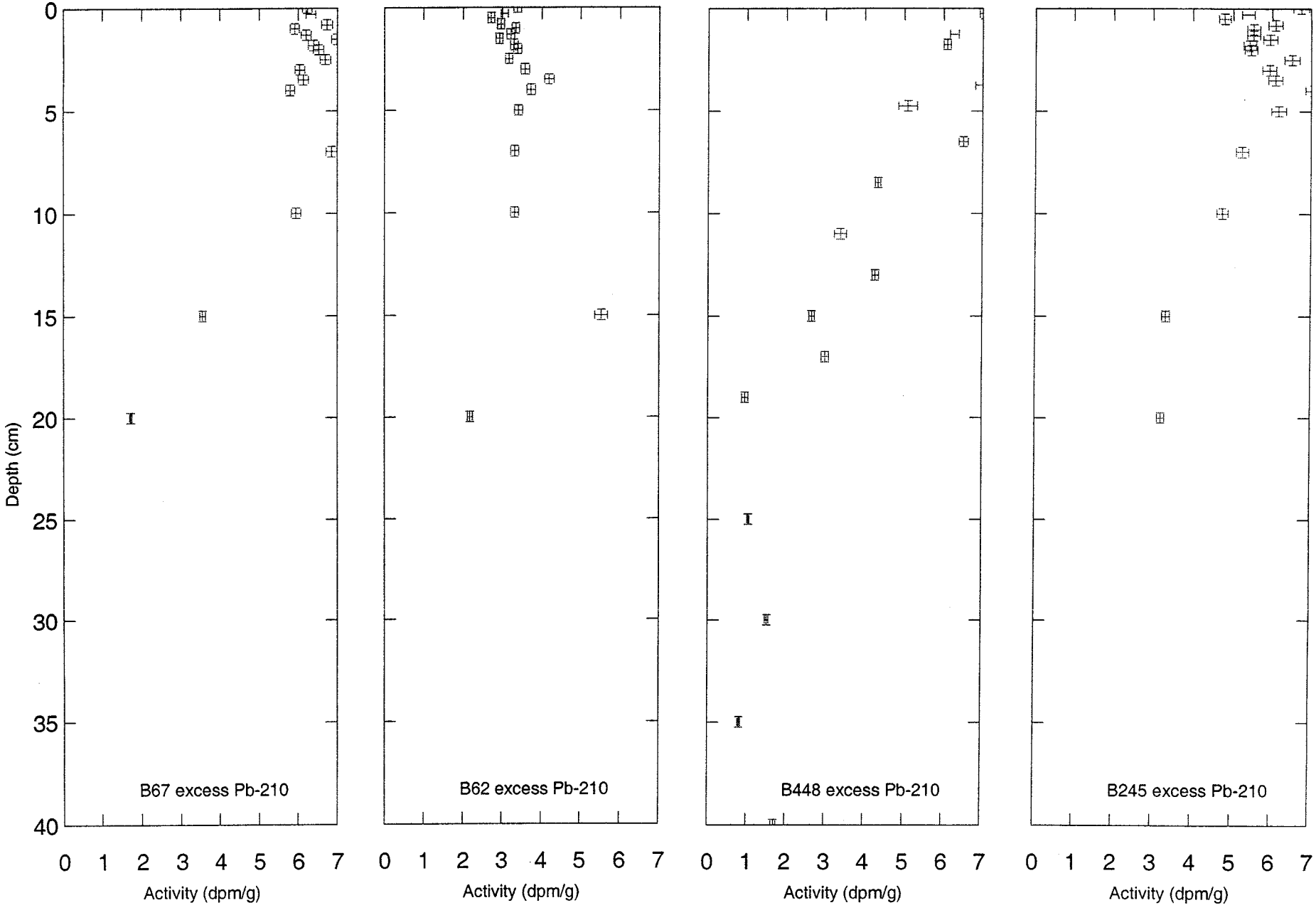
Depth (cm)
0
5
10
15
20
25
30
35
40
B67 excess Pb-210
B62 excess Pb-210
B448 excess Pb-210
B245 excess Pb-210
0 1 2 3 4 5 6 7
Activity (dpm/g)

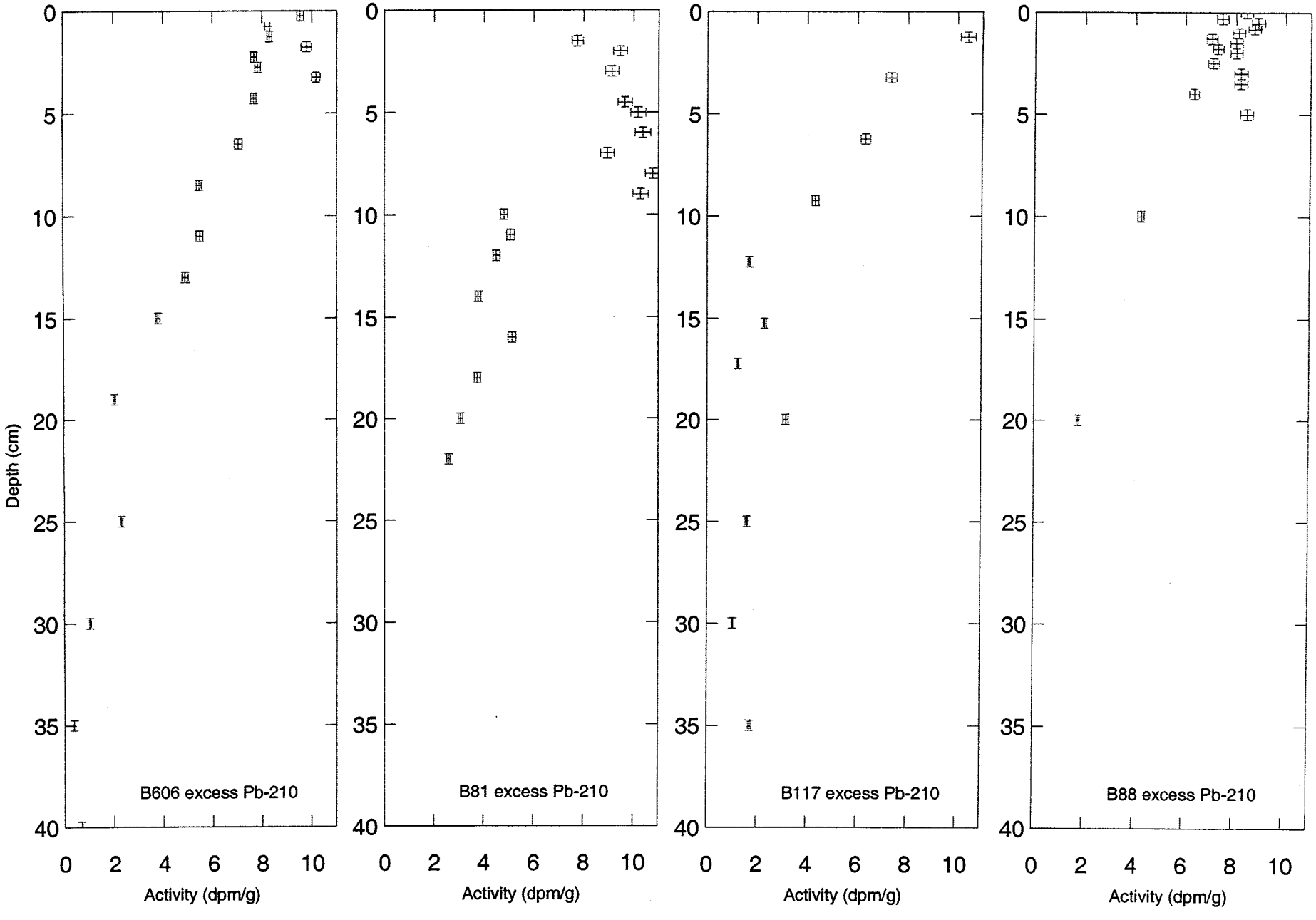
Depth (cm)
0
5
10
15
20
25
30
35
40
0
2
4
6
8
10
Activity (dpm/g)
B606 excess Pb-210
B81 excess Pb-210
B117 excess Pb-210
B88 excess Pb-210

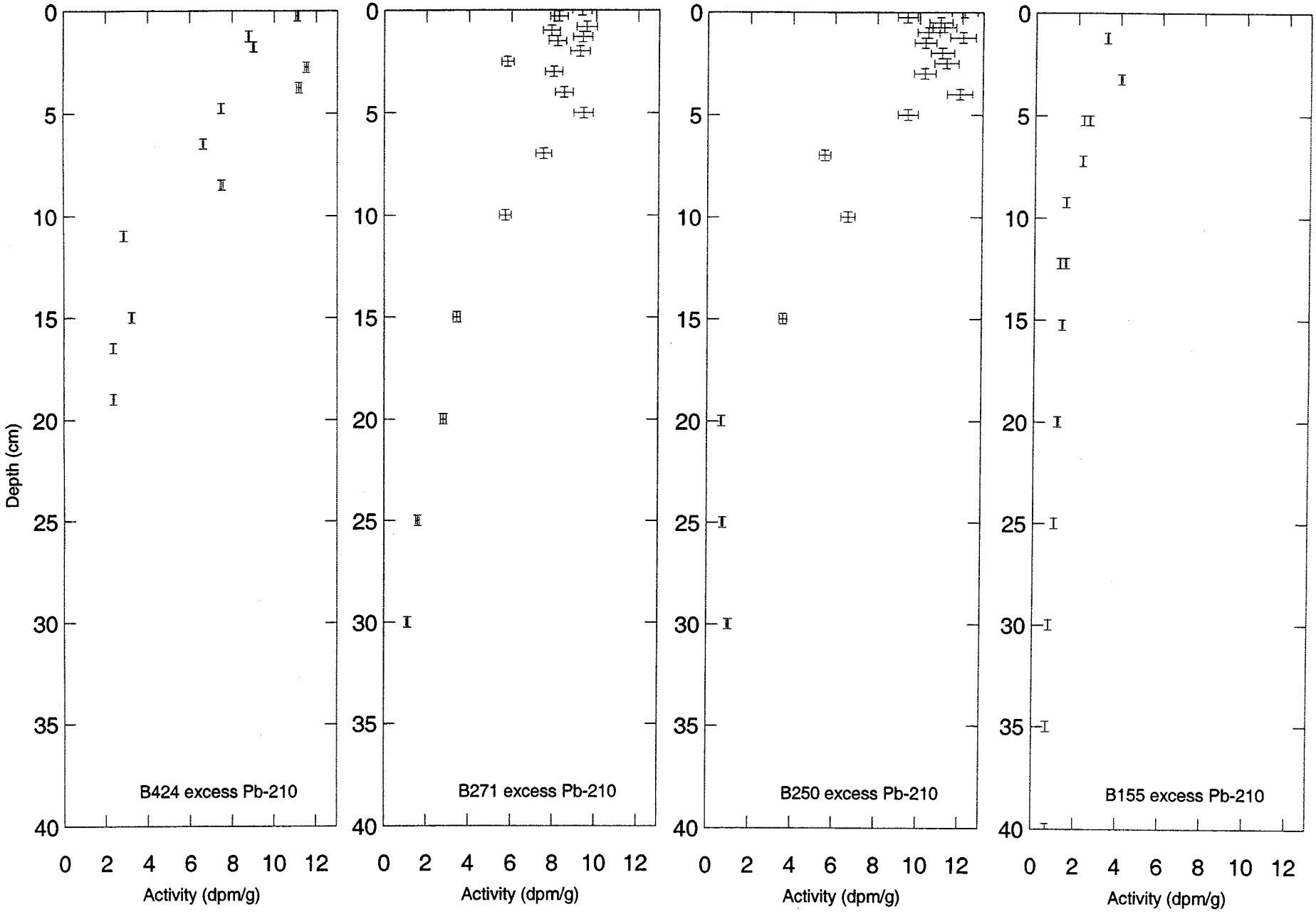
Depth (cm)
0
5
10
15
20
25
30
35
40
0 2 4 6 8 10 12
Activity (dpm/g)
B424 excess Pb-210
B271 excess Pb-210
B250 excess Pb-210
B155 excess Pb-210

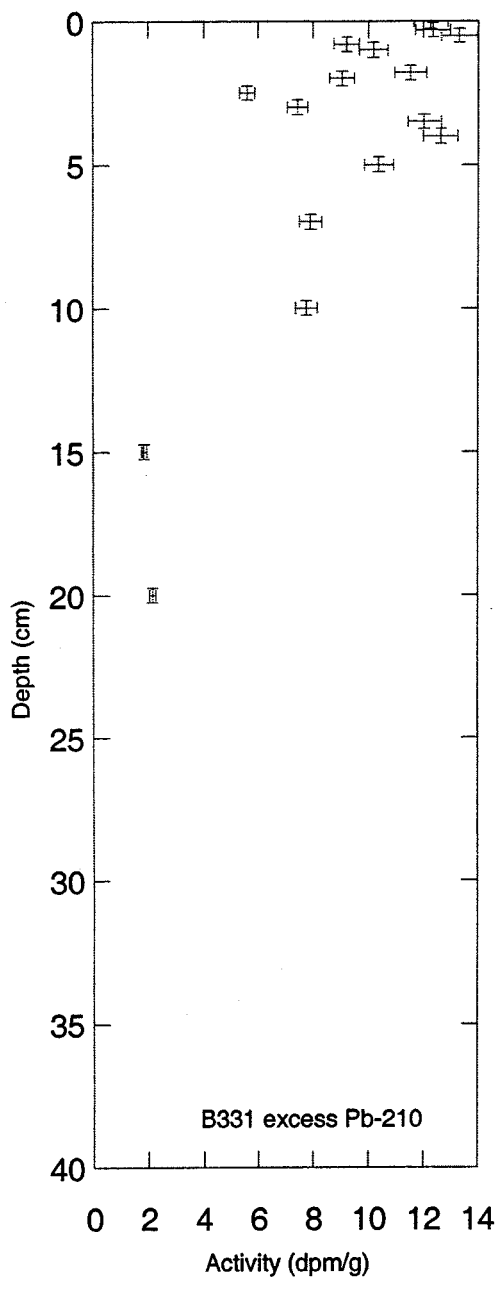
0
5
10
15
20
25
30
35
40
Depth (cm)
B331 excess Pb-210
0 2 4 6 8 10 12 14
Activity (dpm/g)

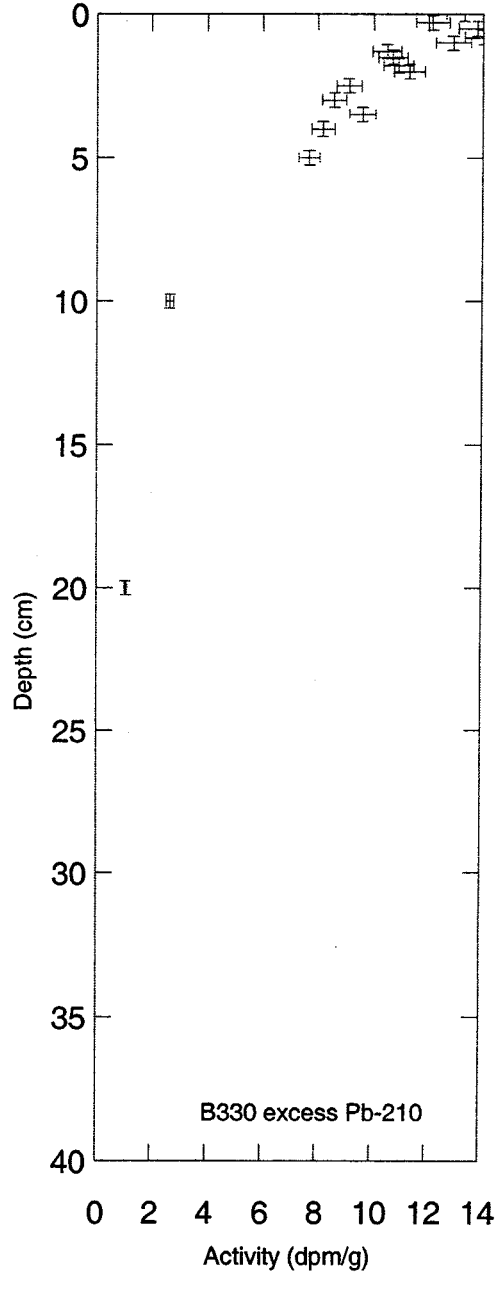
0
5
10
15
20
25
30
35
40
Depth (cm)
B330 excess Pb-210
0 2 4 6 8 10 12 14
Activity (dpm/g)

Appendix C: Tables of radioisotope activity measured by gamma spectrometry

1. Total ^{210}Pb, ^{234}Th, ^{137}Cs, ^{214}Pb, ^{137}Cs, ^{226}Ra, ^{214}Bi in 1B1
2. Total ^{210}Pb, ^{234}Th, ^{137}Cs, ^{214}Pb, ^{137}Cs, ^{226}Ra, ^{214}Bi in 2B1
3. Total ^{210}Pb, ^{234}Th, ^{137}Cs, ^{214}Pb, ^{137}Cs, ^{226}Ra, ^{214}Bi in 3B2
4. Total ^{210}Pb, ^{234}Th, ^{137}Cs, ^{214}Pb, ^{137}Cs, ^{226}Ra, ^{214}Bi in 7B1
5. Total ^{210}Pb, ^{234}Th, ^{137}Cs, ^{214}Pb, ^{137}Cs, ^{226}Ra, ^{214}Bi in 8B1
6. Total ^{210}Pb, ^{234}Th, ^{137}Cs, ^{214}Pb, ^{137}Cs, ^{226}Ra, ^{214}Bi in 13B1

Core No.	Depth (cm)	Mean Depth (cm)	Loss On Ignition (% Dry Wt.)	Tot Pb-210 (dpm/g)	Tot Pb-210 Err (+/-)	Cs-137 Activity (dpm/g)	Cs-137 err +/-	Pb-214 Activity (dpm/g)	Pb-214 err +/- (dpm/g)	Bi-214 Activity (dpm/g)	Bi-214 err +/- (dpm/g)	Ra-226 Activity (dpm/g)	Ra-226 err +/- (dpm/g)	Th-234 Activity (dpm/g)	Th-234 err +/- (dpm/g)
MB 1B1	0-1	0.5	5.2	11.02	0.166	0.21	0.05	1.60	0.13	1.73	0.15	1.67	0.14	3.93	0.38
MB 1B1	1-2	1.5	5.0	10.20	0.238	0.14	0.05	1.57	0.13	1.48	0.14	1.52	0.13	2.93	0.34
MB 1B1	2-3	2.5	4.8	10.63	0.153	0.22	0.05	1.47	0.12	1.45	0.14	1.46	0.13	2.45	0.35
MB 1B1	3-4A	3.5	4.4	9.80	0.135	0.24	0.05	1.56	0.13	1.56	0.14	1.56	0.14	2.44	0.33
MB 1B1	3-4B	3.5	4.6	9.64	0.135	--	--	--	--	--	--	--	--	--	--
MB 1B1	3-4C	3.5	4.4	9.45	0.133	--	--	--	--	--	--	--	--	--	--
MB 1B1	4-5	4.5	4.6	11.34	0.172	0.24	0.06	1.57	0.12	1.48	0.13	1.52	0.12	2.02	0.30
MB 1B1	5-6	5.5	4.4	10.05	0.149	0.10	0.05	1.44	0.12	1.46	0.14	1.45	0.13	1.75	0.32
MB 1B1	6-7	6.5	4.6	11.25	0.178	0.24	0.05	1.41	0.12	1.41	0.13	1.41	0.12	1.90	0.35
MB 1B1	7-8	7.5	4.8	8.82	0.134	0.23	0.05	1.59	0.13	1.53	0.14	1.56	0.13	2.01	0.33
MB 1B1	8-9	8.5	4.8	8.24	0.122	0.15	0.04	1.33	0.10	1.38	0.11	1.36	0.11	2.04	0.29
MB 1B1	9-10	9.5	5.2	7.28	0.112	0.20	0.05	1.33	0.12	1.39	0.13	1.36	0.12	1.70	0.36
MB 1B1	10-12A	11	5.0	6.77	0.102	0.13	0.04	1.43	0.11	1.44	0.19	1.43	0.15	1.74	0.31
MB 1B1	10-12B	11	5.0	6.32	0.102	--	--	--	--	--	--	--	--	--	--
MB 1B1	10-12C	11	5.0	6.94	0.107	--	--	--	--	--	--	--	--	--	--
MB 1B1	12-14	13	6.8	3.60	0.056	0.08	0.04	1.37	0.09	1.28	0.16	1.32	0.13	2.33	0.29
MB 1B1	14-16	15	7.2	3.32	0.070	Tr	--	1.32	0.12	1.30	0.13	1.31	0.12	2.10	0.32
MB 1B1	16-18	17	6.6	2.66	0.057	**	--	1.39	0.11	1.35	0.13	1.37	0.12	2.07	0.31
MB 1B1	18-20	19	7.0	2.10	0.046	**	--	1.24	0.10	1.20	0.12	1.22	0.11	1.96	0.31
MB 1B1	22-24	23	6.8	1.91	0.069	**	--	1.34	0.10	1.24	0.12	1.29	0.11	2.18	0.35
MB 1B1	24-26	25	7.4	1.85	0.071	**	--	1.25	0.09	1.26	0.10	1.25	0.10	2.00	0.25
MB 1B1	28-30	29	6.2	2.06	0.046	**	--	1.30	0.10	1.23	0.11	1.26	0.10	1.75	0.27
MB 1B1	32-34	33	6.8	1.49	0.039	**	--	1.32	0.11	1.27	0.13	1.29	0.12	2.04	0.27
MB 1B1	36-38A	37	6.4	1.39	0.035	**	--	1.40	0.09	1.32	0.16	1.36	0.12	2.04	0.23
MB 1B1	36-38B	37	6.2	1.32	0.033	--	--	--	--	--	--	--	--	--	--
MB 1B1	36-38C	37	6.2	1.28	0.032	--	--	--	--	--	--	--	--	--	--
MB 1B1	40-42	41	5.6	1.48	0.037	**	--	1.47	0.09	1.46	0.19	1.47	0.14	2.36	0.23
MB 1B1	44-46	45	6.2	1.24	0.029	**	--	1.35	0.10	1.35	0.18	1.35	0.14	1.53	0.33

Tr = Trace quantity, too low to quantify.
** = Not detected.

Excess Pb-210 Inventory = 118.84 dpm/cm^2

Core No.	Depth (cm)	Mean Depth (cm)	Loss On Ignition (% Dry Wt.)	Be-7 Activity (dpm/g)	Be-7 Activity +/- (dpm/g)	Cs-137 Activity (dpm/g)	Cs-137 Activity +/- (dpm/g)	Tot Pb-210 Activity (dpm/g)	Tot Pb-210 Activity Error (+/-)	Ra-226 Activity (dpm/g)	Ra-226 Activity +/- (dpm/g)	Th-234 Activity (dpm/g)	Th-234 Activity +/- (dpm/g)
MB 2B1	0-1	0.5	2.59	Tr	--	0.16	0.04	5.81	0.108	1.90	0.15	5.91	0.34
MB 2B1	1-2	1.5	3.80	**	--	0.18	0.05	6.01	0.104	1.96	0.15	2.84	0.39
MB 2B1	2-3	2.5	3.99	**	--	0.18	0.04	6.19	0.090	1.90	0.11	2.88	0.29
MB 2B1	3-4A	3.5	4.38	**	--	0.15	0.05	6.91	0.102	1.97	0.14	2.55	0.35
MB 2B1	3-4B	3.5	4.38	--	--	--	--	6.64	0.082	--	--	--	--
MB 2B1	3-4C	3.5	4.39	--	--	--	--	6.51	0.079	--	--	--	--
MB 2B1	4-5A	4.5	3.78	**	--	0.19	0.05	6.79	0.086	1.83	0.14	2.07	0.38
MB 2B1	4-5B	4.5	--	**	--	0.20	0.05	--	--	1.64	0.13	2.21	0.29
MB 2B1	5-6A	5.5	3.59	**	--	0.20	0.05	6.02	0.084	1.79	0.16	2.09	0.33
MB 2B1	5-6B	5.5	--	**	--	0.17	0.04	--	--	1.80	0.11	2.46	0.31
MB 2B1	6-7	6.5	3.59	**	--	0.21	0.05	6.40	0.085	1.87	0.18	2.05	0.39
MB 2B1	7-8	7.5	2.38	**	--	0.18	0.07	5.41	0.128	1.72	0.15	2.23	0.37
MB 2B1	8-9	8.5	3.59	**	--	0.19	0.05	5.13	0.088	1.83	0.15	2.03	0.45
MB 2B1	9-10A	9.5	3.39	**	--	0.20	0.05	4.72	0.073	1.78	0.14	2.06	0.42
MB 2B1	9-10B	9.5	3.39	--	--	--	--	4.81	0.072	--	--	--	--
MB 2B1	9-10C	9.5	3.39	--	--	--	--	4.51	0.059	--	--	--	--
MB 2B1	10-12	11	3.40	**	--	0.14	0.05	3.67	0.051	1.91	0.18	2.16	0.42
MB 2B1	12-14	13	3.99	**	--	Tr	--	2.60	0.039	1.85	0.14	1.89	0.41
MB 2B1	14-16	15	3.39	--	--	--	--	2.23	0.043	--	--	--	--
MB 2B1	16-18	17	3.59	**	--	Tr	--	1.68	0.031	2.11	0.16	2.44	0.42
MB 2B1	18-20A	19	3.79	--	--	--	--	2.24	0.041	--	--	--	--
MB 2B1	18-20B	19	3.79	--	--	--	--	2.16	0.036	--	--	--	--
MB 2B1	18-20C	19	3.79	--	--	--	--	2.21	0.035	--	--	--	--
MB 2B1	20-22	21	4.99	**	--	**	--	2.33	0.037	1.61	0.15	2.03	0.45
MB 2B1	22-24	23	5.17	--	--	--	--	1.80	0.031	--	--	--	--
MB 2B1	24-26	25	4.99	**	--	**	--	1.71	0.030	1.60	0.17	2.06	0.34

Tr = Trace quantities, too low to quantify.
** = Not detected.
Excess Pb-210 Inventory = 70.83 dpm/cm^2

fixed

Core No.	Depth (cm)	Mean Depth (cm)	Loss On Ignition (% Dry Wt.)	Cs-137 Activity (dpm/g)	Cs-137 Activity +/- (dpm/g)	Total Pb-210 Activity (dpm/g)	Total Pb-210 Activity Error (+/-)	Ra-226 Activity (dpm/g)	Ra-226 Activity +/- (dpm/g)	Th-234 Activity (dpm/g)	Th-234 Activity +/- (dpm/g)
MB 3B2	0-1	0.5	7.98	0.19	0.05	8.34	0.12	1.19	0.13	15.77	0.61
MB 3B2	1-2	1.5	6.97	0.18	0.06	6.48	0.10	1.58	0.15	10.64	0.54
MB 3B2	2-3	2.5	8.35	0.14	0.05	3.58	0.07	1.43	0.12	3.66	0.36
MB 3B2	3-4	3.5	6.99	0.16	0.06	2.76	0.04	1.34	0.12	2.71	0.33
MB 3B2	4-5A	4.5	7.80	0.18	0.05	2.35	0.04	1.30	0.12	1.74	0.29
MB 3B2	4-5B	4.5	8.00	--	--	2.41	0.04	--	--	--	--
MB 3B2	4-5C	4.5	8.18	--	--	2.33	0.03	--	--	--	--
MB 3B2	5-6	5.5	6.39	0.16	0.04	2.22	0.03	1.33	0.13	1.81	0.36
MB 3B2	6-7	6.5	6.59	0.13	0.04	2.13	0.03	1.36	0.10	1.95	0.29
MB 3B2	7-8	7.5	5.80	0.16	0.04	1.99	0.03	1.45	0.15	1.87	0.31
MB 3B2	8-9	8.5	5.40	0.11	0.04	1.71	0.03	1.42	0.13	1.61	0.29
MB 3B2	9-10	9.5	6.96	--	--	2.04	0.04	--	--	--	--
MB 3B2	10-12	11	5.40	0.21	0.05	2.01	0.03	1.52	0.16	1.95	0.38
MB 3B2	12-14	13	5.59	--	--	2.45	0.04	--	--	--	--
MB 3B2	14-16	15	5.79	0.18	0.05	2.63	0.05	1.57	0.13	1.75	0.37
MB 3B2	16-18	17	5.59	--	--	2.35	0.04	--	--	--	--
MB 3B2	18-20	19	4.78	0.14	0.06	2.03	0.04	1.62	0.13	1.80	0.34
MB 3B2	20-22	21	4.80	--	--	2.25	0.04	--	--	--	--
MB 3B2	22-24A	23	6.00	0.21	0.05	2.59	0.07	1.63	0.17	1.88	0.40
MB 3B2	22-24B	23	5.79	--	--	2.83	0.06	--	--	--	--
MB 3B2	22-24C	23	5.59	--	--	2.81	0.05	--	--	--	--
MB 3B2	24-26	25	6.40	--	--	2.58	0.05	--	--	--	--
MB 3B2	26-28	27	5.60	0.19	0.04	2.70	0.04	1.67	0.13	1.92	0.25
MB 3B2	28-30	29	5.98	--	--	2.15	0.07	--	--	--	--
MB 3B2	30-32	31	5.18	0.17	0.05	2.99	0.04	1.54	0.13	1.85	0.33
MB 3B2	32-34	33	5.39	--	--	2.73	0.04	--	--	--	--
MB 3B2	34-36	35	4.99	0.14	0.04	2.52	0.03	1.67	0.11	1.63	0.31
MB 3B2	36-38	37	4.39	0.15	0.05	5.94	0.07	1.79	0.15	2.17	0.39
MB 3B2	38-40	39	4.80	0.25	0.06	17.59	0.19	1.61	0.13	2.05	0.39
MB 3B2	40-42	41	6.19	0.21	0.06	13.87	0.14	1.50	0.13	1.58	0.38
MB 3B2	42-44	43	5.59	0.21	0.05	9.99	0.11	1.49	0.15	1.87	0.32
MB 3B2	44-46	45	5.18	0.20	0.05	6.34	0.11	1.63	0.13	1.79	0.33
MB 3B2	46-48A	47	5.19	0.21	0.05	6.45	0.08	1.51	0.14	2.03	0.30
MB 3B2	46-48B	47	5.38	--	--	6.78	0.09	--	--	--	--
MB 3B2	46-48C	47	5.37	--	--	6.35	0.07	--	--	--	--
MB 3B2	48-50	49	6.80	0.26	0.05	7.68	0.09	1.46	0.12	2.00	0.34
MB 3B2	50-52	51	5.58	0.30	0.06	8.91	0.10	1.58	0.18	1.87	0.38
MB 3B2	52-54	53	5.60	0.26	0.05	8.31	0.10	1.57	0.15	2.05	0.32

Core No.	Depth (cm)	Mean Depth (cm)	Wet Bulk Density (g/cm3)	Loss On Ignition (% Dry Wt.)	Total Pb-210 Activity (dpm/g)	Total Pb-210 Activity Error (+/-)	Cs-137 Activity (dpm/g)	Cs-137 Activity +/- (dpm/g)	Ra-226 Activity (dpm/g)	Ra-226 Activity +/- (dpm/g)	Th-234 Activity (dpm/g)	Th-234 Activity +/- (dpm/g)
MB 7B1	0-1	0.5	0.83	4.00	8.23	0.13	Tr	--	1.36	0.13	7.26	0.43
MB 7B1	1-2	1.5	1.55	3.20	8.18	0.14	0.14	0.05	1.70	0.17	3.27	0.38
MB 7B1	2-3	2.5	1.59	3.40	8.24	0.13	0.15	0.05	1.61	0.14	2.75	0.40
MB 7B1	3-4A	3.5	1.57	3.40	8.79	0.15	Tr	--	1.47	0.12	1.57	0.33
MB 7B1	3-4B	3.5	--	3.40	8.41	0.15	Tr	--	1.43	0.12	1.76	0.28
MB 7B1	3-4C	3.5	--	3.40	7.44	0.12	Tr	--	1.49	0.12	1.71	0.29
MB 7B1	4-5	4.5	1.70	3.20	8.03	0.14	Tr	--	1.45	0.12	1.59	0.29
MB 7B1	5-6	5.5	1.63	3.00	7.91	0.14	0.12	0.04	1.28	0.10	1.74	0.24
MB 7B1	6-7	6.5	1.60	2.80	6.79	0.12	0.12	0.03	1.40	0.09	1.72	0.22
MB 7B1	7-8	7.5	1.73	2.80	7.66	0.13	0.09	0.04	1.48	0.12	1.69	0.26
MB 7B1	8-9	8.5	1.62	2.80	6.56	0.11	0.08	0.04	1.46	0.12	1.72	0.27
MB 7B1	9-10	9.5	1.71	2.80	6.09	0.10	0.14	0.04	1.36	0.12	1.76	0.32
MB 7B1	10-12	11	1.69	3.00	5.35	0.09	0.15	0.04	1.43	0.13	1.81	0.32
MB 7B1	12-14	13	1.65	3.00	5.28	0.09	0.14	0.05	1.42	0.12	2.02	0.30
MB 7B1	14-16A	15	1.61	3.40	4.95	0.09	0.15	0.04	1.30	0.11	1.87	0.26
MB 7B1	14-16B	15	--	3.40	4.43	0.07	--	--	--	--	--	--
MB 7B1	14-16C	15	--	3.40	4.86	0.09	--	--	--	--	--	--
MB 7B1	16-18	17	1.61	3.20	4.68	0.08	--	--	--	--	--	--
MB 7B1	18-20	19	1.64	3.00	3.38	0.09	0.07	0.04	1.50	0.09	1.85	0.24
MB 7B1	20-22	21	1.76	2.80	2.92	0.06	--	--	--	--	--	--
MB 7B1	22-24	23	1.70	2.80	2.27	0.05	**	--	1.50	0.16	2.00	0.29
MB 7B1	24-26	25	1.64	2.80	1.80	0.04	--	--	--	--	--	--
MB 7B1	26-28	27	1.72	3.00	1.43	0.03	**	--	1.49	0.12	2.03	0.29
MB 7B1	28-30	29	1.58	3.20	1.51	0.03	--	--	--	--	--	--
MB 7B1	30-32A	31	1.67	3.20	1.20	0.03	**	--	1.37	0.12	1.89	0.22
MB 7B1	30-32B	31	--	3.20	1.18	0.03	--	--	--	--	--	--
MB 7B1	30-32C	31	--	3.20	1.30	0.03	--	--	--	--	--	--
MB 7B1	32-34	33	1.67	3.00	0.90	0.02	--	--	--	--	--	--
MB 7B1	32-34*	33	1.66	3.00	0.85	0.02	--	--	--	--	--	--
MB 7B1	34-36	35	1.67	3.00	0.70	0.02	**	--	1.24	0.13	1.87	0.27

Tr = Trace quantities, too low to quantify.
** = Not detected.
Excess Pb-210 Inventory = 128.74 dpm/cm^2

Core No.	Depth (cm)	Mean Depth (cm)	Loss On Ignition (% Dry Wt.)	Tot Pb-210 Activity (dpm/g)	Tot Pb-210 Activity Error (+/-)	Cs-137 Activity (dpm/g)	Cs-137 Activity +/- (dpm/g)	Pb-214 Activity (dpm/g)	Pb-214 Activity +/- (dpm/g)	Bi-214 Activity (dpm/g)	Bi-214 Activity +/- (dpm/g)	Th-234 Activity (dpm/g)	Th-234 Activity +/- (dpm/g)
MB 8B1	0-1	0.5	4.60	11.07	0.19	Tr	--	1.49	0.19	1.33	0.19	3.74	0.52
MB 8B1	1-2A	1.5	4.00	11.60	0.20	0.13	0.05	1.44	0.12	1.44	0.13	2.77	0.37
MB 8B1	1-2B	1.5	--	--	--	0.12	0.03	1.45	0.09	1.31	0.16	1.68	0.25
MB 8B1	2-3A	2.5	4.20	11.20	0.20	0.15	0.04	1.36	0.11	1.41	0.12	3.34	0.31
MB 8B1	2-3B	2.5	--	--	--	0.10	0.04	1.32	0.10	1.40	0.12	1.95	0.27
MB 8B1	3-4A	3.5	4.20	11.72	0.19	0.08	0.04	1.29	0.11	1.26	0.12	1.87	0.30
MB 8B1	3-4B	3.5	4.20	11.52	0.18	--	--	--	--	--	--	--	--
MB 8B1	3-4C	3.5	4.20	10.95	0.17	--	--	--	--	--	--	--	--
MB 8B1	4-5	4.5	3.80	10.76	0.18	0.13	0.04	1.36	0.12	1.34	0.12	1.71	0.32
MB 8B1	5-6	5.5	3.60	9.86	0.17	Tr	--	1.39	0.11	1.32	0.13	1.76	0.29
MB 8B1	6-7	6.5	4.00	9.54	0.18	0.14	0.05	1.22	0.11	1.20	0.12	1.71	0.29
MB 8B1	7-8	7.5	3.60	7.95	0.15	0.13	0.04	1.30	0.11	1.26	0.12	1.69	0.28
MB 8B1	8-9	8.5	3.80	6.43	0.11	0.11	0.04	1.29	0.11	1.27	0.12	1.91	0.32
MB 8B1	9-10	9.5	4.00	6.36	0.12	0.11	0.04	1.28	0.09	1.18	0.10	1.69	0.26
MB 8B1	10-12	11.0	3.60	5.30	0.09	0.11	0.05	1.34	0.11	1.34	0.13	2.31	0.34
MB 8B1	12-14A	13.0	4.00	4.51	0.11	--	--	--	--	--	--	--	--
MB 8B1	12-14B	13.0	4.00	4.44	0.07	--	--	--	--	--	--	--	--
MB 8B1	12-14C	13.0	3.80	4.75	0.09	--	--	--	--	--	--	--	--
MB 8B1	14-16	15.0	3.80	4.04	0.09	Tr	--	1.44	0.12	1.39	0.13	1.97	0.31
MB 8B1	16-18	17.0	4.60	3.05	0.06	--	--	--	--	--	--	--	--
MB 8B1	18-20	19.0	4.60	1.66	0.04	**	--	1.14	0.10	1.19	0.12	2.03	0.28
MB 8B1	20-22	21.0	4.20	1.60	0.04	--	--	--	--	--	--	--	--
MB 8B1	22-24	23.0	4.00	1.56	0.03	**	--	1.20	0.10	1.18	0.11	2.30	0.28
MB 8B1	24-26	25.0	4.00	1.03	0.03	--	--	--	--	--	--	--	--
MB 8B1	26-28	27.0	4.20	0.82	0.02	**	--	1.10	0.10	1.13	0.12	2.22	0.34
MB 8B1	28-30	29.0	4.20	0.88	0.02	--	--	--	--	--	--	--	--
MB 8B1	30-32A	31.0	4.00	0.76	0.02	**	--	1.16	0.10	1.13	0.12	2.42	0.31
MB 8B1	30-32B	31.0	3.80	0.69	0.02	--	--	--	--	--	--	--	--
MB 8B1	30-32C	31.0	4.40	0.75	0.02	--	--	--	--	--	--	--	--
MB 8B1	32-34	33.0	4.00	0.69	0.02	--	--	--	--	--	--	--	--
MB 8B1	34-36	35.0	4.40	0.79	0.02	**	--	1.27	0.11	1.13	0.12	2.40	0.31
MB 8B1	36-38	37.0	4.60	0.82	0.02	--	--	--	--	--	--	--	--
MB 8B1	38-39	38.5	4.60	0.87	0.02	**	--	1.34	0.12	1.30	0.13	2.28	0.34

Tr = Trace quantities, too low to quantify.
** = Not detected.

Excess Pb-120 Inventory = 126.52 dpm/cm^2

Core No.	Depth (cm)	Mean Depth (cm)	Loss On Ignition (% Dry Wt.)	Total Pb-210 (dpm/g)	Total Pb-210 Error (+/-)	Cs-137 Activity (dpm/g)	Cs-137 err +/- (dpm/g)	Pb-210 Activity (dpm/g)	Pb-210 err +/- (dpm/g)	Pb-214 Activity (dpm/g)	Pb-214 err +/- (dpm/g)	Bi-214 Activity (dpm/g)	Bi-214 err +/- (dpm/g)	Th-234 Activity (dpm/g)	Th-234 err +/- (dpm/g)
MB 13B1	0-1	0.5	5.6	10.24	0.15	0.20	0.06	15.61	1.10	1.26	0.15	1.11	0.16	9.48	0.60
MB 13B1	1-2	1.5	6.6	9.54	0.15	0.21	0.05	13.93	0.83	1.28	0.13	1.30	0.14	5.51	0.44
MB 13B1	2-3	2.5	7.8	8.17	0.18	0.29	0.06	11.32	0.73	1.26	0.13	1.19	0.14	4.61	0.12
MB 13B1	3-4A	3.5	6.8	8.71	0.14	0.25	0.05	10.83	0.63	1.15	0.10	1.07	0.12	1.75	0.26
MB 13B1	3-4B	3.5	6.8	8.94	0.13	--	--	--	--	--	--	--	--	--	--
MB 13B1	3-4C	3.5	6.6	8.50	0.14	--	--	--	--	--	--	--	--	--	--
MB 13B1	4-5	4.5	6.6	8.88	0.13	0.24	0.05	12.34	0.68	1.21	0.11	1.36	0.13	1.85	0.32
MB 13B1	5-6	5.5	5.6	9.94	0.15	0.19	0.05	12.13	0.66	1.31	0.11	1.23	0.12	1.72	0.31
MB 13B1	6-7	6.5	4.6	9.23	0.15	0.22	0.05	11.80	0.68	1.26	0.10	1.30	0.12	1.55	0.30
MB 13B1	7-8	7.5	4.4	8.40	0.14	0.15	0.04	12.26	0.61	1.27	0.10	1.24	0.11	1.57	0.26
MB 13B1	8-9	8.5	4.2	7.77	0.13	0.19	0.05	11.96	0.68	1.29	0.11	1.26	0.12	1.77	0.29
MB 13B1	9-10	9.5	4	7.82	0.12	0.22	0.04	11.48	0.57	1.23	0.09	1.27	0.16	1.77	0.24
MB 13B1	10-12	11.0	4.2	6.83	0.11	0.17	0.05	9.25	0.58	1.25	0.10	1.13	0.11	1.80	0.29
MB 13B1	12-14A	13.0	3.8	5.30	0.09	--	--	--	--	--	--	--	--	--	--
MB 13B1	12-14B	13.0	3.8	5.30	0.09	--	--	--	--	--	--	--	--	--	--
MB 13B1	12-14C	13.0	3.8	5.62	0.10	--	--	--	--	--	--	--	--	--	--
MB 13B1	14-16	15.0	3.8	4.74	0.09	0.22	0.04	7.41	0.43	1.35	0.08	1.31	0.15	1.62	0.24
MB 13B1	16-18	17.0	3.4	4.38	0.09	--	--	--	--	--	--	--	--	--	--
MB 13B1	18-20	19.0	4	5.03	0.14	0.11	0.03	5.08	0.36	1.33	0.08	1.37	0.15	1.95	0.24
MB 13B1	20-22	21.0	3.6	1.69	0.04	--	--	--	--	--	--	--	--	--	--
MB 13B1	22-24	23.0	3.4	1.58	0.03	Tr	--	3.22	0.42	1.44	0.11	1.40	0.12	1.85	0.29
MB 13B1	24-26	25.0	3.2	1.31	0.03	--	--	--	--	--	--	--	--	--	--
MB 13B1	26-28	27.0	3.2	1.23	0.03	**	--	2.54	0.35	1.33	0.09	1.30	0.16	1.78	0.23
MB 13B1	28-30	29.0	3	0.84	0.02	--	--	--	--	--	--	--	--	--	--
MB 13B1	30-32	31.0	3	0.97	0.03	**	--	2.10	0.38	1.36	0.12	1.40	0.13	2.13	0.32
MB 13B1	32-34	33.0	3.2	0.86	0.02	--	--	--	--	--	--	--	--	--	--
MB 13B1	34-36	35.0	3.2	0.78	0.02	**	--	1.95	0.34	1.35	0.10	1.35	0.17	1.92	0.27
MB 13B1	36-38A	37.0	3	0.66	0.02	--	--	--	--	--	--	--	--	--	--
MB 13B1	36-38B	37.0	3	0.61	0.02	--	--	--	--	--	--	--	--	--	--
MB 13B1	36-38C	37.0	3.2	0.58	0.02	--	--	--	--	--	--	--	--	--	--
MB 13B1	38-40	39.0	2.8	0.63	0.02	**	--	1.89	0.45	1.46	0.11	1.40	0.13	1.79	0.29
MB 13B1	40-41	40.5	2.8	0.75	0.01	--	--	--	--	--	--	--	--	--	--

Tr = Trace quantities, too low to quantify.

** = Not detected.

Excess Pb-210 Inventory = 127.42 dpm/cm^2

Appendix D: Plots of radioisotope activity measured by alpha spectrometry

1. Excess ^{210}Pb in core B557, B558, B554, B555, B556, B561
2. Excess ^{210}Pb in core B582, B505, B506, B509, B504, B49
3. Excess ^{210}Pb in core B67, B62, B448, B245, B606, B81
4. Excess ^{210}Pb in core B117, B88, B424, B271, B250, B155
5. Excess ^{210}Pb in core B330 and B331

B557

depth interval (cm)	Po-210 activity (dpm/g)	counting error +/- (dpm/g)
0-0.5	1.00	0.04
1-1.5	1.50	0.05
1.5-2	1.21	0.04
2.5-3	0.87	0.03
3.5-4	0.89	0.03
4.5-5	0.98	0.03
6-7	1.02	0.03
8-9	0.89	0.03
10-12	0.93	0.03
14-16	0.77	0.02
16-18	0.50	0.02
18-20	0.36	0.02
12-14	0.50	0.02

[assumed supported =0.72]

B558

depth interval (cm)	Po-210 activity (dpm/g)	counting error +/- (dpm/g)
1-1.5	1.93	0.03
1.5-2	1.99	0.03
2.5-3	2.23	0.04
4.5-5	1.83	0.05
6-7	1.67	0.04
8-9	2.44	0.07
10-12	1.65	0.02
14-16	1.53	0.02
16-18	0.93	0.02
18-20	0.94	0.02
0-0.5	2.47	0.04
3.5-4	2.54	0.05
12-14	1.81	0.04

[assumed supported =0.72]

561

depth interval (cm)	Po-210 activity (dpm/g)	counting error +/- (dpm/g)
0-0.5	1.97	0.04
1.5-2	1.57	0.03
2.5-3	1.65	0.03
3.5-4	1.91	0.07
4.5-5	1.45	0.05
6-7	1.41	0.04
8-9	1.57	0.05
10-12	1.51	0.03
14-16	0.84	0.02
16-18	0.88	0.02
18-20	0.75	0.02
12-14	1.29	0.03

[assumed supported =0.72]

B556

depth interval (cm)	Po-210 activity (dpm/g)	counting error +/- (dpm/g)
1-1.5	1.78	0.01
1.5-2	1.75	0.02
2.5-3	2.21	0.03
3.5-4	1.98	0.03
4.5-5	1.94	0.02
6-7	1.77	0.02
8-9	1.88	0.02
10-12	2.09	0.03
16-18	1.59	0.01
18-20	1.74	0.02
12-14	1.92	0.02
14-16	1.69	0.01
24.5-25	1.46	0.01

[assumed supported =0.72]

555

depth interval (cm)	Po-210 activity (dpm/g)	counting error +/- (dpm/g)
0-0.5	2.80	0.09
1-1.5	2.56	0.07
1.5-2	2.42	0.06
2.5-3	2.76	0.08
3.5-4	2.96	0.06
4.0-4.5	3.06	0.06
6-7	2.58	0.06
8-9	3.01	0.09
10-12	2.86	0.05
12-14	2.23	0.04
14-16	1.93	0.03
16-18	1.62	0.03
18-20	2.02	0.04
22.5	1.29	0.02
25.5	1.27	0.03
27	1.47	0.05
30	1.20	0.04
32	1.09	0.05
35	0.68	0.03
40	0.57	0.03

[supported =0.53]

554

depth interval (cm)	Po-210 activity (dpm/g)	counting error +/- (dpm/g)
0-0.5	4.14	0.12
1-1.5	3.47	0.07
1.5-2	3.48	0.08
2.5-3	4.31	0.12
3.5-4	4.45	0.16
4.5-5	3.64	0.13
6-7	3.32	0.12
8-9	4.05	0.17
10-12	3.91	0.08
12-14	3.43	0.06
14-16	3.12	0.07
16-18	2.59	0.07
18-20	3.18	0.08
22	2.59	0.08
25	2.29	0.04
27	0.96	0.02
30	0.81	0.03
32	0.50	0.01
35	0.50	0.02

[supported = 0.44]

B582

depth interval (cm)	Po-210 activity (dpm/g)	counting error +/- (dpm/g)
0-0.5	3.91	0.03
1-1.5	3.02	0.02
1.5-2	3.29	0.02
2.5-3	4.16	0.03
3.5-4	4.06	0.02
4.5-5	2.37	0.01
6-7	3.22	0.02
8-9	3.63	0.03
10-12	3.67	0.05
14-16	2.69	0.03
16-18	2.00	0.03
18-20	1.33	0.03
12-14	2.68	0.01
25	3.24	0.02
30	4.01	0.03
32	3.84	0.03

[assumed supported =0.72]

B505

depth interval (cm)	Po-210 activity (dpm/g)	counting error +/- (dpm/g)
0-0.5	0.11	0.03
1-1.5	0.09	0.02
1.5-2	0.09	0.03
2.5-3	0.11	0.03
3.5-4	0.14	0.04
4.5-5	0.06	0.02
6-7	0.12	0.03
8-9	0.12	0.03
10-12	0.07	0.02
12-14	0.04	0.01
14-16	0.05	0.02
16-18	0.06	0.02
18-20	0.06	0.02
22	0.04	0.04
25	0.02	0.03
27	0.04	0.07
30	0.02	0.03
33	0.03	0.05

[supported =0.54]

506

depth interval (cm)	Po-210 activity (dpm/g)	counting error +/- (dpm/g)
0-0.5	5.89	0.10
1.5-2	4.72	0.07
2.5-3	5.41	0.09
3.5-4	4.98	0.19
6-7	4.49	0.08
8-9	3.84	0.07
10-12	2.28	0.11
14-16	1.49	0.04
16-18	1.56	0.05
18-20	1.12	0.09

[assumed supported =0.72]

B509

depth interval (cm)	Po-210 activity (dpm/g)	counting error +/- (dpm/g)
0-0.5	4.50	0.10
1-1.5	3.75	0.07
1.5-2	3.62	0.06
2.5-3	4.12	0.19
3.5-4	3.18	0.13
4-4.5	4.26	0.08
6-7	4.75	0.23
8-9	3.99	0.13
10-12	3.94	0.09
12-14	3.95	0.07
14-16	2.95	0.09
16-18	2.99	0.11
18-20	2.47	0.13

[assumed supported =0.72]

B504

depth interval (cm)	Po-210 activity (dpm/g)	counting error +/- (dpm/g)
0-0.5	3.97	0.03
0.5-1.0	3.36	0.02
1.0-1.5	3.78	0.02
1.5-2.0	4.45	0.05
2.5-3.0	3.40	0.02
3.5-4.0	3.39	0.03
4.5-5.0	4.02	0.05
6-7	3.57	0.02
8-9	3.35	0.02
10-12	3.72	0.03
12-14	2.75	0.01
14-16	2.21	0.01
18-20	1.49	0.01
22	1.36	0.03
25	0.42	0.01
27	0.39	0.01
30	0.49	0.01

[supported =0.35]

B49

depth interval (cm)	Po-210 activity (dpm/g)	counting error +/- (dpm/g)
0.00	5.07	
0.25	5.22	
0.50	5.63	
0.75	4.79	
1.25	4.26	
1.50	5.02	
1.75	5.15	
2.00	5.25	
2.50	4.94	
4.00	5.47	
5.00	4.76	
7.00	4.81	
10.00	4.84	
15.00	4.11	
20.00	3.13	

[assumed supported =0.72]

B67

depth interval (cm)	Po-210 activity (dpm/g)	counting error +/- (dpm/g)
0.0	6.23	
0.3	6.32	
0.5	8.89	
0.8	6.73	
1.0	5.91	
1.3	6.20	
1.5	6.99	
1.8	6.39	
2.0	6.52	
2.5	6.69	
3.0	6.04	
3.5	6.13	
4.0	**5.79**	
5.0	**7.20**	
7.0	**6.85**	
10.0	**5.95**	
15.0	**3.55**	
20.0	**1.72**	

[supported =0.44]

*

B62

depth interval (cm)	Po-210 activity (dpm/g)	counting error +/- (dpm/g)
0.0	3.38	
0.3	3.05	
0.5	2.71	
0.8	2.96	
1.0	3.34	
1.3	3.21	
1.5	2.92	
1.8	3.30	
2.0	3.39	
2.5	3.17	
3.0	3.58	
3.5	4.19	
4.0	3.73	
5.0	3.41	
7.0	3.32	
10.0	3.32	
15.0	5.53	
20.0	2.18	

[assumed supported =0.72]

*

B448

depth interval (cm)	Po-210 activity (dpm/g)	counting error +/- (dpm/g)
0-0.5	7.04	0.12
1-1.5	6.27	0.11
1.5-2	6.09	0.09
2.5-3	8.01	0.13
3.5-4	7.09	0.27
4.5-5	5.09	0.24
6-7	6.51	0.12
8-9	4.34	0.07
10-12	3.39	0.16
12-14	4.27	0.08
14-16	2.66	0.07
16-18	3.00	0.09
18-20	0.95	0.08
25	1.04	0.03
30	1.52	0.05
35	0.81	0.03
40	1.71	0.06

[supported =1.26]

B245

depth interval (cm)	Po-210 activity (dpm/g)	counting error +/- (dpm/g)
0.0	6.75	
0.3	5.39	
0.5	4.79	
0.8	6.08	
1.0	5.52	
1.3	5.52	
1.5	5.95	
1.8	5.42	
2.0	5.46	
2.5	6.51	
3.0	5.93	
3.5	6.08	
4.0	7.07	
5.0	6.17	
7.0	5.24	
10.0	4.75	
15.0	3.33	
20.0	3.21	

[assumed supported =0.72]

*

B606

depth interval (cm)	Po-210 activity (dpm/g)	counting error +/- (dpm/g)
0-0.5	9.53	0.14
0.5-1	8.23	0.10
1-1.5	8.30	0.10
1.5-2	9.79	0.21
2-2.5	7.68	0.12
2.5-3	7.84	0.12
3-3.5	10.16	0.17
4-4.5	7.67	0.11
6-7	7.05	0.15
8-9	5.47	0.10
10-12	5.49	0.13
12-14	4.91	0.11
14-16	3.81	0.08
18-20	2.04	0.06
25	2.32	0.05
30	1.04	0.03
35	0.37	0.01
40	0.69	0.02

[supported =0.53]

*

B81

depth interval (cm)	Po-210 activity (dpm/g)	counting error +/- (dpm/g)
0.0	12.01	
0.5	15.26	
1.0	15.54	
1.5	7.75	
2.0	9.46	
2.5	13.31	
3.0	9.12	
3.5	11.70	
4.0	11.52	
4.5	9.65	
5.0	10.19	
6.0	10.38	
7.0	8.95	
8.0	10.79	
9.0	10.29	
10.0	4.81	
11.0	5.08	
12.0	4.51	
14.0	3.78	
16.0	5.14	
18.0	3.75	
20.0	3.07	

B117

depth interval (cm)	Po-210 activity (dpm/g)	counting error +/- (dpm/g)
1-1.5	10.41	0.12
3-3.5	7.36	0.21
6-6.5	6.34	0.06
9-9.5	4.34	0.05
12-12.5	1.69	0.03
15-15.5	2.32	0.02
17-17.5	1.24	0.02
20	3.16	0.05
25	1.60	0.02
30	1.03	0.02
35	1.73	0.01
45	1.36	0.01

[supported =1.1]

B88

depth interval (cm)	Po-210 activity (dpm/g)	counting error +/- (dpm/g)
0.0	8.44	
0.3	7.47	
0.5	8.89	
0.8	8.74	
1.0	8.12	
1.3	7.06	
1.5	8.02	
1.8	7.31	
2.0	8.03	
2.5	7.13	
3.0	8.21	
3.5	8.21	
4.0	6.37	
5.0	8.45	
10.0	4.25	
20.0	1.77	

[supported =1.05]

B424

depth interval (cm)	Po-210 activity (dpm/g)	counting error +/- (dpm/g)
0-0.5	11.10	0.08
1-1.5	8.79	0.04
1.5-2	9.01	0.04
2.5-3	11.54	0.09
3.5-4	11.17	0.11
4.5-5	7.48	0.03
6-7	6.64	0.03
8-9	7.52	0.07
10-12	2.87	0.03
14-16	3.25	0.04
16-18	2.37	0.02
18-20	2.37	0.03

[supported =1.03]

B271

depth interval (cm)	Po-210 activity (dpm/g)	counting error +/- (dpm/g)
0.0	9.32	
0.3	8.22	
0.8	9.55	
1.0	7.88	
1.3	9.36	
1.5	8.16	
2.0	9.24	
2.5	5.80	
3.0	7.99	
4.0	8.48	
5.0	9.40	
7.0	7.53	
10.0	5.72	
15.0	3.44	
20.0	2.82	
25.0	1.61	
30.0	1.13	

B250

depth interval (cm)	Po-210 activity (dpm/g)	counting error +/- (dpm/g)
0.00	12.11	
0.25	9.42	
0.50	11.00	
0.75	11.17	
1.00	10.42	
1.25	12.06	
1.50	10.28	
2.00	11.09	
2.50	11.29	
3.00	10.26	
4.00	11.91	
5.00	9.46	
7.00	5.54	
10.00	6.64	
15.00	3.56	
20.00	0.67	
25.00	0.75	
30.00	1.02	

B155

depth interval (cm)	Po-210 activity (dpm/g)	counting error +/- (dpm/g)
1-1.5	3.37	0.03
3-3.5	4.05	0.05
5-5.5	2.30	0.01
5-5.5	2.57	0.02
7-7.5	2.24	0.02
9-9.5	1.48	0.02
12-12.5	1.20	0.02
12-12.5	1.47	0.03
15-15.5	1.32	0.03
20	1.14	0.04
25	0.99	0.02
30	0.76	0.01
35	0.68	0.01
40	0.69	0.01

B331		
depth interval (cm)	Po-210 activity (dpm/g)	counting error +/- (dpm/g)
0.0	12.27	
0.3	12.35	
0.5	13.31	
0.8	9.22	
1.0	10.19	
1.3	16.06	
1.5	15.32	
1.8	11.53	
2.0	9.05	
2.5	5.61	
3.0	7.44	
3.5	12.04	
4.0	12.63	
5.0	10.39	
7.0	7.91	
10.0	7.76	
15.0	1.84	
20.0	2.15	

[supported =0.75]

*

B330		
depth interval (cm)	Po-210 activity (dpm/g)	counting error +/- (dpm/g)
0.0	13.32	
0.3	12.15	
0.5	13.79	
0.8	14.02	
1.0	12.90	
1.3	10.49	
1.5	10.71	
1.8	10.91	
2.0	11.31	
2.5	9.12	
3.0	8.58	
3.5	9.61	
4.0	8.18	
5.0	7.68	
10.0	2.66	
20.0	1.07	

[supported =0.68]

Appendix E: Table of abundance of significant diatoms

Abundance of Significant Diatoms in core PS-1

depth (cm)	mass scanned (mg)	total per gram	fragments per gram	*Chaetoceros* per gram	*Thalasionema nitzschiodes* per gram	*pseudo-nitzschia* per gram	ratio *Chaetoceros* to *T.nitzschiodes*
6	0.039	5692	3744	718	256	51	2.8
12	0.027	18704	9852	4333	444	0	9.8
18	0.026	19231	9654	5231	500	615	10.5
24	0.028	17893	9679	4000	750	0	5.3
33	0.032	9531	4438	2938	188	31	15.7
39	0.028	14893	8429	4250	536	214	7.9
45	0.027	11370	5481	4185	407	0	10.3
51	0.035	3514	2314	486	29	57	17.0
57	0.031	8452	3677	3484	226	0	15.4
63	0.035	10114	4657	3857	171	0	22.5
69	0.041	10854	5439	3951	317	24	12.5
75	0.042	6929	3905	1667	238	71	7.0
81	0.029	2724	1759	483	0	0	
87	0.039	9436	6026	1231	769	51	1.6
93	0.026	3731	2615	385	77	77	5.0
99	0.047	2511	1596	362	64	43	5.7
105	0.031	3194	2742	97	0	0	
111	0.042	10286	6000	2810	238	95	11.8
117	0.045	11222	5400	3911	289	0	13.5
123	0.042	5667	4048	786	95	95	8.3
129	0.047	3872	2000	1085	191	0	5.7
135	0.045	2533	2067	178	89	0	2.0
141	0.029	1690	1448	34	103	0	0.3
147	0.032	3094	2656	63	188	0	0.3

Appendix E: Table of abundance of significant diatoms

Abundance of Significant Diatoms in core PS-1

* age (y)	year	depth (cm)	mass scanned (mg)	total per gram	fragments per gram	*Chaetoceros* per gram	*Thalasionema nitzschiodes* per gram	*pseudo-nitzschia* per gram	ratio *Chaetoceros* to *T.nitzschiodes*
0	1999	6	0.039	5692	3744	718	256	51	2.8
0	1999	12	0.027	18704	9852	4333	444	0	9.8
0	1999	18	0.026	19231	9654	5231	500	615	10.5
0	1999	24	0.028	17893	9679	4000	750	0	5.3
11	1988	33	0.032	9531	4438	2938	188	31	15.7
18	1981	39	0.028	14893	8429	4250	536	214	7.9
26	1973	45	0.027	11370	5481	4185	407	0	10.3
34	1965	51	0.035	3514	2314	486	29	57	17.0
42	1957	57	0.031	8452	3677	3484	226	0	15.4
50	1949	63	0.035	10114	4657	3857	171	0	22.5
58	1941	69	0.041	10854	5439	3951	317	24	12.5
66	1933	75	0.042	6929	3905	1667	238	71	7.0
74	1925	81	0.029	2724	1759	483	0	0	
82	1917	87	0.039	9436	6026	1231	769	51	1.6
89	1910	93	0.026	3731	2615	385	77	77	5.0
97	1902	99	0.047	2511	1596	362	64	43	5.7
105	1894	105	0.031	3194	2742	97	0	0	
113	1886	111	0.042	10286	6000	2810	238	95	11.8
121	1878	117	0.045	11222	5400	3911	289	0	13.5
129	1870	123	0.042	5667	4048	786	95	95	8.3
137	1862	129	0.047	3872	2000	1085	191	0	5.7
145	1854	135	0.045	2533	2067	178	89	0	2.0
153	1846	141	0.029	1690	1448	34	103	0	0.3
161	1838	147	0.032	3094	2656	63	188	0	0.3

* Sediments in the upper 25cm reflect a modern flood deposit. The age of deeper sediment horizons were estimated by subtracting 25 cm from the depth and dividing by a sedimentation rate of 0.76 cm/y.